UNIVERSITY OF OKLAHOMA

GRADUATE COLLEGE

THE *ALAN SHEPARD* (*SHEP*) GENE REGULATES NEURONAL REMODELING DURING METAMORPHOSIS

A DISSERTATION

SUBMITTED TO THE GRADUATE FACULTY

in partial fulfillment of the requirements for the

Degree of

DOCTOR OF PHILOSOPHY

By

DAHONG CHEN
Norman, Oklahoma
2014

THE *ALAN SHEPARD* (*SHEP*) GENE REGULATES NEURONAL REMODELING DURING METAMORPHOSIS

A DISSERTATION APPROVED FOR THE
DEPARTMENT OF BIOLOGY

BY

_____
Dr. Randall Hewes, Chair

_____
Dr. Ben Holt

_____
Dr. David Durica

_____
Dr. David McCauley

_____
Dr. JP Masly

© Copyright by DAHONG CHEN 2014
All Rights Reserved.

Dedication

To my fiancée Silu Wang for her inspiration, support, and understanding on my career. Her encouragement helps me proceed with firm faith.

To my parents for their understanding and support on my decision to start my career on the other side of the earth. They are tremendously contributing to my life, as always.

Acknowledgements

I would like to gratefully say thanks for the continuous support from Dr. Randall Hewes, my mentor and friend. His guidance on both research and personality will have a lifetime impact on my career development. I would like also to thank my committee members, Dr. Ben Holt, Dr. Bing Zhang (previous committee member), Dr. David Durica, Dr. David McCauley, and Dr. JP Masly, for their critical comments and suggestions to help me improve my research. Also, thanks to previous and current members of the Hewes' lab, Chunjing Qu, Tingting Gu, Tao Zhao, and a number of undergraduate students for their help in making it through the graduate student life.

I also want to express my sincere appreciation to Dr. Ingo Schlupp, Dr. Richard Broughton, and Dr. Ben Smith for their help with statistics, phylogeny, and imaging, respectively. I also am thankful for the important assistance and guidance from Dr. Rosemary Knapp in leading me through all kinds of official regulations in my graduate student life. Thanks to our department staff members, Robbie Stinchcomb, Carol Baylor, George Davis, George Martin, Elizabeth Cooley, Marie Brooks, and Kaye Carter for their help in coordinating my daily activities in the Department of Biology at OU.

Sincere thanks are also to Dr. Cunming Duan (University of Michigan) as well as members in his lab. They have been providing supportive suggestion and recommendation since I applied for graduate school in 2008.

I am lucky to have a number of kind friends, David Chen, Feifei Zhang, Feng Wu, Mingzi Xu, Yue Ban, Zhaozhe Hao, and all my other friends. Special thanks to Mingyan Lin, who initiated my training in bioinformatics. These friends supported me through the graduate program, especially during those tough periods. Many thanks to the badminton club members in OU – weekly badminton practice in these six years has been the best relaxation and refreshment.

It is such a pity that I missed a lot of important events in the lives of my relatives in China. I would like to sincerely appreciate their understanding and support in my career development. Best wishes to the newborn baby.

Last but not least, thanks for the funding granted to R.S.H. from the National Science Foundation (IBN-0344018 and IOS-0744447).

Table of Contents

Dedication iii

Acknowledgements iv

List of Tables viii

List of Figures ix

Abstract xi

Chapter I: Introduction 1

1. Neuropeptides 1

1.1 Neuropeptides and peptidergic neurons 2

1.2 Neuropeptides are widely expressed in nervous system and regulate various behaviors 4

1.3 Neuroendocrine control of wing expansion behavior by bursicon and other neurons 6

2. Neuronal plasticity 7

2.1 Nervous system is highly dynamic 7

2.2 *Drosophila melanogaster* as an excellent model for neuronal remodeling 9

2.3 Signaling pathways that regulate neurite pruning and outgrowth during neuronal remodeling in *Drosophila* 11

2.4 The bursicon neuron as an excellent model system to study neuronal remodeling during metamorphosis. 16

3. Interaction between SHEP and *gypsy* insulator complexes 17

4. Summary 18

Chapter II: The *alan shepard (shep)* gene regulates neuronal remodeling during metamorphosis in *Drosophila melanogaster* 20

Abstract 21

Introduction 22

Materials and Methods 24

Results 32

Discussion 49

Chapter III: A deficiency screen for modifiers of *alan shepard* (*shep*) function in nervous system metamorphosis 100

Abstract 101

Introduction 102

Materials and Methods 104

Results 107

Discussion 122

References 159

List of Tables

Chapter II.

Table 1 Insertion sites, trapped genes, co-localized neuropeptide markers, and mutant phenotypes for insertions obtained through the splice-trap screen 54

Chapter III.

Table 1 The 17 suppressor deficiencies obtained in the *shep* modifier screen 128

Table 2 Progeny lethality of crosses with the tester stock and deficiencies..... 157

Table 3 Progeny lethality of crosses with the tester strain to RNAi strains..... 158

List of Figures

Chapter II.

Figure 1 Co-localization of splice-trap reporter gene expression with PHM 62

Figure 2 *shep* mRNA and protein expression in embryonic and larval stages 64

Figure 3 SHEP is the *Drosophila* ortholog to MSSP 66

Figure 4 Defects following pan-neuronal *shep* RNAi 69

Figure 5 Virgin *shep* mutant females displayed increased rejection of courting 71

Figure 6 Cellular defects in $shep^{BG00836}/shep^{ED210}$ animals 73

Figure 7 Reporter gene expression patterns for the selected 30 insertions 75

Figure 8 Reporter gene expression in CCAP neurons larval CNS 77

Figure 9 Reporter gene expression of *BG00836* and *BG01322* in neurons 79

Figure 10 Selected splice-trap expression patterns containing bursicon neurons 81

Figure 11 Ectopic wing veins and loss of wing sensory neurons in *shep* mutants 83

Figure 12 Embryonic *shep* mRNA and SHEP protein expression patterns 85

Figure 13 Loss of *shep* led to reduced levels of multiple presynaptic markers 87

Figure 14 Loss of *shep* resulted in reduced life span 89

Figure 15 Pan-neuronal loss of *shep* produced larvae that remained in center 91

Figure 16 Loss of SHEP resulted in smaller bursicon neurons in P14 stage pharate adults but not in wandering 3rd instar larvae 93

Figure 17 Bursicon neuron peripheral axon projections and synaptic terminals were visualized by anti-BURS immunostaining or genetic labeling with the membrane-localized fusion protein, mCD8::GFP 95

Figure 18 *shep* promoted outgrowth of the peripheral projections of the bursicon

neurons during metamorphosis..... 97

Video 1 Mounting of an *Oregon R* female by an *Oregon R* virgin male 99

Video 2 Kicking of an *Oregon R* male by a $shep^{BG00836}/shep^{ED210}$ virgin female 99

Video 3 Three-leg grooming by a $shep^{BG00836}/shep^{ED210}$ female after copulation..... 99

Video 4 Two-leg grooming of an *Oregon R* female immediately after copulation 99

Video 5 Expulsion of seminal fluid and the mating plug by a $shep^{BG00836}/shep^{ED210}$ virgin female immediately after copulation 99

Chapter III.

Figure 1 Wing expansion defects and lethality produced by loss of *shep* in peptidergic neurons 132

Figure 2 Loss of *shep* reduced soma area and neurite branching of bursicon neurons at the P14 pharate adult stage 134

Figure 3 Plots of wing expansion scores for all deficiencies 137

Figure 4 Suppression of bursicon neuron phenotypes by selected deficiencies..... 139

Figure 5 Mapping of candidate *shep* suppressor genes by RNAi 141

Figure 6 Suppression of the wing expansion defects and bursicon cellular defects by *Dad* and *Oli* alleles 144

Figure 7 Wing expansion percentages for test crosses with deficiencies..... 146

Figure 8 Wing expansion rates in control crosses with two separate test stocks 149

Figure 9 Bursicon neurons were a subgroup of neurons in the *386-Gal4* pattern..... 151

Figure 10 Suppressor deficiencies did not affect growth or expression of an mCD8::GFP reporter in the B_{AG} neurons at the pharate adult stage 153

Abstract

Peptidergic neurons are a group of neuronal cells that synthesize and secrete peptides to regulate a variety of biological processes. To identify genes controlling the development and function of peptidergic neurons, our lab conducted a screen of 545 splice-trap lines and identified 28 loci that drove expression in peptidergic neurons when crossed to a GFP reporter transgene. Based on these expression pattern results, I selected the *alan shepard* (*shep*) gene for further study since an insertion in *shep* drove expression specifically in most peptidergic neurons. *shep* transcripts and SHEP proteins were detected primarily and broadly in the central nervous system (CNS) in embryos, and this expression continued into the adult stage. Loss of *shep* resulted in late pupal lethality, reduced adult life span, wing expansion defects, uncoordinated adult locomotor activities, rejection of males by virgin females, and reduced neuropil area and reduced levels of multiple pre-synaptic markers throughout the adult CNS. Examination of the bursicon neurons in *shep* mutant pharate adults revealed smaller somata and fewer axonal branches and boutons, and all of these cellular phenotypes were fully rescued by expression of the most abundant wild-type *shep* isoform. In contrast to *shep* mutant animals at the pharate adult stage, *shep* mutant larvae displayed normal bursicon neuron morphologies. Similarly, *shep* mutant adults were uncoordinated and weak, while *shep* mutant larvae displayed largely, though not entirely, normal locomotor behavior. Thus, *shep* played an important role in the metamorphic development of many neurons. To shed light on the molecular mechanisms by which SHEP regulates metamorphic outgrowth of neurons, I conducted a genetic modifier screen for *shep* suppressors. I screened a total of 702 deficiencies

that covered 86% of the euchromatic genes, and isolated 33 deficiencies as candidate suppressors. From this set, I identified 12 deficiencies that partially suppressed the morphological defects seen in *shep* mutant bursicon neurons. RNAi tests and crosses with mutant alleles for individual genes led to the identification of *Daughters against dpp* (*Dad*) and *Olig family* (*Oli*) as *shep* suppressor genes, and both rescued neurites of the bursicon neuron in the subesophageal ganglia. *Oli* encodes a transcription factor with unknown downstream targets. *Dad* encodes an inhibitory Smad protein that inhibits phosphorylation of R-Smad by activated Bone morphogenetic protein (BMP) receptors, thus implicating BMP signaling in the control of neurite outgrowth from the bursicon neurons during metamorphosis. In addition, I found that the *su(Hw)* gene, which encodes a *gypsy* insulator protein that is known to interact with SHEP, suppressed the wing expansion defects caused by loss of *shep*, although I did not observe rescue of bursicon neuron outgrowth by *su(Hw)*. These findings highlight novel genetic interactions that are important for controlling neurite growth in mature, terminally differentiated neurons.

Chapter I: Introduction

1. Neuropeptides

1.1 Neuropeptides and peptidergic neurons

Neurons employ neurotransmitters to communicate with each other and regulate a variety of biological activities in their target cells and tissues. The first known neurotransmitter, acetylcholine, was discovered for its action on heart tissues in 1915 (VOGT 1969), and it was confirmed as a transmitter in 1921 (MCCOY and TAN 2014). In the following decades, many other molecules, such as gamma-aminobutyric acid (GABA), glutamine, and glycine, have been identified for their small molecular sizes and shared mechanisms for signal transduction, and these have been collectively categorized as small molecule transmitters. These small molecule transmitters are released from pre-synaptic active zones through exocytosis, travel tens of nanometers across synapses, and bind receptors to activate or inhibit activities of post-synaptic cells through binding to cell surface receptors (KUO *et al.* 1978; MACDONALD *et al.* 2006). Subsequently, these small molecule transmitters are rapidly degraded, and the products of these degradation reactions are transported back to pre-synaptic cells for recycling (VAN DER KLOOT *et al.* 2000).

In addition to these small molecule transmitters, some large, brain-derived molecules were found to be produced and released by neurons to act on neural and other substrates. Several of these molecules were previously defined as biologically active hormones, such as vasopressin and oxytocin, and their structures—long chains of amino acids—were determined in the middle of the 19th century (DU VIGNEAUD 1953). These large polypeptides were then called neuropeptides. There have been more than 90

mammal genes (DATABASE) and 42 genes in the fruit fly *Drosophila melanogaster* (NASSEL and WINTHER 2010) that have been found to encode neuropeptides. The products of these genes are translated as neuropeptide precursors that then undergo a series of modifications that may include cleavage by endopeptidases and exopeptidases, C-terminal amidation, folding and formation of di-sulfide bonds, phosphorylation, and other chemical modifications to become biologically active and mature neuropeptides. They are stored in large dense core vesicles and transported to synapses and boutons for release in response to appropriate signals (NEWCOMB *et al.* 1985; MCKELVY and WHITE 1987; EIPPER *et al.* 1992). Once released, neuropeptides bind to receptors (most often G protein-coupled receptors) and regulate biological activities in various ways. As the largest and the most diverse group of signaling molecules in the nervous system, these neuropeptides can act as direct transmitters (ANDERSON *et al.* 1988), modulators of other transmitters (YANG and IADAROLA 2006), autocrine or paracrine regulators (JAN and JAN 1982), or distantly regulatory hormones through the circulation (PEABODY *et al.* 2008).

Unlike small molecule transmitters that are rapidly degraded, collected, and locally synthesized for reuse, neuropeptides are rapidly degraded after release and receptor binding, but they are not collected for recycling and synthesis in nerve cell terminals (HENS *et al.* 1998). Neuropeptides are often secreted into the circulation and must travel long distances and overcome dilution in order to send effective signals to target cells. Thus, peptidergic neurons are often characterized by their ability to synthesize and store large amounts of neuropeptides (HEWES *et al.* 2006). Although a number of

groups have been studying the genetic and molecular mechanisms responsible for development of these peptidergic cell-characteristic properties, only a handful of factors that regulate this process have been identified (JIANG *et al.* 2000; HEWES *et al.* 2003; PARK *et al.* 2008; VEVERYTSA and ALLAN 2011).

One of the best known examples of this class of factors is *dimm*, which encodes a basic helix-loop-helix transcription factor and is selectively expressed in both central and peripheral neuroendocrine cells in *Drosophila melanogaster* (HEWES *et al.* 2003). The *dimm* gene is required for the differentiation of many different types of peptidergic neurons, and loss of *dimm* leads to reduced mRNA and protein levels for diverse neuropeptides. More strikingly, over-expression of *dimm* in non-peptidergic neurons is sufficient to induce ectopic peptidergic cell properties, suggesting a fundamental role of *dimm* in the differentiation of these cells (HEWES *et al.* 2003). One of the direct targets of *dimm* is peptidylglycine-alpha-hydroxylating monooxygenase (PHM), an enzyme required for neuropeptide amidation, a feature found in more than 90% of all known insect neuropeptides (JIANG *et al.* 2000; PARK *et al.* 2008). By interacting with three E-boxes within introns of the *Phm* gene, *dimm* controls PHM expression and thus the neurosecretory capacity of peptidergic neurons (PARK *et al.* 2008).

1.2 Neuropeptides are widely expressed in nervous system and regulate various behaviors

Peptidergic neurons are widely distributed in the central nervous system (CNS) and regulate a variety of biological activities, such as growth (JETTE *et al.* 2005),

metabolism (TAYLOR *et al.* 1990), and fertility (CHEE *et al.* 2013). Neuropeptides also play an essential role in the regulation of many behaviors. In mammals, for example, the hypothalamus synthesizes and secretes many neuropeptides, such as orexin, neuropeptide Y, and gonadotropin-inhibitory hormone to regulate feeding and drinking behaviors, sexual behaviors, and social behaviors (STANLEY and LEIBOWITZ 1985; MCCARTHY *et al.* 1991; SAKURAI *et al.* 1998; CHEE *et al.* 2013; UBUKA *et al.* 2014). In addition to the hypothalamus, many other regions of the brain, including the anterior pituitary, posterior pituitary, and amygdala, have also been studied for their expression of neuropeptides and regulation of social, emotional, and depression-related behaviors (BOHUS 1977; CALDWELL *et al.* 2008; TASAN *et al.* 2010). Behavioral regulation by neuropeptides has been studied in diverse animals, and many studies have revealed evolutionarily conserved neuropeptide functions. For example, the melanocortins play a role in metabolism and feeding behaviors in mammals (VERGONI *et al.* 2000), and a similar function of melanocortins has been also identified in chicks and toads (HORN and HORN 1982; SHIRAISHI *et al.* 2008). Another neuropeptide, β-endorphin, regulates feeding behaviors in mammals, birds, and fish (MCKAY *et al.* 1981; DEVICHE and SCHEPERS 1984; DE PEDRO *et al.* 1995).

The fruit fly is a model organism that has been used for over two decades to study neuropeptides and peptidergic neurons (SCHNEIDER and TAGHERT 1990; HEWES *et al.* 1998; JIANG *et al.* 2000; PARK *et al.* 2008; CLYNEN *et al.* 2010; CHEN *et al.* 2014). Most peptidergic neurons are broadly distributed in the brain (often innervating other neurons) and ventral nerve cord (VNC) (often with efferent projections that secrete

neuropeptides into the blood or onto peripheral targets. These neuropeptides regulate diverse biological activities, which include metabolism, growth, circadian rhythms, and many behaviors, such as general locomotion, ecdysis, feeding, and aggression behaviors (PARK *et al.* 2003; LEE and PARK 2004; DIERICK and GREENSPAN 2007; MCNEILL *et al.* 2008; WALKIEWICZ and STERN 2009; HE *et al.* 2013).

1.3 Neuroendocrine control of wing expansion behavior by bursicon neurons and other neurons

One insect neuropeptide with well defined roles in the regulation of behavior is bursicon. Bursicon is one of the larger known neuropeptides, and it exists as a heterodimer of Burs-α and Burs-β glycoprotein subunits (DEWEY *et al.* 2004). Upon secretion in the adult, bursicon initiates post-eclosion cuticle tanning and wing expansion behaviors via its receptor, *rickets* (SUDO *et al*. 2005). Over 20 neurons synthesize and secrete bursicon, and most fall into one of two groups with differing structures and functions (LUAN *et al.* 2006). Two bursicon neurons in the suboesophageal ganglia (B_{SEG}) are required for the wing expansion behaviors, and they also act as commander cells that promote bursicon secretion by 14 additional neurons in the abdominal ganglia (B_{AG}) (PEABODY *et al.* 2008). Loss of the *rickets* receptor in the B_{AG} neurons leads to reduced secretion of bursicon into the hemolymph, suggesting that bursicon from B_{SEG} works as a neuronal modulator to promote the B_{AG} bursicon secretion. Bursicon secreted by B_{AG} neurons enters the hemolymph after eclosion to initiate cuticle tanning and the wing expansion program (LUAN *et al.* 2006; PEABODY *et al.* 2008). Conversely, the forced activation of bursicon neurons is sufficient to initiate

wing expansion (PEABODY *et al.* 2009). Environmental perturbation, such as reduced space, delays the wing expansion after eclosion. Forced activation of bursicon neurons can rescue this delay by promoting wing expansion behaviors (PEABODY *et al.* 2009).

In addition to the bursicon neurons, other undefined neuropeptide-secreting cells have also been implicated in the control of wing expansion. For example, Zhao et al. found genetic manipulations that produce wing expansion defects when they are targeted to broad populations that include both bursicon-positive and bursicon-negative neurons, but the same genetic manipulations in the bursicon neurons alone had no impact on wing expansion (ZHAO *et al.* 2008). This implied that there might be other unknown neuronal circuits that also regulate the wing expansion.

2. Neuronal plasticity

2.1 Nervous system is highly dynamic

Nervous systems undergo anatomical and functional modifications in the context of developmental transitions, learning and memory formation, and in response to environmental changes and injury. These changes can happen on a small scale, such as in the case of synaptic plasticity, or they can happen on a large scale, in some cases involving the entire nervous system. For example, two or more consecutive action potentials can increase synaptic strength within a few milliseconds, due to elevated intracellular Ca^{2+} concentration and Ca^{2+}-dependent transmitter secretion. This stimulus-mediated enhancement of synaptic strength, such as synaptic augmentation and synaptic potentiation, has been well studied at millisecond or second scales

(ECCLES 1983; LLEDO *et al.* 1995; DENG and KLYACHKO 2011). Over longer periods, the modification of synaptic strength can be established through gene expression and last for hours to years. One well-known mechanism for long-term plasticity is seen following repeating stimuli that lead to a persistent increase of protein kinase A (PKA) activity, which in turn activates the transcription factors CREB and C/EBP to promote the addition of more synapses between pre- and post-synaptic neurons. This is also thought to be an important mechanism for learning and memory (ECCLES 1983; KANDEL 2012).

The above examples of neuronal plasticity are often limited to just a few cells, but broad reorganization or remodeling of the nervous system also occurs. This has been intensively studied for neuronal development during various stages such as puberty (SISK and FOSTER 2004), metamorphosis in insects (see below), and neuronal regeneration after injury (CURT *et al.* 2008). This process generally consists of pruning of unnecessary or injured neural structures such as synapses, neurites or neurons, and regrowth of more complex and/or efficient structures to the demands of new functions. Take puberty as an example: The gonadotropin releasing hormone (GnRH) neurons release hormone at the onset of puberty to initiate gametogenesis and hormone secretion from gonads. The gonadal steroid hormones in turn mediate the remodeling of the GnRH neurons in the nervous system to promote the development of sexual motivation and copulatory behaviors in adults (CROWLEY *et al.* 1985; SCHIML and RISSMAN 2000). This remodeling requires the removal of dendritic branches that exist in the early postnatal stages, and the outgrowth of new and adult specific dendritic spines of the

GnRH neurons (COTTRELL *et al.* 2006). A similar remodeling process happens to many other neurons to complete the transition from juvenile to adult (WRAY and HOFFMAN 1986; NUNEZ *et al.* 2002).

2.2 *Drosophila melanogaster* as an excellent model for neuronal remodeling

Nervous systems of holometabolism insects undergo substantial modifications during metamorphosis. An important genetic model of this process is the metamorphosis of the nervous system of the fruit fly *Drosophila melanogaster* as the organism transitions through metamorphosis from a crawling worm into a flying insect. During this process, many neurons prune away larva-specific neurites, migrate into new locations, and grow adult-specific neurites. This process is known as neuronal remodeling (BROWN 2007), and it has been well characterized for a number of different types of neurons, thus allowing people to comprehensively study the mechanisms of neuronal remodeling.

The mushroom body (MB) neurons are one of the best examples of metamorphic remodeling. They consist of three different types of cells: γ, αβ and α'β' neurons (LEE *et al.* 1999). The γ neurons are born in the larval stages with clustered dendrite branches and bifurcated axonal projections, and these are the only class of MB cells that undergo neuronal remodeling during metamorphosis. Most dendritic and axonal neurites of the γ neurons are pruned between 4-8 h and 12-18 h, respectively, after puparium formation (APF), and adult specific neurites regrow by 24 h APF (LEE *et al.* 1999; ZHU *et al.* 2003). With mosaic analysis with a repressible cell marker (MARCM), it is possible to monitor the development and remodeling of single MB

neurons during metamorphosis, therefore enabling studies of the regulation of neuronal remodeling with detailed timing and high resolution (LEE *et al.* 2000). Another well-documented instance of remodeling is seen in the ddaC neurons, which are a group of sensory neurons along the larval body wall. Exuberant dendrites of ddaC neurons start breaking between 5 to 12 h APF, and these dendrites are completely removed by 16 to 18 h APF, while the axons and somata remain largely intact. Adult specific dendrites complete growth by ~24 h APF (KUO *et al.* 2005; WILLIAMS and TRUMAN 2005a; BOULANGER and DURA 2014). A number of other types of *Drosophila* neurons also undergo well documented metamorphic remodeling. These include the Tv neurons (BROWN *et al.* 2006), motorneurons (LIU *et al.* 2010), and olfactory circuits (MARIN *et al.* 2005). All of these finely defined remodeling processes provide excellent models to study neuronal remodeling.

In addition to a well-characterized nervous system, fruit flies provide many advantages over other species for studying neuronal remodeling. They have high fertility and can provide hundreds of progeny within just two weeks, and they have relatively low requirements for space and food sources, as compared to other model organisms such as mice (XIAO *et al.* 2003). The powerful GAL4-UAS binary system and its variants enable genetic manipulation in either all neurons or single neurons (DUFFY 2002). Plus, it is possible to activate or inactivate these genetic manipulations with temperature/ligand-dependent stimuli, and create transgenic flies of interest commercially within two months. Together, these convenient tools and advantages

make *Drosophila* ideal for molecular genetic studies of the mechanisms governing long-term neuronal plasticity.

2.3 Signaling pathways that regulate neurite pruning and outgrowth during neuronal remodeling in *Drosophila*

A number of signaling pathways are known to regulate neuronal remodeling during insect metamorphosis. Among them, ecdysone signaling plays a central role. Ecdysone signaling regulates developmental timing of molts and ecdysis, the molting behaviors used to shed the old cuticle at the end of each molt (TRUMAN 1996). Before each larval and pupal ecdysis, the primary active steroid hormone, 20-hydroxyecdysone (ecdysone) acts as a molting hormone to promote larva-larva or larva-adult transitions (TRUMAN 1996). Most of the effects of ecdysone are mediated by its binding to heterodimeric nuclear receptors, consisting of the ecdysone receptor (EcR) and Ultraspiracle (USP), the *Drosophila* homolog of the vertebrate RXR proteins. The ecdysone-EcR-USP complex binds to specific DNA elements to manipulate expression of early genes, which include *Broad-Complex* (*BR-C)*, *E74*, *E75*, and *E93* (WOODARD *et al.* 1994; THUMMEL 2001b). These early genes encode transcription factors and regulate the expression of late genes that are thought to have more direct effects on metamorphosis. These late genes, which include glue genes, L71 genes, *reaper*, and *hid*, play important roles in puparation, metamorphic growth and programmed cell death during metamorphosis (THUMMEL 2001a).

In the nervous system of *Drosophila*, expression of these key regulators may contribute to the differential responses of neurons to 20-hydroxyecdysone in the context of remodeling. For example, the *EcR* gene encodes three different ecdysone receptor isoforms, EcR-A, EcR-B1, and EcR-B2. The expression of EcR-A is strong in larval neurons that undergo programmed cell death during metamorphosis, whereas the expression of EcR-B1 is detected in those neurons undergoing remodeling to perform new, adult-specific functions (ROBINOW *et al.* 1993; TRUMAN 1996; SCHUBIGER *et al.* 1998). This cell-type specific expression of EcR-B1 implied involvement of EcR-B1 in the regulation of neuronal remodeling.

At least three signaling pathways have been identified to regulate the expression of EcR-B1 to control metamorphic neuronal pruning. The first discovered regulator of EcR-B1 expression was TGF-β signaling (ZHENG *et al.* 2003). TGF-β receptors on the cell membrane are activated by secreted ligands, and these activated receptors phosphorylate intracellular target proteins, which then travel into nuclei and function as transcription factors to regulate expression of various genes (HUANG and CHEN 2012). In MB γ neurons, myoglianin ligands that are secreted by glia cells activate the TGF-β receptors, which in turn up-regulate the expression of EcR-B1. Loss of myoglianin leads to decreased EcR-B1 expression and results in pruning defects in the neurites of γ neurons (ZHENG *et al.* 2003; AWASAKI *et al.* 2011; YU *et al.* 2013).

The second category of factors known to regulate the expression of EcR-B1 includes the ecdysone-responsive transcription factors, FTZ-F1 and HR39. During metamorphic

remodeling of the MB γ neurons, FTZ-F1 activates the expression of EcR-B1 by directly binding to the EcR-B1 locus (BOULANGER *et al.* 2011). Loss of FTZ-F1 leads to down-regulated expression of EcR-B1, and consequently defects of the remodeling of MB γ neurons (BOULANGER *et al.* 2011). Suppression on HR39 activities is required for normal remodeling of MB γ neurons. Artificial overexpression of HR39 leads to reduction of EcR-B1 expression, and inhibits the neuronal pruning of the MB γ neurons (DURA *et al.* 2009; BOULANGER *et al.* 2011).

The third known factor known to regulate EcR-B1 during neuronal pruning is cohesin, which controls cohesion of sister chromatids during meiosis (NASMYTH 2005). The cohesin complex binds directly to the EcR-B1 locus and positively regulates the expression of EcR-B1, which is required for neurite pruning during metamorphosis (MISULOVIN *et al.* 2008; SCHULDINER *et al.* 2008). Overexpression of EcR-B1 rescues pruning defects seen in γ neuron axons of cohesin complex gene ($SMC1^{-/-}$) mutants, suggesting transcriptional regulation of EcR-B1 by cohesin signaling (SCHULDINER *et al.* 2008).

A number of EcR-B1 targets have also been identified for their roles in metamorphic neuronal pruning. Loss of EcR-B1 blocks expression of *Sox14*, suggesting that this known ecdysone-responsive transcription factor is an EcR-B1 target (OSTERLOH and FREEMAN 2009). Loss of *Sox14* disrupts neurite pruning in both ddaC neurons and MB γ neurons, and overexpression of *Sox14* results in pre-mature neurite pruning in ddaC neurons. Thus, *Sox14* is necessary and sufficient to induce neurite pruning (KIRILLY *et*

al. 2009; RITTER and BECKSTEAD 2010). The chromatin remodeler *brahma* (*brm*) and a CREB binding protein (CBP) with histone acetyltransferase (HAT) activity are known as coactivators of EcR-B1 to regulate the expression of *Sox14* (KIRILLY *et al.* 2011). In response to ecdysone, BRM promotes the formation of an EcR-CBP complex, which leads to acetylation of histone H3 at the *Sox14* locus. These three factors interact to coordinately establish a transcriptionally active chromatin state, allowing the expression of their common target, *Sox14* (KIRILLY *et al.* 2011). Two independent targets of *Sox14*, *Mical* and *Cullin1*, have been found to regulate neurite pruning (KIRILLY *et al.* 2009; WONG *et al.* 2013). *Cullin1* mediates inactivation of TOR pathway through ubiquitin ligase activity to regulate neurite pruning of the ddaC neurons (WONG *et al.* 2013). This action is independent from the other *Sox14* target, *Mical*, loss of which blocks neurite pruning in the ddaC neurons, but not the MB γ neurons (KIRILLY *et al.* 2009). These findings suggest that *Sox14* serves as a target of EcR-B1 to promote neurite pruning by regulating the expression of *Mical* and *Cullin1* in specific neurons (KIRILLY *et al.* 2009; OSTERLOH and FREEMAN 2009).

Up-regulation of the ubiquitin proteasome system (UPS) and of an RNA binding protein, BOULE, has also been found in EcR-B1 mutant MB γ neurons (HOOPFER *et al.* 2008). BOULE is an evolutionarily conserved protein required for spermatogenesis in both flies and vertebrates. A reduction in the expression of BOULE is necessary to allow the initiation of MB γ neurite pruning, and forced expression of BOULE is sufficient to inhibit this process (HOOPFER *et al.* 2008). Therefore, EcR-B1 may also regulate neurite pruning through these candidate target genes.

In addition to pruning, ecdysone signaling is also known to regulate metamorphic neuronal outgrowth. *Kruppel-homolog 1* (*Kr-h1*) encodes a zinc-finger transcription factor that interacts with ecdysone-regulated transcriptional pathways (SHI *et al.* 2007). The expression of *Kr-h1* requires USP, and in turn it regulates the expression pattern of EcR-B1 in the late larval CNS. The expression of *Kr-h1* drops during early metamorphosis, and forced overexpression of *Kr-h1* reduces neurite outgrowth in the MB neurons, while the loss of *Kr-h1* does not lead to any obvious phenotype. Therefore, *Kr-h1* coordinates ecdysone signaling during metamorphic neuronal outgrowth (SHI *et al.* 2007; HEWES 2008).

Apart from ecdysone, there are other signals that are known to regulate metamorphic neuronal remodeling. For instance, inhibition of valosin-containing protein (VCP), a ubiquitin-selective AAA chaperone, interrupts dendritic pruning and leads to cell apoptosis in *Drosophila* da neurons (RUMPF *et al.* 2011). Wnt signaling proteins regulate dendritic remodeling and the shape of olfactory circuits (CHIANG *et al.* 2009; SINGH *et al.* 2010). An orphan nuclear receptor, UNF, promotes MB neurite outgrowth during metamorphosis through activation of TOR signaling (YANIV *et al.* 2012).

In spite of all these findings, the molecular and genetic mechanisms of neuronal remodeling—particularly the outgrowth phase—remain poorly understood. Even less is known about the metamorphosis of important neuroendocrine systems, although several reports have focused on remodeling of peptidergic neurons. The Tv neurons (thoracic ventral neurosecretory cells) undergo remodeling, and ecdysone signaling through EcR

regulates both pruning and outgrowth of the Tv neurons, although no downstream effectors have been identified (BROWN *et al.* 2006; BROWN 2007). Another example of identified signaling that regulates remodeling of peptidergic neurons is the insulin/insulin-like growth factor pathway. Loss of receptors of the insulin/insulin-like growth factor leads to outgrowth defects of CCAP/bursicon neurons, leaving larval CCAP/bursicon neurons largely normal (GU *et al.* 2014).

2.4 The bursicon neuron as an excellent model system to study neuronal remodeling during metamorphosis.

The bursicon neurons are a group of neurons in the CNS that secrete bursicon, CCAP and MiP neuropeptides to regulate wing expansion, cuticle tanning and heart contractions in *Drosophila* (DULCIS *et al.* 2005; PEABODY *et al.* 2008; LOVEALL and DEITCHER 2010; VEVERYTSA and ALLAN 2011). There are about ~30 neurons expressing bursicon peptides in the 3rd larval instar ventral nerve cord (VNC) (PEABODY *et al.* 2008; LOVEALL and DEITCHER 2010). These neurons send projections to muscles along the body wall (CHEN *et al.* 2014; GU *et al.* 2014). During metamorphosis, these neurons prune their peripheral projections, relocate their cell bodies (which grow more than two-fold in size) to the distal tip of the VNC, and grow adult-specific and highly branched axonal projections (ZHAO *et al.* 2008). Along these projections, numerous *en passant* boutons (neuropeptide releasing sites) form during metamorphosis and secrete bursicon into the circulating system to promote post-eclosion wing expansion behaviors and cuticle tanning (PEABODY *et al.* 2008). At the time of adult emergence, only 16 of those ~30 neurons prominently express bursicon (ZHAO *et al.* 2008; CHEN *et al.* 2014).

These dramatic changes of morphology during metamorphosis, and the obvious wing expansion defects caused by disrupted development of function of the bursicon neurons, make them excellent models for the study of metamorphic neuronal remodeling through large-scale genetic screens.

3. Interaction between SHEP and *gypsy* insulator complexes

The *alan shepard* (*shep*) gene is predicted to encode RNA/DNA binding proteins, and it is required for neuronal remodeling during metamorphosis in *Drosophila* (CHEN *et al.* 2014). Loss of *shep* leads to locomotion defects, reduced neuropil areas, smaller neuron soma sizes, and fewer neurite branches. Strikingly, these phenotypes are mostly detected in the adult, and mutant larvae are largely normal (see Chapter II).

The only factors previously known to interact with SHEP are two insulator proteins, Suppressor of Hairy Wings [SU(HW)] and modifier of mdg4 [MOD(MDG4)]. SHEP binds to these two proteins and suppresses their insulator activity specifically within nervous system (MATZAT *et al.* 2012). Insulators are DNA sequences that serve as docking sites to recruit insulator proteins, and these proteins could further interact with each other to form insulator complexes in both vertebrate and invertebrates. These insulator complexes regulate gene expression by interfering with enhancer-promoter interactions or by protecting gene regions from silencing by spreading heterochromatin (BARKESS and WEST 2012). One of the most thoroughly studied insulators is *gypsy*, which is an enhancer-blocking insulator. Insertion of each *gypsy* insulator into the genome provides a set of 12 binding sites for SU(HW) (ADRYAN *et al.* 2007), which in

turn recruit two other insulator proteins, MOD(MDG4) and centrosomal protein 190kD (CP190), to form functional insulators (KARAKOZOVA *et al.* 2004; PAI *et al.* 2004). The *gypsy* insulator has been studied for its enhancer blocking activity for the *yellow* and *cut* genes, which are required for pigmentation and wing-margin sensory organ specification, respectively. Insertion of *gypsy* insulators between enhancers and promoters of these two genes blocks enhancer function, therefore leading to loss of cuticle pigmentation and misshaped wing margins (MELNIKOVA *et al.* 2002; KRUPP *et al.* 2005). The extent of these phenotypes has been employed as indicators of insulator activities to study insulator signaling (ROY *et al.* 2011; MATZAT *et al.* 2012).

Given the CNS-specific interactions between SHEP and insulator proteins and the *shep* regulation of neuronal remodeling, it is very likely that *shep* regulates neuronal development through the regulation of insulator activities.

4. Summary

Neuropeptides are important signaling molecules that regulate many biological phenomena such as development, physiology, and behavior. There are more than 100 known neuropeptides, and we have a good general understanding of the process involved in their synthesis, secretion, signaling transduction, and biological functions across many different species.

However, apart from several key regulators, we know very little about the mechanisms governing the development of peptidergic cell-specific properties. Furthermore, in spite

of what is known from a handful of recent studies on the metamorphic pruning of the MB neurons and ddaC neurons, the processes controlling metamorphic outgrowth, and controlling peptidergic neuron remodeling in general, are not well understood. Here, my goal was to identify genes that help to build peptidergic neuron identity. During differentiation, which genes are required for the development of peptidergic neuron capacity to synthesize and secrete neuropeptides? During subsequent development, which factors govern metamorphic development of these neurons? In Chapter II, I followed up on a splice-trap screen that sought genes that are expressed in peptidergic neurons, and studied *alan shepard* (*shep*) for its role in neuronal remodeling during metamorphosis. In Chapter III, I conducted a modifier screen to identify *shep*-interacting genes that regulate the outgrowth of peptidergic neurons during metamorphosis. My findings identified a gene, *shep*, that regulates neuronal remodeling and determined genetic mechanisms through which *shep* regulates the development of peptidergic neurons.

Chapter II: The *alan shepard* (*shep*) gene regulates neuronal remodeling during metamorphosis in *Drosophila melanogaster*

This chapter was published as D. Chen, Qu, C., & Hewes, R.S. (2014). Neuronal remodeling during metamorphosis is regulated by the *alan shepard* (*shep*) gene in *Drosophila melanogaster*. *Genetics*, 197(4):1267-1283.

Abstract

Peptidergic neurons are a group of neuronal cells that synthesize and secrete peptides to regulate a variety of biological processes. To identify genes controlling the development and function of peptidergic neurons, a previous graduate student in our lab, Chunjing Qu, conducted a screen of 545 splice-trap lines and identified 28 loci that drove expression in peptidergic neurons when crossed to a GFP reporter transgene. Among these lines, an insertion in the *alan shepard* (*shep*) gene drove expression specifically in most peptidergic neurons. *shep* transcripts and SHEP proteins were detected primarily and broadly in the central nervous system (CNS) in embryos, and this expression continued into the adult stage. Loss of *shep* resulted in late pupal lethality, reduced adult life span, wing expansion defects, uncoordinated adult locomotor activities, rejection of males by virgin females, and reduced neuropil area and reduced levels of multiple pre-synaptic markers throughout the adult CNS. Examination of the bursicon neurons in *shep* mutant pharate adults revealed smaller somata and fewer axonal branches and boutons, and all of these cellular phenotypes were fully rescued by expression of the most abundant wild-type *shep* isoform. In contrast to *shep* mutant animals at the pharate adult stage, *shep* mutant larvae displayed normal bursicon neuron morphologies. Similarly, *shep* mutant adults were uncoordinated and weak, while *shep* mutant larvae displayed largely, though not entirely, normal locomotor behavior. Thus, *shep* played an important role in the metamorphic development of many neurons.

Introduction

Peptidergic neurons produce small peptides, called neuropeptides, which are secreted within the nervous system to influence the activity of other neurons or into the blood to act on other tissues. Through these targets, neuropeptides regulate a wide range of processes, which include development, feeding, growth, aggression, reproduction and learning and memory (McShane *et al.* 1992; Park *et al.* 2003; Luquet *et al.* 2005; Crown *et al.* 2007; Nephew *et al.* 2009; Slaidina *et al.* 2009; Goncalves *et al.* 2012).

One of the first genes identified to play a specific role in the development of peptidergic neurons was *dimmed* (*dimm*), which encodes a basic helix-loop-helix transcription factor that is required for the differentiation of diverse peptidergic neurons (Hewes *et al.* 2003; Park *et al.* 2008; Hamanaka *et al.* 2010). DIMM is a key regulator of expression of the neuropeptide biosynthetic enzyme, peptidylglycine-alphahydroxylating monooxygenase (PHM) (Park *et al.* 2008), and it promotes the differentiation of neurosecretory properties in many neurons (Hamanaka *et al.* 2010). Both DIMM and PHM are expressed widely and specifically in peptidergic neurons (Michaud *et al.* 1998; Acampora *et al.* 1999; Jiang *et al.* 2000; Hewes *et al.* 2003). In fact, DIMM was first identified by virtue of its pattern of peptidergic neuron expression through an enhancer-trap screen (Hewes *et al.* 2003). Similar expression pattern-based strategies may be useful for identification of other factors critical for peptidergic neuron development.

In this current study, we sought to identify similar factors through a splice-trap screen for genes with peptidergic cell-specific expression patterns. Chunjing Qu identified 28 insertions with different patterns of peptidergic cell reporter gene expression, driven by *P* element splice-trap insertions in specific loci. These insertions drove reporter expression in insulin-like peptide 2 (ILP2), crustacean cardioactive peptide (CCAP)/bursicon, -RFamide, Furin 1, and leucokinin (LK) cells and often caused defects typical of disrupted neuropeptide signaling. Thus, all 28 of these genes are strong candidate regulators of peptidergic cell development or function.

We mapped one of the splice-trap insertions to an exon of the *alan shepard* (*shep*) gene, and I chose this insertion for further analysis because it displayed an expression pattern that was highly similar to PHM and DIMM. *shep in situ* hybridization and anti-SHEP immunostaining later revealed that both the *shep* mRNA and SHEP protein expression is enriched in most neurons, yet *shep* mutants displayed defects in adult eclosion and wing expansion that suggested specific disruptions in signaling by bursicon and other neuropeptides. Consistent with these behavioral phenotypes, the *shep* mutant bursicon neurons had smaller somata, fewer axon branches, and smaller and fewer neuroendocrine boutons, and all of these phenotypes were rescued by expression of a wild-type *shep* cDNA. Interestingly, pan-neuronal RNA interference to *shep* produced smaller CNS neuropils and defects in general locomotor behaviors, such as flipping and climbing. Most of the locomotor phenotypes were restricted to the adult stage, and the effects of *shep* mutations on neuronal growth were restricted to pupal development.

Thus, *shep* regulates metamorphic growth of the bursicon neurons, and it may also serve as a general regulator of neuronal growth during metamorphic remodeling.

Materials and methods

Stocks: *Drosophila melanogaster* stocks and crosses were cultured on standard cornmeal–yeast–agar media at 25°. We obtained splice-trap strains, deficiency strains and *Gal4* strains from the Bloomington *Drosophila* Stock Center. I used three *shep* deficiencies: *Df(3L)ED210* (FBab0035327), *Df(3L)Exel6104* (FBab0038124) and *Df(3L)Exel6103* (FBab0038123). The *Gal4* lines used were *386-Gal4* (FBti0020938) (BANTIGNIES *et al.* 2000), *en-Gal4* (FOX *et al.* 2010), *D42-Gal4* (YEH *et al.* 1995), *elav-Gal4* (FBti0002575) (SHAKIRYANOVA *et al.* 2005), and *ccap-Gal4* (FBti0037998) (PARK *et al.* 2003) . The *UAS-shep-RNAi* stock was obtained from the Vienna *Drosophila* RNAi Center (w^{1118}*; P{GD5125v37863}*; FBst0462204).

EST sequence verification: I randomly selected six *shep* EST clones that shared the 5' end represented by isoforms RE, RH and RI and amplified them with forward primer 5'-GCCGAATTCTGAGCAACACGACGAACAC-3' and reverse primer 5'-CGCAGATCTTGGCTTTTCCGCTTCTC-3'. Subsequent sequencing of each EST clone for the RE isoform-specific sequence 'CAACAG' in exon 13 (FBgn0052423:13) was done with the forward primer in order to distinguish RE from RH and RI.

***UAS-shep*:** A *shep-RE/RG* isoform cDNA was generated from a male wild-type fly (*Oregon R*) by RT-PCR with forward primer 5'-

GCCGAATTCTGAGCAACACGACGAACAC-3' and reverse primer 5'-CGCAGATCTTGGCTTTTCCGCTTCTC-3'. The cDNA was inserted into pUAST between the *Eco*RI and *Bgl*II sites in the polylinker and transformed into DH5α *E. coli*, and a single transformant colony was selected for sequence verification. The forward primer 5'-GCCGAATTCTGAGCAACACGACGAACAC-3' was used to check for the sequence 'GTGGGTATCTGGGTGCTTCATAGGCCGGCCATTCAACAG' in exon 14 (FBgn0052423:14) and sequence 'AAAGGT', which spans exons 14 and 16 (FBgn0052423:16), to rule out isoforms RA, RB, RD, RF, RH, and RI. Thus, the clone represents either *shep-RE* or *shep-RG*, which are identical throughout the region amplified for cDNA cloning. These primers and a third primer 5'-CCTGCTGGTTAAGTTTGCCGATGGCG-3' were used to sequence verify all of the cDNA coding sequence except the first 29 bp at the 5' end. The pUAST construct was injected into embryos by BestGene (Chino Hills, CA) to obtain *UAS-shep-RE/RG* insertions on the second chromosome.

Splice-trap expression patterns: Each splice-trap line was crossed with *UAS-mCD8::GFP*, and the 3rd instar larvae were collected and examined under a compound epifluorescence microscope without dissection. Larvae with CNS expression were dissected in Ca^{2+} free saline solution [182 mM KCl, 46 mM NaCl, 2.3 mM $MgCl_2 \cdot 6H_2O$, 10 mM 2-Amino-2-(hydroxymethyl) propane-1, 3-diol (Tris), pH=7.2], and processed for immunostaining.

Immunostaining: Immunostaining was performed as previously described (HEWES *et al.* 2003). After dissection in Ca^{2+}-free saline, tissues were fixed for 1 hr in 4% paraformaldehyde (PFA), 4% paraformaldehyde with 7% picric acid (PFA/PA), or Bouin's fixative. I used antibodies against the following proteins: Bursicon α-subunit (1:5000, PFA/PA) (LUAN *et al.* 2006), PHM (1:750, Bouin's) (JIANG *et al.* 2000), LK (1:500, PFA/PA), ILP2 (1:50, PFA/PA), Furin 1 (1:1000, Bouin's), -RFamide (PT2 antiserum) (1:2000, PFA/PA), SHEP (1:1000, PFA/PA) (provided by K. Beckingham, Rice University), Choline Acetyltransferase (1:100, PFA) (Developmental Studies Hybridoma Bank, DSHB, Iowa City, Iowa), Synapsin (1:20, PFA) (DSHB), Bruchpilot (1:20, PFA) (DSHB) and green fluorescent protein (GFP) (1:500, PFA) (Invitrogen, Carlsbad, CA). Secondary antibodies conjugated with Cy3 or ALEXA 488 from goat, mouse and rat were each used at a 1:500 dilution. After incubation for 30 min in 70% glycerol, tissues were mounted in Vectashield (Vector Labs, Burlingame, CA), and confocal z-series projections were obtained with an Olympus (Center Valley, PA) Fluoview FV500 confocal microscope. For the isolated adult CNS images in Figure 4, I mounted the tissues between two cover slips and imaged from both sides; one of each pair of images was flipped horizontally and merged with the image from the other side in Adobe Photoshop (San Jose, CA) for better resolution of deep structures.

Immunostaining quantification: Cells and projections were imaged as confocal z-series scans, and identical settings were used in parallel for all of the samples in each experiment. Neuropil and soma areas were measured with Adobe Photoshop by manually tracing the structures and counting the bordered pixels on 2D maximum

intensity projection images. For the larval stage, I measured the area of the more intensely immunostained bursicon neuron on the left side of abdominal segments 1-6 (A1-A6)—these cells survive through metamorphosis into the adult stage (ZHAO *et al.* 2008). When the cells could not be clearly distinguished from each other (e.g., due to close apposition), I substituted the cell from the right side in the same segment. The soma area for all six cells was then averaged to obtain a single value for each preparation. For the pharate adult stage, I measured the average soma area of the six most anterior bursicon neurons in the abdominal ganglia; preparations in which these six neurons could not be clearly delineated in the images (e.g., due to physical juxtaposition of the cells) were discarded. Axonal branches of the bursicon cells were counted in Adobe Illustrator by Sholl analysis (MILOSEVIC and RISTANOVIC 2007) after overlaying a grid of nested, concentric circles, each with a radius 50 μm larger than the previous circle, over the image. In order to measure the size of boutons within the axon projections of pharate adult bursicon neurons, I obtained confocal images (2D projections of z-series stacks) of the first left branch of the bursicon neuron axons within the abdominal nerve from the 2nd abdominal segment (Ab_2Nv) (DEMEREC 1994). To ensure imaging of any more faintly immunostained boutons, the photomultiplier voltage was set to a level at which the centers of some boutons were saturated. I used the inversion and threshold functions in Adobe Photoshop (with the same threshold of 170 for all images) to convert the background to white and all remaining pixels, which were the boutons, to black. Boutons located within 50 μm distal and proximal of the first left branch in the Ab_2Nv were traced manually in Photoshop to obtain a count of the number of pixels, or cross-sectional area, for each bouton. For the quantification of

wandering 3rd instar larval bouton areas, I applied a similar strategy for the bursicon cell neuromuscular junctions (NMJs) on muscles 12-13 of the 2nd abdominal segment.

***In situ* hybridization:** I used sense probe primer 5'-CGCGAATTCGCTTTGCCCGCATGGAGAGT-3' and anti-sense primer 5'-GCGTCTAGAACCTGAGTCATCATGTAACCCGGAAT-3' to demonstrate the expression pattern of *shep*. Single-strand DNA probes were amplified and labeled with digoxigenin by PCR, and *in situ* hybridization was conducted with probes at a 1:100 dilution using a previously described protocol (HEWES *et al.* 2003). For *in situ* hybridization on embryos, collections of embryos were made from apple juice-agarose plates every 24 hr.

Longevity assays under fed and starved conditions: For fed condition treatments, six vials each containing ten 3-5 day old mated female flies were maintained at 25° and flipped to fresh food every day. The number of dead flies in each vial was scored every morning. For the starved condition, three to six vials of ten 1-2 day old mated female flies of each genotype were maintained at 25° in vials with 1% agarose, which supplied water but no nutrients. Flies were scored every 3-4 hr from 8:00 am to midnight, and the morning 8:00 am count represented an 8 hr collection.

Flipping behavior assays: Larvae were placed on their backs on a piece of tissue that was soaked with 200 µl of phosphate buffered saline (PBS, 137 mM NaCl, 2.7 mM KCl, 10 mM Na_2HPO_4 and 1.8 mM KH_2PO_4) and set upon an apple juice-agarose plate,

and the time required for each larva to right itself (so that the ventral surface was in contact with the tissue) was measured. Five measurements were obtained for each larva. For adults, the wings were removed and flies were allowed two hours to recover from the CO_2 anesthesia. Flies were placed individually in a 10 cm petri dish, which was tapped to flip each fly onto its back, and then the time for the fly to right itself was measured. Three trials were performed to obtain an average value for that fly; the n for each experiment indicates the number of animals tested.

Larval crawling behavior assay: I divided 100 mm plastic petri dishes evenly (by radius) into four concentric zones, numbered 1-4 from the center to the periphery. Dishes were filled with apple juice-agarose, and a thin layer of 200 µl PBS buffer solution was applied to the surface immediately prior to the assay. Each larva was placed into the center of zone 1 (center of the dish), and I recorded the total time the larva spent in each zone over a 10-min period.

Locomotor activity assays: Larval locomotor activity was scored on apple juice-agarose plates with a thin layer of PBS (200 µl) on the surface. Larvae were placed in the center of the plate and were allowed 2 min to acclimate. After that, I immediately began tracing the trail of the larva on the petri dish lid (viewed from directly above the plate) for 5 min. The trail of each larva was then placed on a square grid pattern (the side of each square was 6.35 mm), and I counted the number of squares traversed, counting squares more than once if the larva doubled back over a previous area. For the adult stage, flies were individually placed in an empty plastic vial that was vertically

marked at 1 cm intervals. Flies were allowed to climb along the vial wall, and the maximum height attained in five seconds was recorded. If flies fell off the side of the vial during the trial, the highest point attained was counted (rounding to the closest cm mark). If flies started climbing but failed to reach the first 1 cm mark, their maximum height attained was scored as 1 cm. Flies that did not climb during the test (approximately 10% of the experimental group and none of the controls) were discarded.

Phylogenetic and sequence analysis: BLASTP searches with SHEP isoform PE were performed at NCBI (ALTSCHUL *et al.* 1997; ALTSCHUL *et al.* 2005) and Flybase (http://flybase.org/blast/) to obtain the top annotated vertebrate matches (domain similarity >=50%, non-redundant, precalculated data version: cdd.v.3.10, database: cdsearch/cdd, E-value threshold: 0.01) and single representatives of each of the top three *Drosophila* protein family hits, respectively. The RNA recognition motif sequences of SHEP isoform PE, the vertebrate BLASTP matches, the *Drosophila* BLASTP matches and their vertebrate homologs, and two *Drosophila* outgroup RNA binding proteins were aligned and used to build a neighbor-joining phylogenetic tree in MEGA5 (BAINBRIDGE and BOWNES 1981a). Total percentage identity was calculated with LALIGN (HUANG and MILLER 1991), and the percentage identity for specific motifs was calculated using the NCBI BLASTP server. The sequence accession numbers for the proteins in the analysis were as follows: hMSSP-2, human MSSP-2 (*c-myc* single strand binding protein 2) (NM002898); xMSSP-2, *Xenopus laevis* MSSP-2 (NM001086938); heMSSP-2, *Heterocephalus glaber* MSSP-2 (EHB06530); rMSSP-2,

Rattus norvegicus MSSP-2 (NP001020574); mMSSP-2a, *Mus musculus* MSSP-2a (NP062685); zELAV-like 2, *Danio rerio* ELAV-like protein 2 (NM001002172); hRBP-PH, human RBP-PH (AAA69698); RBP9-PH, *Drosophila melanogaster* RBP9-PH (FBti0114122); FNE-PB, *Drosophila melanogaster* FNE-PB (FBpp0112400); hELAV, human ELAV (NP001410).

Mating behavior assay: All male and female flies for mating behavior assays were collected as isolated pharate adult pupae and were tested 3-5 days after eclosion. *Oregon R* was used as the wild-type control. Video-recordings were obtained with a Sony DCR-SX45 camcorder, and they were stopped 10 min after copulation was completed (the recording in Video 5 was obtained by using an iPhone 4 to capture the monitor screen display obtained with a Sony ExwaveHAD camera on an Olympus SZX12 microscope). Flies that failed to initiate copulation within 30 min were discarded. Copulation latency was measured as the time required for the pair of flies to begin copulation. Mount latency was the time it took for the male to climb onto the back of the female (with both of the male's prothoracic legs clasping the base of the female's wings) after copulation started. The kicking index was calculated as the fraction of time the female spent kicking the male with her metathoracic legs during copulation. Grooming index was defined as the fraction of time the female spent grooming during the 10 min recording window after copulation. Some of the experimental flies displayed an unusual 3-leg grooming behavior in which they rubbed both of the metathoracic legs together with one of the mesothoracic legs. The 3-leg

grooming index was calculated as the fraction of time each female fly spent performing this behavior out of the total time spent grooming during the recording window.

Statistics: All statistical tests were performed in SPSS 20.0 (IBM, Armonk, NY). Tukey HSD was used for all ANOVA post-hoc tests. Statistical significance was indicated as $*P<0.05$, $**P<0.01$, $***P<0.001$.

Results

Screen for loci with peptidergic neuron expression: Chunjing Qu conducted a screen of 545 splice-trap insertion strains to identify genes with expression that was enriched in or specific to peptidergic neurons. Each splice-trap strain contained a *P* element insertion with a *Gal4*-encoding exon that may be joined through alternative splicing with exons from a native gene into which the *P* element is inserted. *Gal4* is therefore expressed in a pattern driven by the native gene (LUKACSOVICH *et al.* 2001). Chunjing Qu used these lines to drive expression of membrane tagged GFP (*UAS-mCD8::GFP*) to identify 38 insertions with reporter gene expression in the central nervous system (CNS) of 3rd instar larvae. Although this set yielded useful lines (below) and we therefore did not perform further screening, the number of insertions with CNS expression was unexpectedly low, given the large number of genes expressed in selected CNS cells (cf., BERGER *et al.* 2012; FONTANA and CREWS 2012). Two factors may have contributed to this low recovery rate: our live larval screening method, in which weaker CNS expression may have been missed, and the observation that 12-52%

of splice-trap insertion sites with this vector (the rates co-vary with eye color) result in no detectable Gal4 activity (LUKACSOVICH *et al.* 2001).

Thirty of these insertions drove expression in neurons (Figure 7), and these were retained for further analysis. The other eight insertions drove expression in putative glia, ring gland cells, and/or neurites of undefined origin (data not shown) and were discarded. To identify insertions with expression in peptidergic neurons, Chunjing Qu performed immunostaining for PHM in the 30 lines with expression of mCD8::GFP in CNS neurons. The PHM enzyme is required for amidation of most insect neuropeptides (JIANG *et al.* 2000) and is thus a global marker for peptidergic neurons (HEWES *et al.* 2003). We observed prominent PHM staining in 126 CNS neurons that could be reliably identified based on size, shape, and location (Figure 1A), and the insertion-driven expression patterns that included any of these cells were documented. Of the original 30 insertions with CNS reporter gene expression, 28 drove expression in different groups of PHM neurons, which included but were not limited to the brain insulin-producing cells (IPCs), medial protocerebrum neuron 2 (MP2), superior protocerebrum neuron 1 (SP1), medial protocerebrum neuron 1 (MP1), lateral cluster neurons (LC), adipokinetic hormone neurons (AKH) (LEE and PARK 2004), dorsal chain neurons 1-11 (d1-d11), and posterior abdominal neurons (PA) (HEWES *et al.* 2003; LEE and PARK 2004). Some of the insertions drove largely peptidergic cell-specific expression that was restricted to small cell groups (Figure 1, B and E; Figure 2A), and some drove broader expression that included many other types of neurons (Figure 1, C and D).

To further characterize the peptidergic neurons included in each pattern, Chunjing Qu double-labeled the 28 lines that displayed peptidergic neuron mCD8::GFP expression with immunostaining for different neuropeptides that included crustacean cardioactive peptide **(**CCAP**)**, bursicon (BURS), insulin-like protein 2 (ILP2), peptides with -RFamide C-terminal sequences, and leucokinin (LK), as well as the neuropeptide biosynthetic enzyme, Furin 1. We documented 17 insertions that drove expression in CCAP neurons, eight with expression in ILP2 neurons, and 2-6 lines with expression in LK neurons, Furin 1 neurons, -RFamide neurons, and/or bursicon neurons (Figures 8-10 and Table 1).

Based on the genomic insertion sites, we were able to putatively identify the trapped gene for each of the 28 insertions (Table 1). When homozygous, four of the 28 insertions produced defects in ecdysis, post-ecdysis behaviors, and cuticular tanning, all of which are processes that are regulated by neuropeptides (HEWES *et al.* 2000; PARK *et al.* 2002; PARK *et al.* 2003). Other mutant phenotypes included reduced adult tanning, appearance of multiple mouthparts in larvae, an ectopic wing vein, and wing expansion defects (Figure 11, A-D and Table 1). Given the expression patterns and mutant phenotypes produced by these insertions, we deemed it likely that some of the trapped genes regulate the development or function of selected peptidergic neurons. This part of work has been modified from Chunjing Qu's splice-trap data, and integrated as a portion of a published paper (CHEN *et al.* 2014).

***shep* is expressed in a broad CNS pattern:** One insertion, *BG00836*, had a reporter gene expression pattern that closely matched the cellular distribution of PHM (Figure 2A). At least three factors with similar expression patterns are known—DIMM, PHM, and PC2/amontillado—and all are key regulators of neuropeptide expression and/or peptidergic neuron development (SIEKHAUS and FULLER 1999; HEWES *et al.* 2000; JIANG *et al.* 2000). The peptidergic neurons contained within the *BG00836* expression pattern included neurons expressing ILP2, LK (Table 1), Furin 1 and -RFamide (Figure 9), and bursicon (Figure 10). In addition, homozygous *BG00836* animals displayed defects in eclosion and wing expansion (Table 1), two behaviors under regulation by peptidergic neurons (PARK *et al.* 2003; PEABODY *et al.* 2008). Since *BG00836* contained a *P* element insertion in an exon of *alan shepard (shep)* (Figure 3A), these behavioral defects, together with the high degree of co-localization between the *BG00836* ($shep^{BG00836}$) expression pattern and peptidergic markers, suggested a key role of *shep* in development or function of peptidergic neurons.

We obtained two other *P* element insertions, $shep^{BG01322}$ and $shep^{G00261}$, in *shep* introns (Figure 3A). The $shep^{BG01322}$ insertion is a second splice-trap insertion in *shep* that we obtained in the initial screen (Figure 7), and it displayed widespread, low-level expression in the CNS (Figure 2B) together with higher-level expression in diverse peptidergic neurons (Figure 8 and Figure 9; and data not shown). The $shep^{G00261}$ insertion is a protein-trap element, which attaches a GFP tag to the native protein (MORIN *et al.* 2001), and this line displayed an even broader, more uniform pattern of CNS expression (Figure 2C). Thus, the SHEP expression pattern appeared to be

broader than indicated by *shep*^{BG00836}, although two of the three lines displayed selected or stronger expression in some peptidergic neurons.

I employed *shep in situ* hybridization to confirm the *shep* mRNA expression pattern. In order to verify the specificity of the *in situ* probes, I first conducted hybridization with antisense probes to *shep* in *engrailed-Gal4/UAS-shep* (*engrailed>shep*) embryos, and I found the expected *engrailed* stripes (Figure 12A) in stage 11 embryos (FOX *et al.* 2010); *engrailed* stripes were not observed in wild-type embryos (Figure 2). This result confirmed both the function of the *UAS-shep* construct and hybridization of the antisense probe to *shep* transcripts. Sense probes were used as a control (Figure 12X).

In wild-type animals, I first observed hybridization to *shep* transcripts in oocytes, suggesting that *shep* is maternally loaded (Figure 12C). In syncytial blastoderm embryos at stage 3, *shep* transcripts were detected ubiquitously in a granular pattern surrounding nuclei (Figure 2D and Figure 12E). The level of *shep* transcripts decreased sharply in stage 4 embryos (Figure 12G and Figure 12H) and became undetectable by stage 5 (Figure 12I and Figure 12J). At stage 7, zygotic *shep* expression first appeared in the pro-cephalic neurogenic region (Figure 2E; Figure 12, K and L). The expression of *shep* transcripts was strongly upregulated in stage 8 and stage 9 (Figure 12, M-P) and expanded to a midline region, putatively mesectoderm, beginning in stage 10 (Figure 12Q and Figure 12R, arrows). Strong expression in the ventral neurogenic region started during stage 12 (Figure 12S and Figure 12T, open arrowheads) and spread to the entire CNS as well as to the peripheral nervous system (PNS) in stage 13 (Figure 2F

arrows; Figure 12, U and V, arrowheads). A developmental RNA-Seq expression profile from modENCODE (GRAVELEY *et al.* 2011) largely mirrors the above results, with moderate expression in 0-2 hr embryos, a sharp drop in expression in 2-4 hr embryos, and a jump in expression in 12-14 hr embryos, when *shep* expression in our *in situ* analysis became strong and widespread throughout the CNS.

To determine the SHEP protein expression pattern, I performed immunostaining with a polyclonal anti-SHEP antiserum. I confirmed the specificity of the antiserum in *engrailed>shep* embryos, and the expected stripes were observed in stage 12 (Figure 12B). In wild-type animals, SHEP was first detected in the cytoplasm of oocytes (Figure 12D), and in syncytial blastoderm embryos it showed a granule-like distribution around the nuclei (Figure 12F), as I observed in the *shep in situ* hybridization. I did not observe strong zygotic SHEP expression in embryos until stage 17, when SHEP was detected in the cytoplasm of CNS and PNS neurons (Figure 12W, arrows). In stage 17, I also observed SHEP expression in the antennomaxillary complex and labral sensory complex (Figure 12W, arrowhead). In 3rd instar wandering larvae, strong staining was broadly detected in the brain, ventral nerve cord, and ring gland (Figure 2H). Moreover, the pattern mirrored the results of *shep in situ* hybridization at this stage (Figure 2G). This broad expression of SHEP in the CNS was also detected at the P14 (BAINBRIDGE and BOWNES 1981a) pharate adult stage (Figure 4A) and was concentrated in neuronal cytoplasm (data not shown).

Lower level expression of *shep* mRNA and SHEP protein was sometimes detectable in many non-neuronal tissues (data not shown), and this has been indicated by Western blot and RNA-Seq analysis (GRAVELEY *et al.* 2011; MATZAT *et al.* 2012). Nevertheless, these spatiotemporal expression data indicated that zygotic *shep* mRNA and SHEP protein was primarily restricted to the nervous system beginning in the late embryo and continuing into the late larval and pharate adult stages.

SHEP is a member of the MSSP RNA/DNA binding protein family: To date, eight *shep* transcripts (RA, RB, and RD-RI) have been identified (Figure 3A) based on expressed sequence tags (ESTs) reported by the Berkeley *Drosophila* Genome Project (BDGP). There are 53 *shep* 5' ESTs, and RE, RH, and RI together represent ~70% of the total. To determine which of the three transcripts is more abundant, I randomly selected six ESTs that have been mapped to the shared 5' end of the three transcripts for amplification and sequencing (see methods). Four out of the six clones contained the RE-specific sequence 'CAACAG' from exon 13, and the other two did not and were therefore RH or RI. Thus, I used an RE/RG cDNA sequence to create a *UAS-shep* line (RG utilizes an alternate transcriptional start site; however, the RE sequence amplified for the cDNA is identical to RG).

The predicted *shep* open reading frame encodes six proteins PA, PB/D, PE/G, PF, PH, and PI (the predicted protein products of transcripts RB and RD are identical, and the products of RE and RG are identical). These isoforms have diverse N termini and largely share the same C terminal sequences, except for two short indels. All six

predicted SHEP isoforms contain two RNA recognition motifs (RRM) (Figure 3C), suggesting possible binding to RNA. According to a protein-sequence-based neighbor-joining phylogenetic tree, SHEP-PE displayed the strongest homology with the MSSP (*c-myc* single strand binding proteins) family, which consists of RNA/DNA binding proteins. The most closely related protein to SHEP in vertebrates was human MSSP-2, with a sequence identity of 60% for conserved feature regions (Figure 3B) (MARCHLER-BAUER *et al.* 2005) and 38% for the global alignment. After MSSP, the next most closely related protein(s) was a family of mRNA binding/alternative splicing factors that includes *Drosophila* ELAV (Figure 3B).

Loss of neuronal *shep* resulted in developmental and behavioral defects: Since *shep* was primarily and broadly expressed in CNS, I obtained pan-neuronal *shep* loss-of-function animals by crossing *elav-Gal4* to *UAS-shep-RNAi, Dicer-2* (*elav>shep-RNAi, Dicer-2*) in order to assay impacts on the CNS. The efficiency of the *shep* RNAi was confirmed by anti-SHEP immunostaining on the CNS of *elav>shep-RNAi, Dicer-2* flies at the P14 pharate adult stage. The levels of SHEP protein were strongly reduced by *shep-RNAi, Dicer-2*, and only a few SHEP-positive neurons throughout the entire CNS were detected (Figure 4, A and D).

I used the presynaptic marker, Bruchpilot (monoclonal antibody nc82) (SEKI *et al.* 2010), as a general counterstain for the above anti-SHEP immunostaining. Interestingly, the expression level of Bruchpilot was also decreased in pharate adults (Figure 4E) and 3rd instar larvae (Figure 13, A and B). Based on this finding, I

examined two other presynaptic markers, Choline acetyltransferase (ChAT) and Synapsin, and both displayed substantially reduced expression throughout the CNS (Figure 13, C-F). These results suggest that *shep* RNAi led to smaller or fewer synapses, or reduced expression of multiple synaptic proteins. This was accompanied by a decrease in neuropil size. In spite of the weak anti-Bruchpilot signal in *elav>shep-RNAi, Dicer-2* flies, I was able to visualize neuropilar regions, and I found a 21%-31% reduction of multiple neuropilar areas, including the antennal lobes, suboesophageal ganglion, and prothoracic ganglion (Figure 4G). Interestingly, I also observed substantial loss of mCD8::GFP reporter gene expression (suggesting failure to differentiate or cell loss) in adult wing sensory neurons following *shep* RNAi with a *D42-Gal4* driver (Figure 11, E-H).

About one third (38%) of *elav>shep-RNAi, Dicer-2* flies died as pupae, while the lethality observed in *elav>Dicer-2* control flies was less than 1% (Figure 4H). Most (74%) of the *elav>shep-RNAi, Dicer-2* lethality occurred late during pupal development in animals that displayed wing pigmentation (stage P12 or later), and the rest of the lethality occurred during eclosion. These flies emerged halfway from the pupal case and then remained stuck there permanently. The half-eclosed phenotype may have been the result of weakened eclosion movements, since *elav>shep-RNAi, Dicer-2* flies that did eclose walked unsteadily and often fell to the bottom of the vial, and *elav>shep-RNAi, Dicer-2* flies during eclosion appeared to display weakened leg movements (data not shown). More than 92% of the escaper *elav>shep-RNAi, Dicer-2* adults also failed to expand their wings after eclosion (Figure 4H). The eclosion defects and wing

expansion defects following *shep* RNAi were consistent with the phenotype observed for homozygous $shep^{BG00836}$ mutant animals (Table 1), indicating that these effects of the *shep* RNAi are due to loss of SHEP function rather than off-target effects of the RNAi.

In addition to the developmental or motor defects, I also observed reduced lifespan. In a lifespan experiment with flies maintained on standard food, all *elav>shep-RNAi, Dicer-2* adults died by the 18th day, while none of the *elav>Dicer-2* control flies died during this time period (Figure 14A). This result is consistent with previous reports of genetic screens, which showed that *shep* mutants might have significantly higher fat accumulation in larvae (REIS *et al.* 2010), possibly reflecting a reduced mobilization of fat reserves, and reduced starvation tolerance in adults (HARBISON *et al.* 2004). I observed similar defects in starvation tolerance in multiple *shep* loss-of-function backgrounds (Figure 14, B-D). Thus, reduced expression of *shep* in the nervous system resulted in weakened adult locomotor behaviors, failure to complete neuropeptide-controlled eclosion and wing expansion behaviors, and shortened lifespan under fed and starved conditions.

In order to quantify the effects of reduced *shep* expression on locomotor behaviors, I measured rates of flipping and climbing in two separate assays. In the flipping assay, I removed the wings of adult flies and then placed them on their backs. Although the *elav>shep-RNAi, Dicer-2* flies waved their legs around rapidly while flipped, they took more than 200 times longer to turn over than the control *elav>Dicer-2* flies (Figure 4I).

I also performed flipping assays on *shep*^{Exel6103}/*shep*^{Exel6104} mutant animals, and they took 10 times longer to flip over than the hemizygous deficiency control animals (data not shown). The *shep*^{Exel6103} and *shep*^{Exel6104} deficiencies share a common breakpoint located within the first exon shared by *shep* transcripts RE/RH/RI; *shep*^{Exel6103} deletes all of the 3' exons, which include the coding sequences for the C-terminal parts of the SHEP protein that are shared by the various SHEP isoforms, and *shep*^{Exel6104} deletes all of the *shep* exons 5' of the breakpoint, which include some coding sequences (Figure 3A). Western blot analysis showed that *shep*^{Exel6103}/*shep*^{Exel6104} mutant animals lack expression of the SHEP-PA and -PB/D isoforms and have reduced expression of SHEP-PE/G (MATZAT *et al.* 2012).

In the climbing assay, which measured the vertical distance traveled in 5 sec after each fly started climbing, *elav>shep-RNAi, Dicer-2* flies traveled only 42% of the vertical distance that was covered by the *elav>Dicer-2* control flies (Figure 4J). The reduced distance climbed appeared to result at least partially from motor defects or weakness, since I observed that the legs of the *elav>shep-RNAi, Dicer-2* flies shook while climbing and these flies often dropped off the side of the vial during the 5 sec period. Taken together, these general locomotor defects, the observed reductions in neuropil area (Figure 4G), the loss of adult wing sensory neurons (Figure 11), and the broad expression of SHEP in the CNS (Figure 4A) suggest that SHEP regulates the development or function of many motorneurons, interneurons, and/or sensory neurons.

Interestingly, the *shep* RNAi did not result in changes in flipping or crawling performance in 3rd instar larvae (Figure 4, I and J). Moreover, the 3rd instar larval neuropil area was also unchanged (Figure 13G), which was in contrast to the reduction in neuropil area that I observed at the P14 pharate adult stage (Figure 4, A-G). The stage-dependence of these behavioral and morphological phenotypes suggested that *shep* might regulate nervous system development primarily during metamorphosis, when the nervous system undergoes dramatic structural remodeling. Consistent with this model, RNA-Seq analysis shows a strong peak of *shep* expression during the first half of metamorphosis, beginning in late 3rd instar wandering larvae (salivary gland puff stages 3-6) and continuing through 2 days after pupariation; levels then decline by about 50% during the third day after pupariation (GRAVELEY *et al.* 2011).

It appeared that SHEP regulated cell growth in the above tests primarily during metamorphosis, but the effects were not exclusive to this stage, and I did detect a subtler behavioral defect in larvae, which displayed more turns and a tendency to remain in the center of the petri dish in the distance crawled assays (Figure 15). These results show that loss of SHEP function in the larval nervous system resulted in some behavioral defects. Nevertheless, the behavioral defects in larvae were qualitatively weaker overall than the ones observed in adults (Figure 4, I-J).

Loss of *shep* resulted in altered mating behaviors: In addition to the general locomotor defects seen in *shep* mutants, I also observed changes in the organization of mating behaviors. I first detected this phenotype in $shep^{Exel6103}/shep^{Exel6104}$ females,

which laid only unfertilized eggs when crossed to $shep^{Exel6103}/shep^{Exel6104}$ males but did produce viable embryos and larvae when crossed to wild-type (*Oregon R*) males. This result led us to examine courtship and mating behaviors in the $shep^{Exel6103}/shep^{Exel6104}$ adults. Virgin $shep^{Exel6103}/shep^{Exel6104}$ females displayed several sexual rejection behaviors. These included decamping, failure to extend the wings to allow copulation, and kicking to push males off during copulation (TAN *et al.* 2013), and expulsion of seminal fluid after copulation.

I quantified these changes in $shep^{BG00836}/shep^{ED210}$ females, which also displayed these defects in courtship and mating behaviors. The $shep^{ED210}$ allele deletes the entire *shep* gene (RYDER *et al.* 2007), and $shep^{BG00836}$ carries a *Gal4* splice-trap element that is inserted in a *shep* exon (Figure 3A), and $shep^{BG00836}/shep^{ED210}$ females display reduced expression of native SHEP protein (Figure 70C) (MATZAT *et al.* 2012). Wild-type males were paired together with wild-type females or $shep^{BG00836}/shep^{ED210}$ females with or without *shep* (*UAS-shep*) rescue. All three genotypes showed similar copulation latencies (Figure 5A). Once copulation started, wild-type virgin females extended their wings and allowed mounting of males within seconds (Video 1), but $shep^{BG00836}/shep^{ED210}$ virgin females vigorously kicked at males while keeping their wings closed, thus preventing the males from mounting and grasping the base of the wings (Figure 5A and Video 2). During copulation, the s$hep^{BG00836}/shep^{ED210}$ females also kicked almost continuously (>90% of the time) at the males with their metathoracic legs, whereas the wild-type females displayed kicking behaviors only 17% of the time (Figure 5B). The copulation duration was reduced in the $shep^{BG00836}/shep^{ED210}$ females

(Figure 5A), and I often observed a burst of intensive kicking prior to the withdrawal of the male (data not shown). Kicking during both mounting and copulation was reduced in $shep^{BG00836}/shep^{ED210}$, *UAS-shep* females, and the copulation duration was restored to the wild-type level (Figure 5, A and B).

After copulation, $shep^{BG00836}/shep^{ED210}$ females displayed extensive grooming, almost exclusively involving just the legs (Figure 5B, grooming index; Video 3). In contrast, control females used the metathoracic legs to alternate grooming of the legs, wings and abdomen (Video 4). Much of the grooming in recently mated $shep^{BG00836}/shep^{ED210}$ females involved one of the mesothoracic legs together with the metathoracic legs (Video 3); this form of 3-leg grooming was rarely observed in wild-type flies (Figure 5B and Video 4). In addition, I observed 8 out of 10 females actively expelling seminal fluids from the reproductive tract (Video 5); I never observed the expulsion of seminal fluids by wild-type females. Females often used their metathoracic legs in this process, and as shown in the video, strands of sticky fluid could be observed. Thus, the presence of these fluids may have contributed to the observed changes in grooming behavior. I did not observe rescue of normal rates of 2-leg grooming in $shep^{BG00836}/shep^{ED210}$, *UAS-shep* females, although this failure to rescue was not completely unexpected, given the heterogeneous pattern of transgene expression (which may not include important grooming circuits) in the $shep^{BG00836}$ line (Figure 2A).

***shep* was required for neuronal outgrowth during metamorphic remodeling:** Since I observed wing expansion defects in *shep* mutants, I examined the function of *shep* in

the bursicon neurons, which play a key role in the regulation of wing expansion behaviors (PEABODY *et al.* 2008). These neurons undergo extensive remodeling during metamorphosis and secrete the neuropeptide bursicon soon after eclosion to promote wing expansion behaviors (PEABODY *et al.* 2008; ZHAO *et al.* 2008). In order to test whether *shep* regulated the development or function of the bursicon neurons, I examined these cells in hemizygous $shep^{BG00836}/shep^{ED210}$ mutant animals. The cells were visualized by immunostaining with an anti-Bursicon (Bursicon α subunit, FBgn0038901) antiserum (anti-BURS) (LUAN *et al.* 2006) or by expressing the membrane tag, mCD8::GFP. Both markers provided excellent resolution of the bursicon neuron somata (Figure 10), and the peripheral axons and axon terminals in both larvae and P14 stage pharate adults in *shep* loss-of-function backgrounds (Figure 17). Thus, I used anti-BURS in most experiments, since this marker did not require the introduction of *UAS-mCD8::GFP* into all genotypes.

At the P14 pharate adult stage, the bursicon neuron somata in $shep^{BG00836}/shep^{ED210}$ animals lost the multi-angular morphology that is characteristic of that stage (Figure 6A) and became more rounded (Figure 6B) together with a 27% reduction in soma area (Figure 6J). In $shep^{Exel6103}/shep^{Exel6104}$ animals, $shep^{BG00836}$ homozygotes, and *ccap>shep-RNAi* animals (the abdominal bursicon neurons are a subset of the CCAP neurons) (LUAN *et al.* 2006), the soma area reductions were all 42-47% (Figure 16F). In the periphery, I also observed reduced branching of the bursicon neuron axons in P14 pharate adult stage animals (Figure 6, D and E), and I quantified the changes in branch numbers by Sholl analysis (MAGARINOS *et al.* 2006) (Figure 6K). I observed no

difference between *shep*^{BG00836}/*shep*^{ED210} animals and *shep*^{BG00836}/*w* controls in the number of efferent bursicon axons at the point where they enter the abdominal nerves or in the maximum extent of these axons in the periphery (Figure 6K). However, the axons in *shep*^{BG00836}/*shep*^{ED210} animals had fewer peripheral branches, resulting in fewer intersections with the intermediate sampling rings (Figure 6K). The reduction in intersections was evident throughout the arbor, and the greatest reduction (10 fewer branches) was observed 450 µm from the posterior tip of the ventral nerve cord. The peripheral bursicon axons in *shep*^{BG00836}/*shep*^{ED210} pupae also displayed fewer boutons than the controls (Figure 6, H and L). I observed similar defects in axonal branching in *shep*^{Exel6103}/*shep*^{Exel6104}, *ccap>shep-RNAi*, and *ccap>shep-RNAi, Dicer-2* animals (Figure 18, A-C). These peripheral axon branches form during outgrowth of the bursicon neurons during metamorphosis, after pruning of the larval, unbranched axons has occurred (ZHAO *et al.* 2008). Taken together, these results show that *shep* promotes formation (or maintenance) of peripheral axon branches in the bursicon neurons during metamorphic remodeling.

To determine whether the cellular defects were solely caused by the loss of *shep*, I took advantage of the fact that the *shep*^{BG00836} mutation can be used to drive transgene expression in *shep*-mutant bursicon neurons. In P14 stage *shep*^{BG00836}/*shep*^{ED210}, *UAS-shep* pharate adults, I found that bursicon neuron soma area, peripheral axon branch number, and bouton number were all fully rescued (Figure 6, C and F; I-L). Since I built *UAS-shep* with *shep-RE/RG,* I conclude that one or both of these isoforms is (are) sufficient to restore normal soma growth, peripheral axon branching, and bouton growth

in the bursicon neurons during metamorphic remodeling. In addition, I observed punctate accumulation of bursicon in the somata (cytoplasm) of *shep*-rescued neurons (Figure 6C), suggesting that *shep* expression can influence the regulated secretory pathway. However, I did not observe changes in bursicon distribution in *shep* mutant cells without rescue, and I therefore cannot exclude the possibility that this observation reflects a gain-of-function effect of transgenic SHEP expression in the $shep^{BG00836}/shep^{ED210}$, *UAS-shep* animals.

Interestingly, loss of *shep* had no impact in our assays of bursicon neuron morphology in wandering 3rd instar larvae. In contrast to pharate adults, bursicon neuron soma area was unchanged in $shep^{BG00836}/shep^{ED210}$ larvae (Figure 6J). Similarly, although $shep^{Exel6103}/shep^{Exel6104}$ and $shep^{BG00836}/shep^{BG00836}$ P14 pharate adults each displayed a 44%-47% reduction in bursicon neuron soma area, these genotypes displayed no change in soma area in the 3rd instar larvae. In addition, there was no change in bursicon neuron soma area in *ccap>shep-RNAi, Dicer-2* larvae (Figure 16G). To test for impacts of the loss of *shep* on larval bouton area, I examined boutons at the bursicon neuron NMJ on muscles 12-13 of the 2nd abdominal segment (HODGE *et al.* 2005). In $shep^{Exel6103}/shep^{Exel6104}$, $shep^{BG00836}/shep^{ED210}$, and *ccap>shep-RNAi, Dicer-2* larvae, we found no change in the number and size distribution of NMJ boutons (Figure 18, D-L), which is in contrast to the clear reductions in bouton area and number in P14 stage pharate adult $shep^{BG00836}/shep^{ED210}$ animals (Figure 6, G-H and L). Taken together, these results suggest that SHEP is required for growth of the bursicon neurons during metamorphosis but not during larval development.

Discussion

Identification of *shep* through splice-trap screening: Through an expression pattern-based splice-trap screen, we identified 28 insertions that drove expression in peptidergic neurons. These included 17 insertion sites with expression in CCAP neurons and several sites with expression in ILP2 neurons, LK neurons, Furin 1 neurons, -RFamide neurons, and/or bursicon neurons (2-8 sites per marker). One of the insertions, $shep^{BG00836}$, drove transgene expression in PHM-positive peptidergic neurons, and homozygous $shep^{BG00836}$ adults displayed defects in wing expansion. These observations implicated *shep* in the development or function of diverse peptidergic neurons, and we selected it for further analysis. Anti-SHEP immunostaining and additional *shep* reporter genes confirmed expression in peptidergic neurons, but these markers and *shep in situ* hybridization also revealed widespread expression in the CNS, with much lower expression in other tissues.

SHEP is orthologous to the *c-myc* single-strand binding protein, MSSP-2: Previous studies have described *shep* as homologous to the vertebrate genes, Rbms2/Scr3 (ARMSTRONG *et al.* 2006) or Rbms1/Scr2/MSSP-2 (WANG *et al.* 2013). Our phylogenetic analysis supported the placement of SHEP in the MSSP family, with the ELAV family of RNA-binding proteins being the next most closely related (Figure 3B). In general, MSSP proteins contain RNA recognition motifs and have been found in vertebrates to bind DNA, RNA, or proteins to regulate a variety of biological processes, including DNA polymerization, gene expression, cell transformation, and apoptosis (BALDUCCI-SILANO *et al.* 1998; KIMURA *et al.* 1998b; NIKI *et al.* 2000b; NIKI *et al.*

2000d; NOMURA *et al.* 2005b). In *Drosophila*, SHEP interacts with the insulator proteins MOD(MDG4)2.2 and SU(HW) to negatively regulate chromosomal insulator activities, specifically in the CNS (MATZAT *et al.* 2012). These molecular insights suggest a gene regulatory mechanism by which SHEP may control aspects of the metamorphic development of the bursicon neurons, as well as other neurons that contribute to the overall structure of adult brain neuropils.

Metamorphic remodeling of the bursicon neurons and stage-dependence of SHEP function: The *shep* mutant defects in wing expansion presented an opportunity to define cellular functions of SHEP in an experimentally accessible cell type, the bursicon neurons. In *shep* mutants, I observed a reduction in the post-pruning growth of the bursicon neurons during metamorphosis, resulting in smaller somata and less branching in the peripheral axon arbor in pharate adult animals (Figure 6).

Interestingly, the regulation of bursicon neuron growth by *shep* was stage-dependent. I observed defects in bursicon neuron soma growth and axon branching during metamorphosis in hypomorphic *shep* mutant animals of multiple genotypes, including $shep^{BG00836}/shep^{BG00836}$, $shep^{Exel6103}/shep^{Exel6104}$ and $shep^{BG00836}/shep^{ED210}$ (Figure 16 and Figure 18). However, in each of these genotypes, the larval cellular morphologies were normal.

I observed other behavioral defects that suggested that the metamorphosis-specific actions of SHEP were not limited to the bursicon neurons. For example, the most

severe *shep* loss-of-function genotype tested (see below) was *elav>shep-RNAi, Dicer*-2, but *elav>shep-RNAi, Dicer*-2 larvae displayed normal crawling distances and self-righting behaviors, while this genotype showed lethality in the late pupal stages and severe locomotor defects in adult animals. Associated with this increase during metamorphosis in the dependence of the nervous system on *shep* activity, there is also a marked increase in the levels of *shep* expression at the onset of metamorphosis (GRAVELEY *et al.* 2011). These results provide indirect evidence to suggest that an increase in *shep* expression during the pupal stage may support neuronal remodeling or other aspects of neuronal function and development in diverse neurons during metamorphosis.

Although most of the larval behaviors assayed were unaffected in *shep* mutant animals, I observed one behavioral phenotype in *elav>shep-RNAi, Dicer-2* larvae, namely a tendency to remain in the center of the apple juice-agarose plate while making many sharp turns along the path of locomotion. Based on anti-SHEP immunostaining (Figure 16, A-E), *UAS-shep-RNAi, Dicer-2* provided a more complete knockdown of anti-SHEP immunostaining in the CNS than *shep* RNAi without *UAS-Dicer-2* or in $shep^{BG00836}$ homozygotes or $shep^{BG00836}/shep^{ED210}$ mutant larvae. Moreover, *shep* RNAi without *UAS-Dicer-2* led to a greater knock-down of SHEP in Western blots than $shep^{Exel6103}/shep^{Exel6104}$ (MATZAT *et al.* 2012). Taken together with the above observation that many of the weaker *shep* loss-of-function genotypes had defects that were only manifest in adults, these findings suggest that *shep* plays a stage-dependent

(largely metamorphosis-specific) role in the maintenance, function, or development of the nervous system.

Broad impacts of *shep* in the nervous system: The SHEP expression pattern and *shep* mutant phenotypes reported here are consistent with broad actions of this protein in neuronal development and functions throughout the nervous system. Pan-neuronal loss of *shep* resulted in late-pupal lethality and reduced adult life span under both fed and starved conditions, as well as diverse developmental and behavioral defects, including failure to complete wing expansion, uncoordinated and weakened adult locomotion, reduced neuropil areas, and altered mating behaviors. Other groups have also shown defects in gravitaxis and reduced starvation resistance in *shep* mutants (HARBISON *et al.* 2004; ARMSTRONG *et al.* 2006).

Such widespread actions may also explain the partial rescue of the mating defects by *UAS-shep* expression in $shep^{BG00836}/shep^{ED210}$ females. Although I cannot exclude the possibility that other SHEP isoforms in addition to SHEP-E/G (used to create *UAS-shep*) were necessary to support the normal function of the post-copulatory grooming circuits, it is also possible that neurons required for female receptivity to the male may have been included in the $shep^{BG00836}$ expression pattern used to drive *shep* rescue, whereas the neurons involved in normal post-copulatory grooming behaviors were not.

The observation of several seemingly independent behavioral defects (e.g., gravitaxis and female receptivity to mating) and reduced neuropil areas, taken together with the

cellular defects described in *shep*-mutant bursicon neurons, suggests that SHEP may have pleiotropic effects on neurite development or other processes throughout the CNS. Such pleiotropic effects of *shep* mutations in the CNS may be due to the loss of SHEP suppression of widely distributed chromatin insulator complexes (MATZAT *et al.* 2012), so as to establish altered chromatin states and gene expression, potentially in multiple signaling pathways controlling a range of developmental and physiological events. In addition, some of the adult *shep* loss-of-function phenotypes, such as reduced lifespan and altered mating behaviors, may reflect adult-specific (acute) effects of SHEP on neuronal activity. Alternatively, the metamorphosis-specific regulation of neurite branching and cell growth in the bursicon neurons may be representative of the actions of SHEP in many neuronal cell types. It will be important in future studies to distinguish among these models, as our results demonstrate that SHEP is a general regulator of the postembryonic development of mature neurons.

Table 1 Insertion sites, trapped genes, co-localized neuropeptide markers, and mutant phenotypes for insertions obtained through the splice-trap screen.

Transposon insertion	Trapped gene(s)	Insertion site	Product(s) of trapped gene(s)	Co-localized neuropeptide markers	Homozygous mutant phenotype
BG00076	*Shal K^+ channel interacting protein (SKIP)*	1st exon	Ion channel regulating protein	DILP2, PHM, -RFamide	Recessive pharate adult lethality
BG00197	*jim*	537 bp upstream	Transcription factor	PHM	Mid-pupal lethality
BG00476	*CG4860*	4 bp upstream; insertion orientation unknown	Short chain acyl-CoA dehydrogenase (SCAD)	PHM	Normal

BG00665	*CG8963*	2nd intron of RA, RC and RD; 1st intron of RB	poly(A) binding protein, middle domain of factor 4G (MIF4G) superfamily	CCAP, PHM	Larval lethality (all stages)
BG00836	*alan shepard (shep)*	1st exon of RC, RE (3rd intron of RB and RA, 2nd intron of RD, and 4th intron of RF)	RNA binding protein	CCAP, DILP2, DIMM, Furin 1, LK, PHM, -RFamide	20% pharate adult lethality; 2% adults failed to fully eclose and died stuck half-way out of the pupal case; 10% adults with wing expansion defects; 40% adults with ectopic longitudinal vein that extended from the posterior cross vein (pcv) (Figure S5)
BG01322	*alan shepard (shep)*	15 bp upstream of RB; 1st intron of	RNA binding protein	CCAP, DILP2 Furin 1, LK,	25% adults with wing expansion defects

		RD; 2nd intron of RA and RF		PHM, -RFamide	
BG00855	*homeodomain interacting protein kinase (hipk)*	1st intron of RA and RB	Serine/threonine kinase	CCAP, PHM	Lethal
BG02654	*homeodomain interacting protein kinase (hipk)*	1st intron of RB	Serine/threonine kinase	CCAP, PHM	Normal
BG01140	*MYPT-75D*	2nd intron of RA, RB and RD	Myosin phosphatase regulator	PHM	Normal
BG01171	*Adult enhancer factor 1 (Aef1)*	1st exon of RB; 1st intron of RA, RC and RD	Transcription factor (C2H2 Zn finger)	CCAP, PHM	Moderate pupal lethality

BG01610	*scribbler (sbb)*	2nd intron of RD, RE, RF and RJ; 3rd intron of RG; insertion orientation unknown	Transcription factor	CCAP, PHM	Embryonic lethality
BG01711	*frizzled 2 (fz2)*	4th intron of RE and 5th intron of RD	Wnt receptor	CCAP, DILP2, PHM, -RFamide	Normal
BG01746	*taiman (tai)*	2nd intron of RD and RG; 3rd intron of RC, RE and RF	PAS domain transcriptional coactivator, signal transduction	CCAP, PHM	Moderate larval lethality associated with appearance of multiple mouthparts; moderate pupal lethality; adult dorsal thorax with darkened trident and less glossy cuticle

BG01766	*Decapping protein 2 (Dcp2)*	1st exon of RA and RE; 2nd intron of RB	mRNA decapping enzyme 2 (Dcp2p)	PHM	Early, mid-, and late pupal lethality
BG01850	*hephaestus (heph)*	1st intron in RB	RNA recognition motif (RRM), RNA binding protein	CCAP, DILP2, LK, PHM, -RFamide	Normal
BG01854	*ERp60*	1st intron	Protein disulfide isomerase	PHM	Normal
BG01894 [a]	*CG11444*	1st exon	Casein kinase substrate, phosphoprotein PP28 superfamily,	CCAP, PHM	Dark cuticle and trident on adult dorsal thorax
	CG32773	2nd intron	Unknown		

BG02142	*cAMP-dependent protein kinase 1 (Pka-C1)*	1st exon of RB and RC	Serine/threonine kinase	PHM	Mid-pupal lethality
BG02222	*CG30127*	2nd intron	Unknown	CCAP, DILP2 PHM	Mid- to late pupal lethality
BG02427	*CG42669*	1st exon of RR, RU, RS and RQ; 2nd intron of RE, RF, RL and RN; 1st intron of RM	Unknown	CCAP, PHM	Normal
BG02721	*brain tumor (brat)*	1st intron of RA and RD	Zn-finger, B-box protein, translation repressor	CCAP, DILP2, LK, PHM	Normal

BG02759	*protein kinase 61C (Pk61C, PDK1)*	1st intron of RI; 2nd intron of RD	Serine/threonine kinase	CCAP, PHM	Normal
BG02772	*CG13791*	1st intron of RA and RB	BTB/POZ protein	CCAP, PHM	Normal
GT-000078	*CG13791*	1st intron of RA; 2nd exon of RB	BTB/POZ protein	CCAP, PHM	Normal
BG02810	*couch potato (cpo)*	2nd intron of RR, RT, RQ, RU, RW and RV	RNA recognition motif (RRM), RNA binding protein	PHM	Lethality in homozygotes
BG02820 [a]	*chiffon (chif)*	1st intron of RA and RB	Zinc finger/DBF-like protein (ZnF-DBF)	PHM	Normal
	CG42231	1st intron of RA	Unknown		
BG02836 [a]	*6-*	1st exon of RB and	6-phosphofructo-2-	DILP2,	Normal

		phosphofructo-2-kinase (Pfrx)	RG; 1st intron of RA, RF, RI and RJ;	kinase (6PF2K)	DIMM, LK, PHM, -RFamide	
		CG14200	1st intron of RA	Zinc finger/C2H2-like protein		
	BG00449	*CG31145*	2nd intron of RA, RB, RC and RD	Unknown	PHM	Mid- to late pupal lethality

For insertions within exons or introns, the distances are provided with respect to the 5' end of the exon or intron. For insertions upstream or downstream of the gene, the distances are relative to the transcriptional start or transcriptional stop site, respectively.

[a]Inserted in two overlapping or nested genes.

Figure legends

Figure 1. Co-localization of splice-trap reporter gene expression with the peptide biosynthetic enzyme, PHM. (A) Schematic diagram of neurons that consistently display strong anti-PHM immunostaining in the wandering 3rd instar larval CNS. For cellular nomenclature, see (HEWES *et al.* 2003). (B-F) Examples of reporter gene expression (green) and anti-PHM immunostaining (magenta) for five selected splice-trap insertions (*BG01850*, *BG01610*, *BG01894*, *BG02721*, and *BG02836*). Arrowheads, MP1 neurons; open arrowheads, LC neurons; asterisks, insulin-producing neurons (IPCs); arrows, dorsal chain neurons. Scale bars: 50 μm.

This figure was adapted and modified from Chunjing Qu's dissertation (QU 2010), and it was part of our publication of this chapter in my dissertation (CHEN *et al.* 2014).

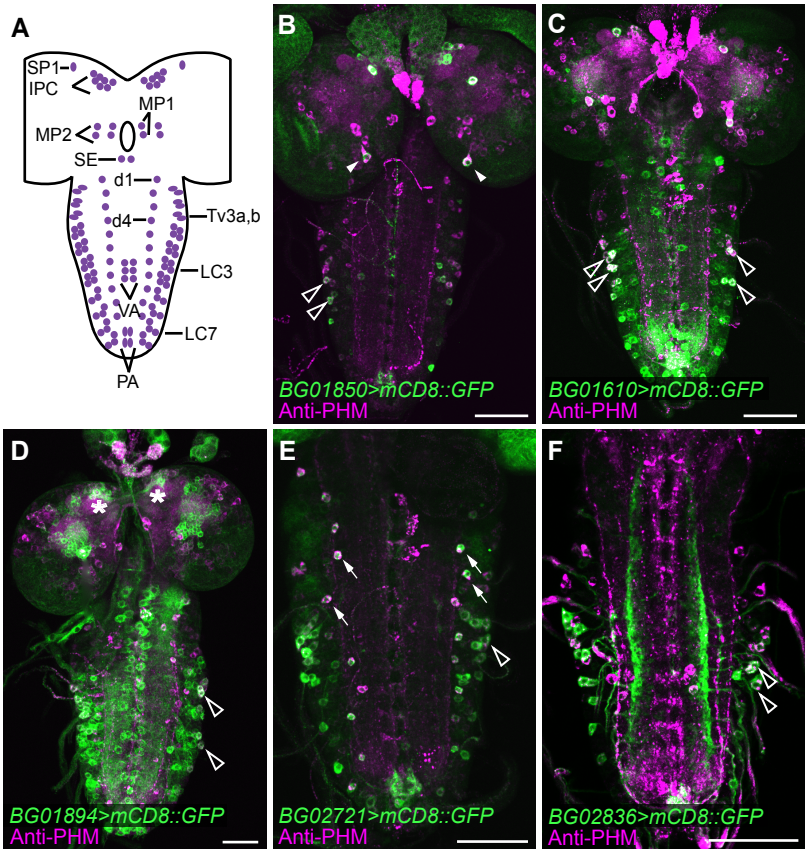
A
SP1
IPC
MP1
MP2
SE
d1
d4
Tv3a,b
LC3
VA
LC7
PA
B
BG01850>mCD8::GFP
Anti-PHM
C
BG01610>mCD8::GFP
Anti-PHM
D
BG01894>mCD8::GFP
Anti-PHM
E
BG02721>mCD8::GFP
Anti-PHM
F
BG02836>mCD8::GFP
Anti-PHM

Figure 2. *shep* mRNA and SHEP protein expression in embryonic and larval stages. (A) $shep^{BG00836}$ displayed an mCD8::GFP reporter gene expression pattern (green) that overlapped extensively with anti-PHM immunostaining (magenta). The areas with the strongest colocalization appear white, but many other cells were labeled with both markers. (B) A second splice-trap insertion in the *shep* gene, $shep^{BG01322}$, showed a broader expression pattern, which included PHM-positive neurons as well as many PHM-negative neurons. (C) The protein-trap insertion, $shep^{G00261}$, also labeled a very broad population of neurons throughout the CNS. (D) In the embryonic syncytial blastoderm stage, *shep in situ* hybridization (blue) showed *shep* transcripts that were clustered around DAPI-labeled nuclei (red). The grayscale DAPI fluorescence image was inverted, with the black pixels (nuclear staining) converted to red, prior to the merge with the *in situ* image. (E) Zygotic transcripts of *shep* first appeared in the pro-cephalic neurogenic region (arrowhead) in stage 7. (F) In late embryonic stages, *shep* transcripts were broadly detected throughout the CNS and PNS (arrows) by *in situ* hybridization. (G-H) In wandering 3rd instar larvae, *shep* transcripts and SHEP protein were broadly detected in the CNS and ring gland (asterisks) by *in situ* hybridization (G) and immunostaining (H), respectively. The distributions of *shep* transcripts and SHEP protein were not uniform, and I observed heterogeneous levels of expression in the brain lobes and ventral nerve cord, with lower level expression in the optic lobes (open arrowheads). Scale bars: 50 μm.

Panel A-C were adapted and modified from Chunjing Qu's dissertation (QU 2010), and they were part of our publication of this chapter in my dissertation (CHEN *et al.* 2014).

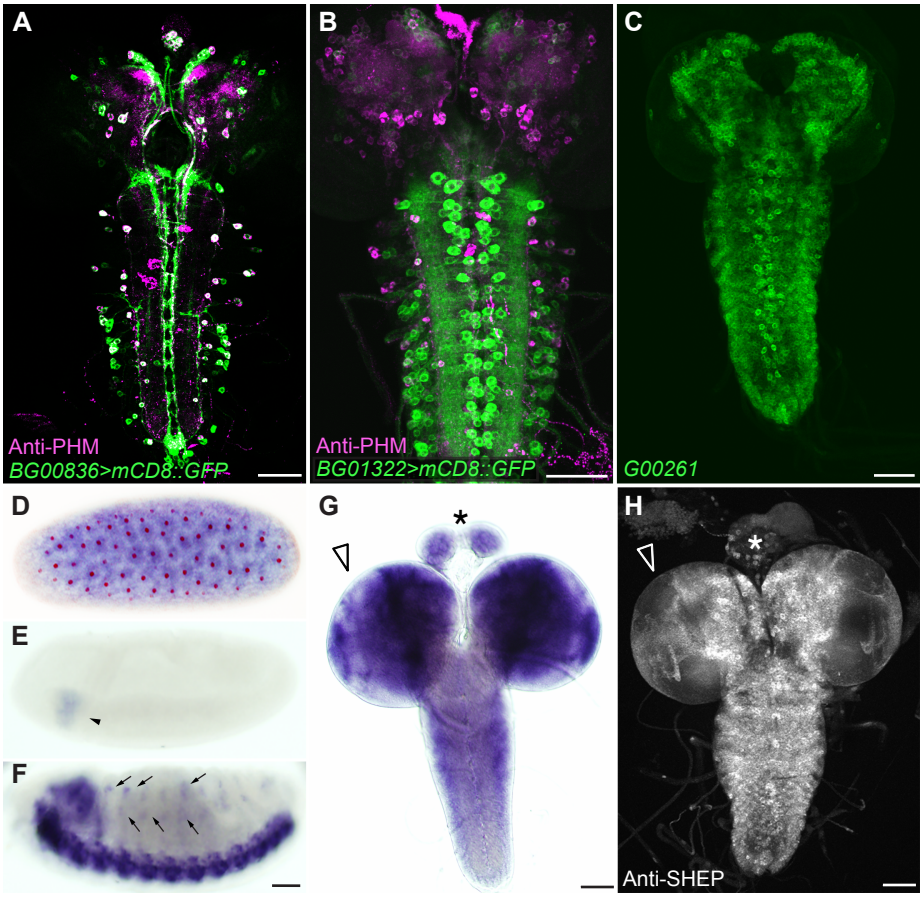
A
Anti-PHM
BG00836>mCD8::GFP
B
Anti-PHM
BG01322>mCD8::GFP
C
G00261
D
E
F
G
H
Anti-SHEP

Figure 3. SHEP is the *Drosophila* ortholog to MSSP. (A) Genomic organization of alternative *shep* transcripts, *P* element insertion sites, and regions deleted by deficiencies. Open triangles indicate the locations of *P* element insertions, and the gray bars indicate regions deleted by deficiencies (with gray arrows indicating that the deficiency deletes flanking regions that are not shown in the figure). RA, RB, and RD-RI are *shep* transcripts arising from a combination of alternative transcriptional start sites (arrows) and alternative mRNA splicing. Vertical lines and bars represent exons, and the lines connecting them indicate introns. (B) A rooted neighbor-joining phylogeny tree for the SHEP-PE/G protein. Accession numbers for sequences in the tree are listed in the Materials and Methods. SHEP belongs to the MSSP family, and human MSSP-2 was the closest vertebrate homolog (shortest horizontal distance). The ELAV family was the next most closely related group, and TAR DNA-binding protein-43 homolog (TBPH) and Transformer 2 (TRA2) were more distantly related. Percentage identities obtained by BLASTP (NCBI) with SHEP-PE/G are shown in parentheses, and bootstrap scores for 100 cycles are indicated on the tree branches. (C) Alignment of RRMs of SHEP-E/G to 10 of the most closely related genes from the MSSP and ELAV families. Identical residues were highlighted in boxes and the most highly conserved residues found more generally in diverse proteins containing ribonucleoprotein domains 1 and 2 (RNP1 and RNP2) (BANDZIULIS *et al.* 1989; MARIS *et al.* 2005) were labeled with triangles across the top of the alignment. Among these most highly conserved residues, aromatic amino acids that form the primary RNA binding surface in each RNP (LORKOVIĆ 2012) were labeled with open triangles.

Panel A was adapted and modified from Chunjing Qu's dissertation (QU 2010), and it was part of our publication of this chapter in my dissertation (CHEN *et al.* 2014).

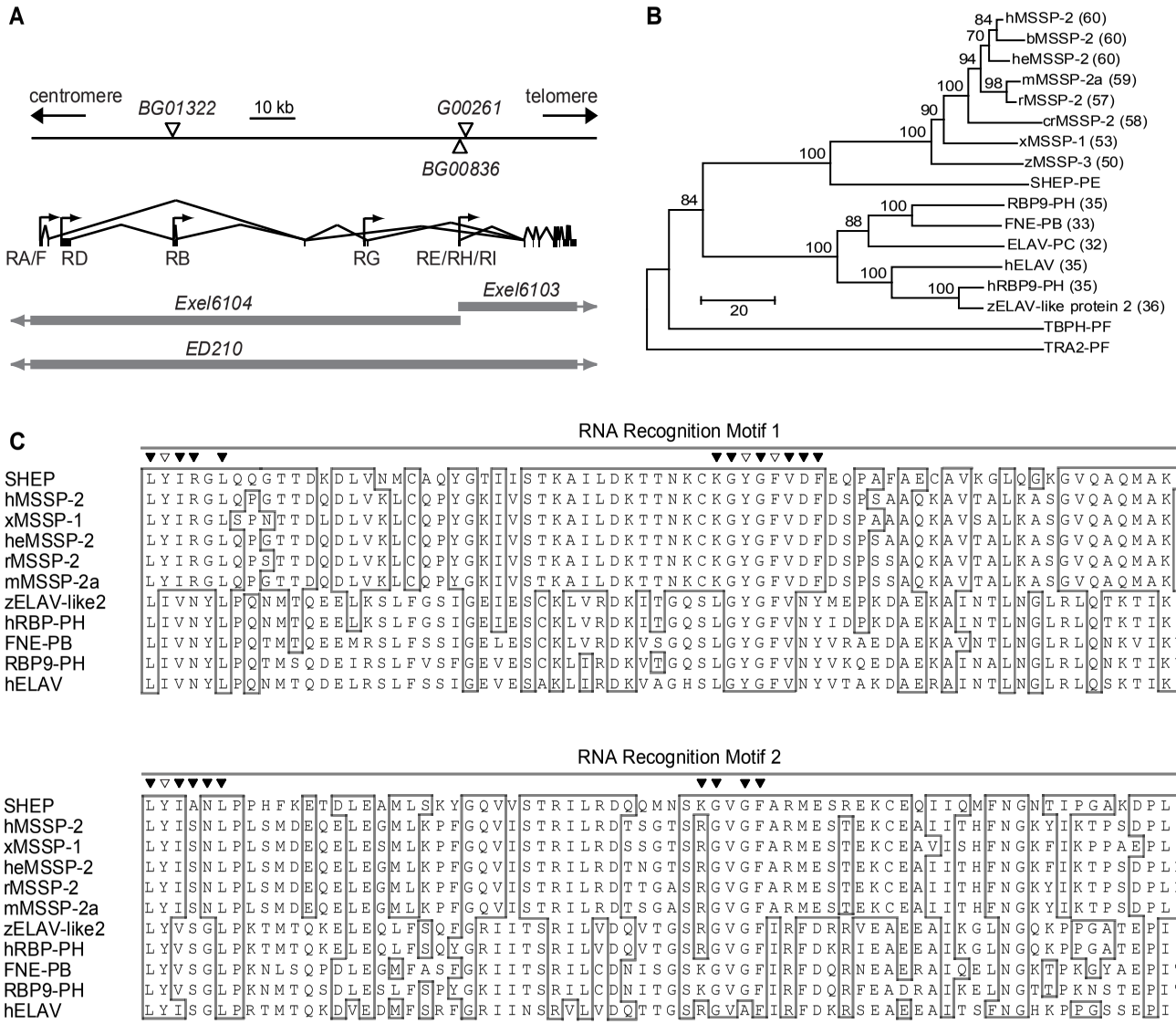
A
centromere
BG01322
10 kb
G00261
telomere
BG00836
RA/F
RD
RB
RG
RE/RH/RI
Exel6104
Exel6103
ED210
B
hMSSP-2 (60)
bMSSP-2 (60)
heMSSP-2 (60)
mMSSP-2a (59)
rMSSP-2 (57)
crMSSP-2 (58)
xMSSP-1 (53)
zMSSP-3 (50)
SHEP-PE
RBP9-PH (35)
FNE-PB (33)
ELAV-PC (32)
hELAV (35)
hRBP9-PH (35)
zELAV-like protein 2 (36)
TBPH-PF
TRA2-PF
20
C
RNA Recognition Motif 1
SHEP
hMSSP-2
xMSSP-1
heMSSP-2
rMSSP-2
mMSSP-2a
zELAV-like2
hRBP-PH
FNE-PB
RBP9-PH
hELAV
RNA Recognition Motif 2
SHEP
hMSSP-2
xMSSP-1
heMSSP-2
rMSSP-2
mMSSP-2a
zELAV-like2
hRBP-PH
FNE-PB
RBP9-PH
hELAV

Figure 4. Developmental and behavioral defects following pan-neuronal *shep* RNAi. (A) Anti-SHEP immunostaining (green) revealed broad expression in the CNS of *elav>Dicer-2* control flies. (B) Immunostaining with anti-nc82 antibodies (magenta) showed the morphology of neuropils in *elav>Dicer-2* CNS. (C) In a merge of the images in panels A and B, strong co-localization of the two signals appears white. (D-E) *elav>shep-RNAi, Dicer-2* flies displayed marked reductions in anti-SHEP (D, green) and anti-nc82 (E, magenta) immunostaining. Neuropil areas were also reduced by 21%-31%. Dashed outlines, left suboesophageal neuropil. Scale bars: 200 μm. (F) Merge of the images in panels D and E after enhancement (using a linear levels function in Photoshop) of the anti-nc82 signal for better visualization of neuropil outlines. (G) Quantification of selected neuropil areas from 2D projections of confocal z-series images. AL, antennal lobe; SOG, suboesophageal ganglion; PTG, prothoracic ganglion. P=0.000022, repeated measures ANOVA; Tukey HSD post hoc *P<0.05, ***P<0.001. The number of animals for each genotype is indicated in parentheses. (H) The final pupal or adult fate of *elav>shep-RNAi, Dicer-2* (n=272) pupae and *elav>Dicer-2* (n=243) controls. Lethal, died as pupae; UEW, adults with unexpanded wings; normal, adults with expanded wings. (I) Box plots of the time needed for larvae and adults to flip over when placed on their backs. The boxes define the interquartile range and the whiskers define the minima and the maxima. Open dots indicate outliers. The number of animals in each group is indicated in parentheses. (J) Distances crawled by *elav>shep-RNAi, Dicer-2* and *elav>Dicer-2* larvae (horizontal distance in 5 min on apple juice-agarose plates, n=15-16) and adults (vertical distance in 5 sec in empty culture vials, n=18-21). ***P<0.001, Student's t-Test.

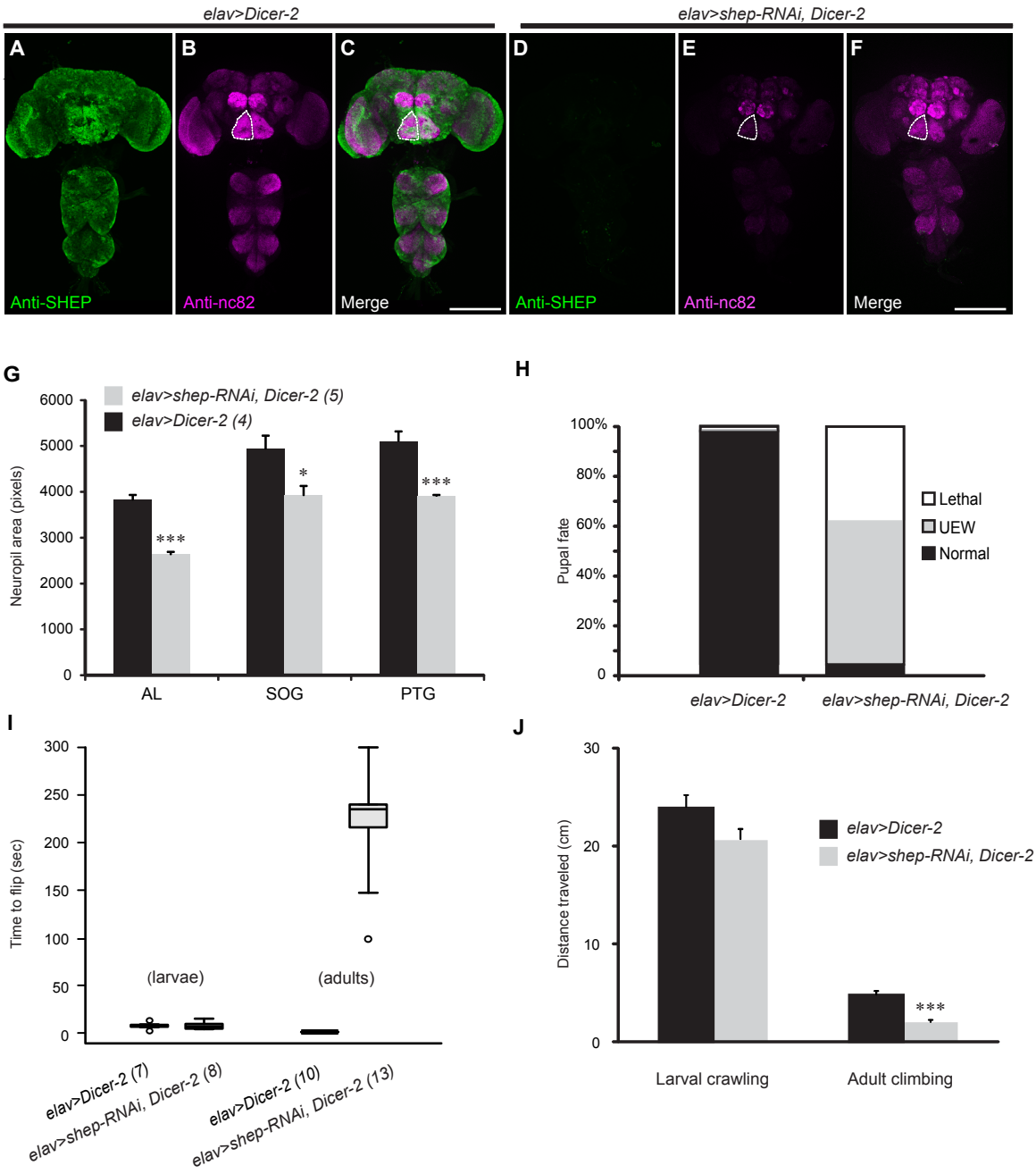
elav>Dicer-2
elav>shep-RNAi, Dicer-2
A
B
C
D
E
F
Anti-SHEP
Anti-nc82
Merge
Anti-SHEP
Anti-nc82
Merge
G
elav>shep-RNAi, Dicer-2 (5)
elav>Dicer-2 (4)
Neuropil area (pixels)
6000
5000
4000
3000
2000
1000
0
***
*
***
AL
SOG
PTG
H
Pupal fate
100%
80%
60%
40%
20%
0
Lethal
UEW
Normal
elav>Dicer-2
elav>shep-RNAi, Dicer-2
I
Time to flip (sec)
300
250
200
150
100
50
0
(larvae)
(adults)
elav>Dicer-2 (7)
elav>shep-RNAi, Dicer-2 (8)
elav>Dicer-2 (10)
elav>shep-RNAi, Dicer-2 (13)
J
Distance traveled (cm)
30
20
10
0
elav>Dicer-2
elav>shep-RNAi, Dicer-2
***
Larval crawling
Adult climbing

Figure 5. Virgin *shep* mutant females displayed increased rejection of courting males. (A) Virgin females of all genotypes displayed the same latency to copulation with *Oregon R* males, but the mount latency was increased and copulation duration was decreased for $shep^{BG00836}/shep^{ED210}$ mutant females. Rescue with *UAS-shep* returned these values to control levels. The numbers following the genotypes are the sample sizes. (B) Post-copulation behaviors for the females in panel A. All latency and duration data were measured in seconds (panel A), and each index is the ratio of the duration of a given behavior over the 10 min post-copulation video recording period. Separate one-way ANOVAs were performed for each behavioral measure (copulation latency, P=0.891; mount latency, P= 0.000015; copulation duration, P= 0.000234; kicking index, P= 0.000027; grooming index, P= 0.035767; 3-leg grooming index, P= 0.000906). *P<0.05, **P<0.01, ***P<0.001, Tukey HSD post hoc test.

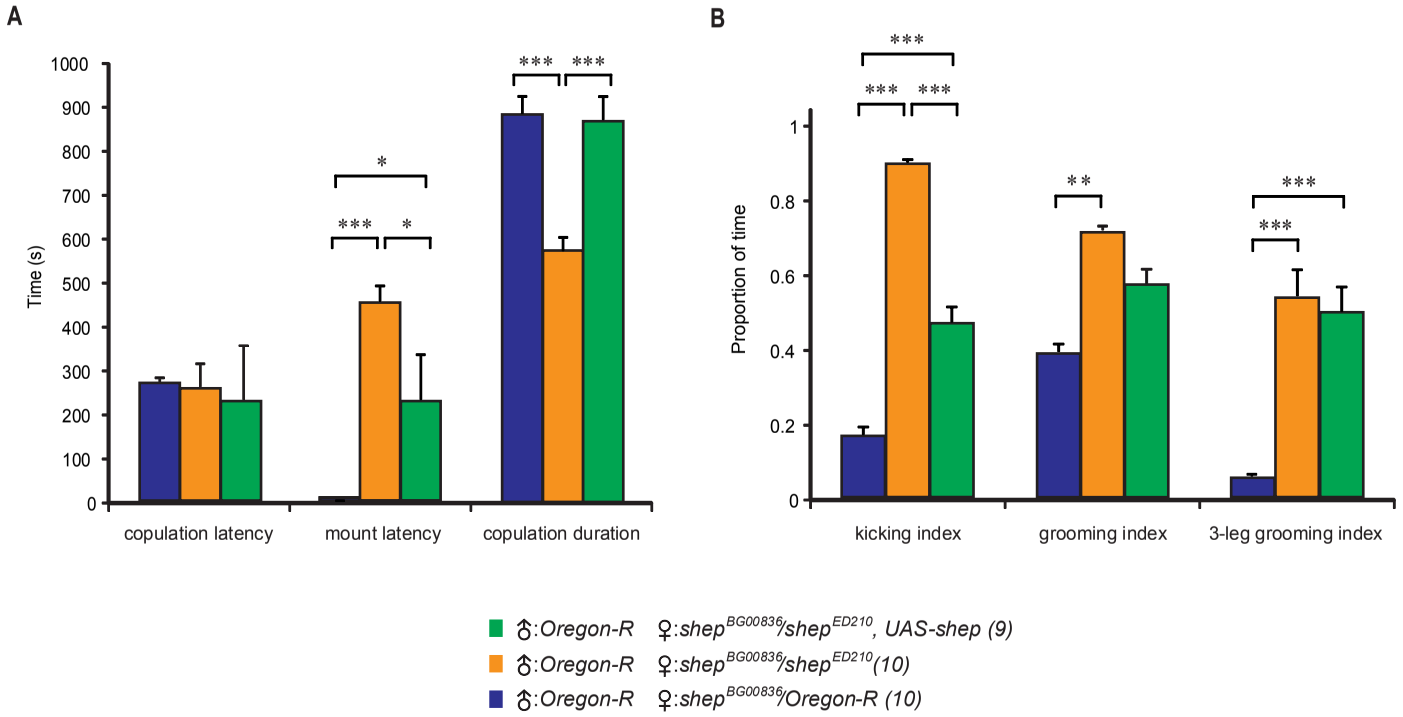
A
B
Time (s)
1000
900
800
700
600
500
400
300
200
100
0
copulation latency
mount latency
copulation duration
*
***
*
***
***
Proportion of time
1
0.8
0.6
0.4
0.2
0
kicking index
grooming index
3-leg grooming index
**
***
♂:Oregon-R ♀:shep^BG00836/shep^ED210, UAS-shep (9)
♂:Oregon-R ♀:shep^BG00836/shep^ED210 (10)
♂:Oregon-R ♀:shep^BG00836/Oregon-R (10)

Figure 6. Loss of *shep* in $shep^{BG00836}/shep^{ED210}$ animals reduced the soma area, branching of peripheral axons, and the bouton size distribution of bursicon neurons at the P14 pharate adult stage. (A-C) Immunostaining with anti-BURS antibodies showed the morphology of bursicon neurons in the abdominal ganglia. The most anterior cell on the right side is shown in the insets, with punctate peptide accumulation in the $shep^{BG00836}/shep^{ED210}$, *UAS-shep* cell labeled by arrows. (D-F) Reduced branching of the bursicon neuron axons in the peripheral arbor in a $shep^{BG00836}/shep^{ED210}$ pharate adult (E) and rescue of branching in a $shep^{BG00836}/shep^{ED210}$, *UAS-shep* animal (F). (G-I) A reduction in bouton sizes in *shep* mutant animals (H) and rescue after targeted expression of *shep* (I) was also observed in the peripheral axon arbor. Scale bars: 50 μm (insets in A-C, 10 μm). (J) Quantification of bursicon neuron soma areas for P14 pharate adults and wandering 3rd instar larvae. I performed a one-way ANOVA ($P<$ 0.000001, Tukey HSD post hoc, ***$P<0.001$) for the pharate adult values and a Student's *t*-test ($P=0.934$) for the wandering 3rd instar larval values. (K) Results of Sholl analysis of branches in the peripheral axon arbor. The space between each of the concentric rings used to count intersecting axons was 50 μm. (L) Counts of boutons along all axons 50 μm proximal and distal to the first branch of the Ab_2Nv nerve (squares). *$P<0.05$ (two-way ANOVA, $P<0.00001$; Tukey HSD post hoc test). Scale bars: 100 μm.

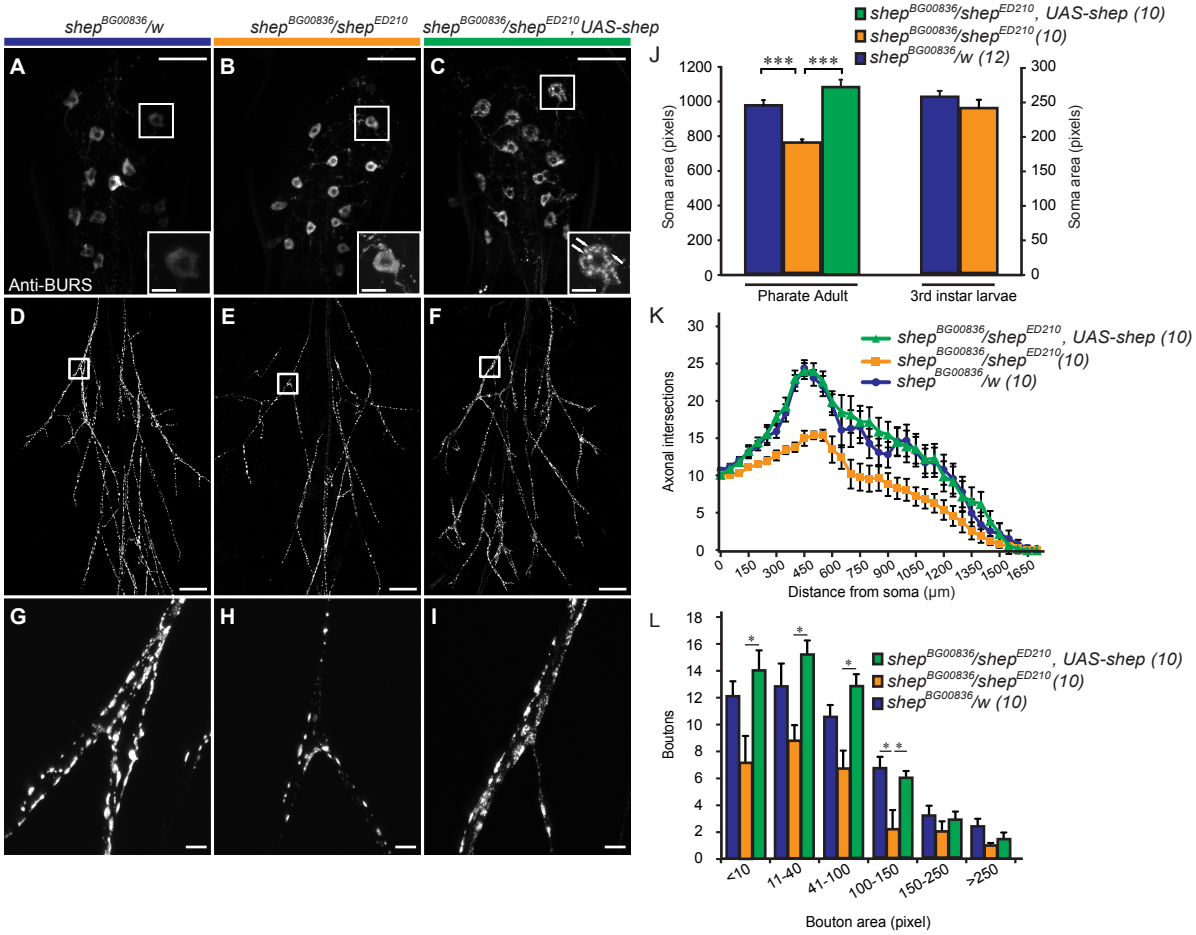
shep^BG00836/w
shep^BG00836/shep^ED210
shep^BG00836/shep^ED210, UAS-shep
A
B
C
Anti-BURS
D
E
F
G
H
I
J
shep^BG00836/shep^ED210, UAS-shep (10)
shep^BG00836/shep^ED210 (10)
shep^BG00836/w (12)
***
***
Soma area (pixels)
Pharate Adult
3rd instar larvae
K
shep^BG00836/shep^ED210, UAS-shep (10)
shep^BG00836/shep^ED210 (10)
shep^BG00836/w (10)
Axonal intersections
Distance from soma (μm)
L
shep^BG00836/shep^ED210, UAS-shep (10)
shep^BG00836/shep^ED210 (10)
shep^BG00836/w (10)
Boutons
<10
11-40
41-100
100-150
150-250
>250
Bouton area (pixel)

Figure 7. Reporter gene expression patterns for 30 insertions with expression in neurons. Each line was crossed to *UAS-mCD8::GFP* prior to isolation of the CNS at the wandering 3rd instar larval stage, and representative confocal z-series projections of fixed tissues are shown. Arrowheads indicate expression in the ring gland, and asterisks denote expression in the mushroom bodies. Scale bar: 50μm.

This figure was adapted and modified from Chunjing Qu's dissertation (QU 2010), and it was part of our publication of this chapter in my dissertation (CHEN *et al.* 2014).

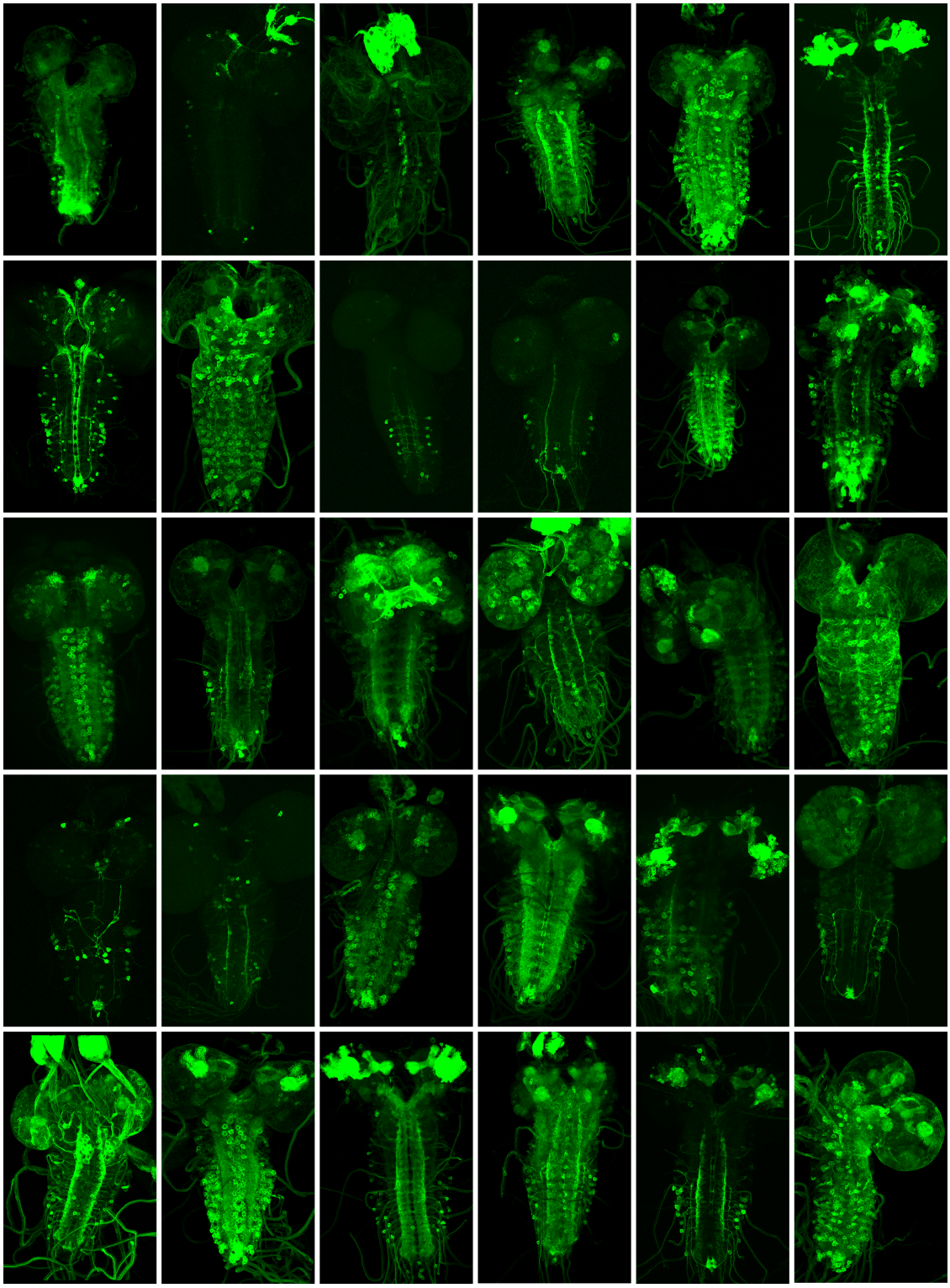

Figure 8. Patterns of splice-trap reporter gene expression in CCAP neurons in the wandering 3rd instar larval CNS. We found 17 insertions that drove expression in CCAP neurons, which are indicated with circles on the schematic CNS diagrams. The relative intensities of GFP reporter expression (mCD8::GFP, subjective scale) are indicated with different colors, and CCAP neurons with no detectable expression of the reporter are indicated with open circles. If there was no reporter expression in the brain lobes or ventral nerve cord, those regions of the CNS are not shown.

This figure was adapted and modified from Chunjing Qu's dissertation (QU 2010), and it was part of our publication of this chapter in my dissertation (CHEN *et al.* 2014).

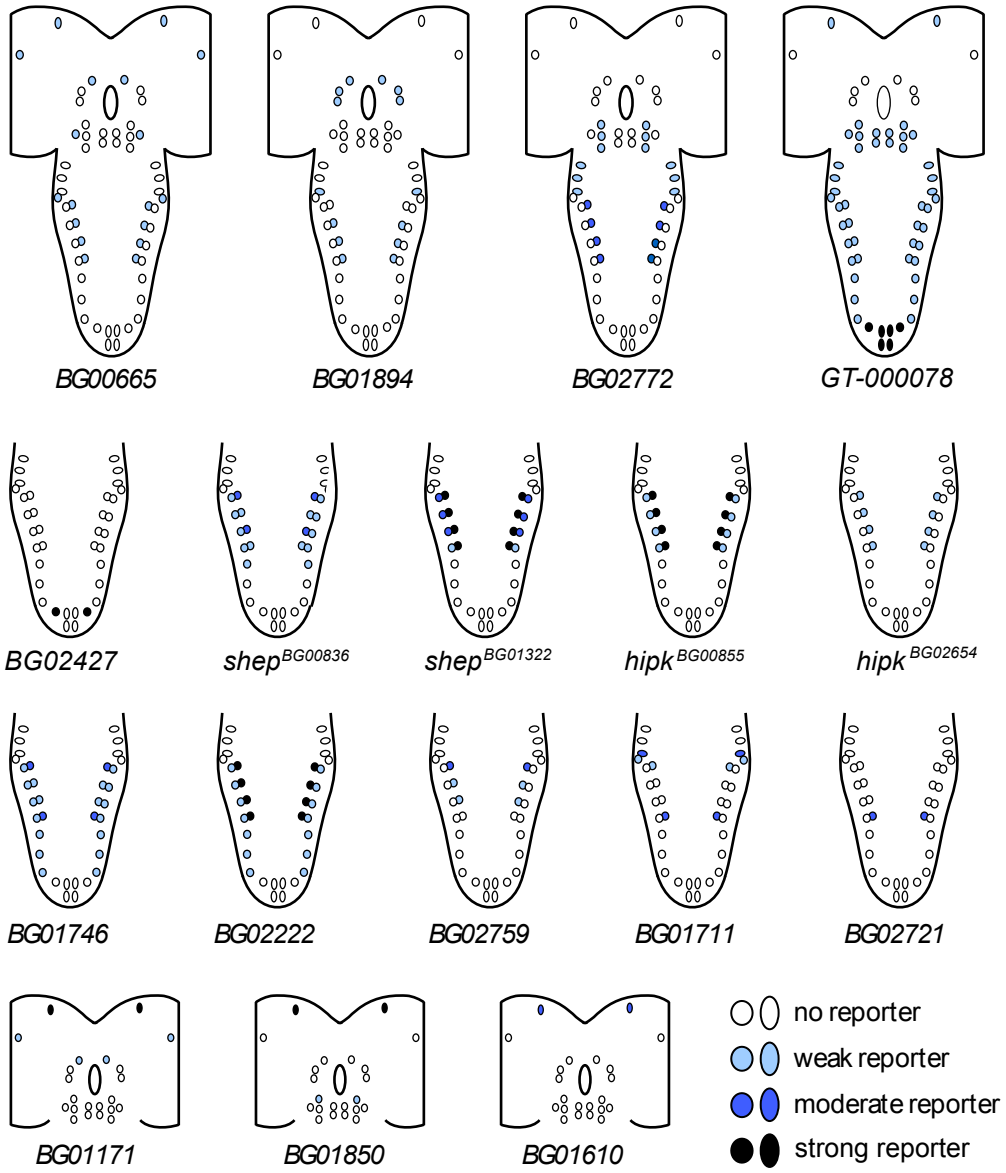
BG00665
BG01894
BG02772
GT-000078
BG02427
shep BG00836
shep BG01322
hipk BG00855
hipk BG02654
BG01746
BG02222
BG02759
BG01711
BG02721
BG01171
BG01850
BG01610
no reporter
weak reporter
moderate reporter
strong reporter

Figure 9. Reporter gene expression for the two *shep* splice-trap insertions, *BG00836* and *BG01322*, in multiple types of peptidergic neurons. (A-B) Co-localization of immunostaining with the PT2 antiserum (magenta) and mCD8::GFP reporter expression driven by *BG00836* (panel A) and *BG01322* (panel B). (C-F) Co-localization of anti-Furin 1 immunostaining (magenta) and mCD8::GFP reporter expression driven by *BG00836* (panels C and E) and *BG01322* (panels D and F). Panels C and D are ventral views of a portion of the ventral nerve cord, and panels E and F are dorsal views. Arrows: examples of colocalization of the immunosignal and reporter gene expression. Scale bars: 50 μm.

This figure was adapted and modified from Chunjing Qu's dissertation (QU 2010), and it was part of our publication of this chapter in my dissertation (CHEN *et al.* 2014).

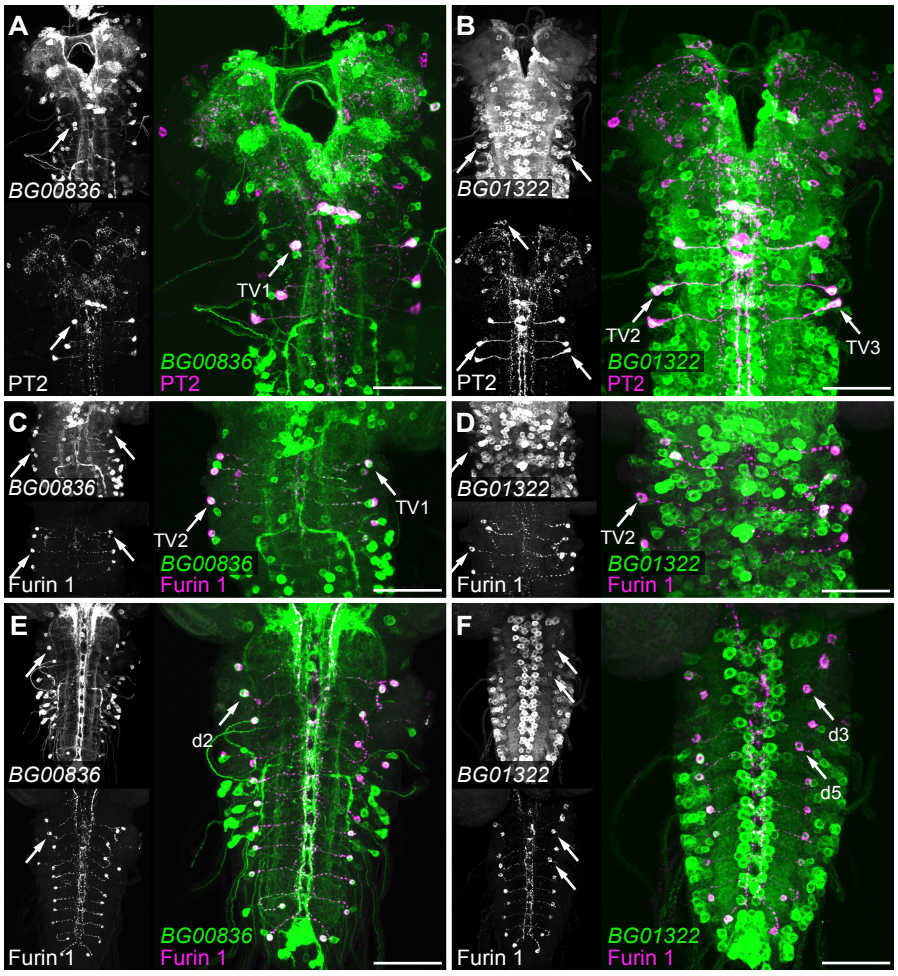
A
BG00836
PT2
TV1
BG00836
PT2
B
BG01322
PT2
TV2
TV3
BG01322
PT2
C
BG00836
Furin 1
TV2
TV1
BG00836
Furin 1
D
BG01322
Furin 1
TV2
BG01322
Furin 1
E
BG00836
Furin 1
d2
BG00836
Furin 1
F
BG01322
Furin 1
d3
d5
BG01322
Furin 1

Figure 10. Selected splice-trap expression patterns that contained bursicon neurons. (A-B) Co-localization of immunostaining with an anti-BURS antiserum (magenta) and mCD8::GFP reporter expression (green) driven by *BG02222* (panel A) and *BG00836* (panel B) in wandering 3rd instar larvae. (C-D) At the P14 pharate adult stage, both *BG02222* and *BG00836* drove reporter expression in all 14 bursicon neurons in the abdominal ganglia. Arrows, examples of abdominal bursicon neurons with co-localization of the two markers. Scale bars: 50 μm.

This figure was adapted and modified from Chunjing Qu's dissertation (QU 2010), and it was part of our publication of this chapter in my dissertation (CHEN *et al.* 2014).

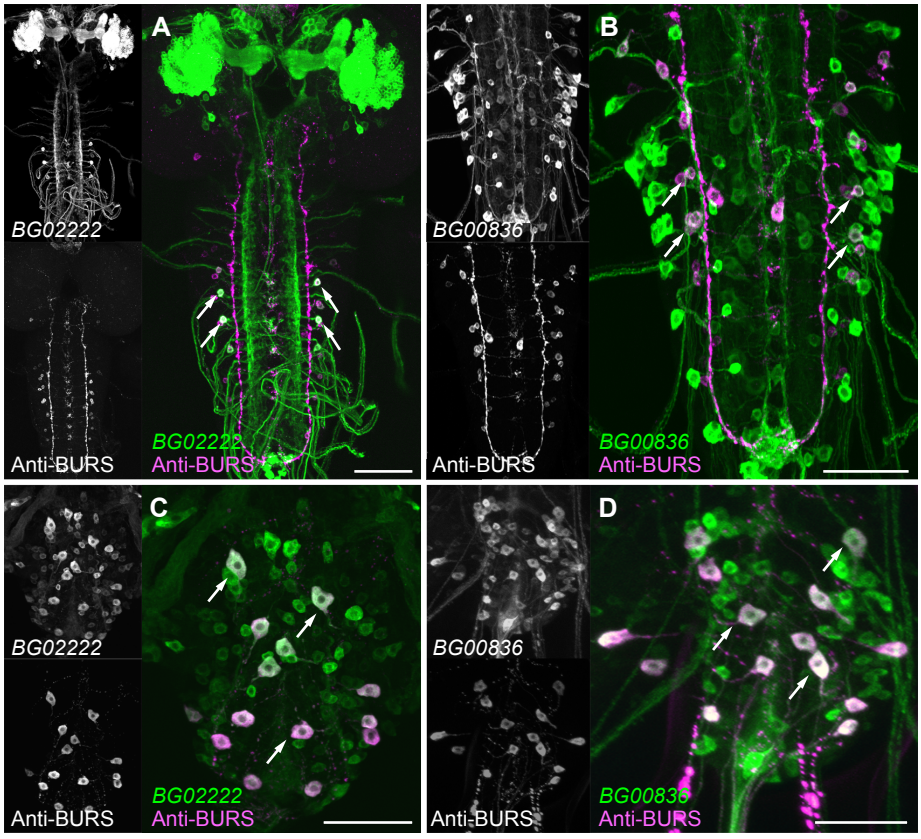
A
BG02222
Anti-BURS
BG02222
Anti-BURS
B
BG00836
Anti-BURS
BG00836
Anti-BURS
C
BG02222
Anti-BURS
BG02222
Anti-BURS
D
BG00836
Anti-BURS
BG00836
Anti-BURS

Figure 11. Loss of wing sensory neurons and appearance of ectopic wing veins following loss of *shep*. (A-D) 40% (23 out of 57) $shep^{BG00836}$ homozygotes had an ectopic vein on the posterior crossvein (arrows) that was not found in $shep^{BG00836}/w$ control flies. Panels C-D are higher magnification views of the region containing the posterior crossvein. Scale bars: A and B, 200 μm; C and D, 100 μm. (E) At the P14 pharate adult stage, sensory neurons on the wings of *D42>Dicer-2, mCD8::GFP* flies had proximal neurite projections. (F) In *shep* RNAi animals (*D42>shep-RNAi, Dicer-2, mCD8::GFP*), the proximal projections and most sensory neuron somata were absent. Scale bars: 100 μm. (G-H) Higher magnification views of the developing wing border in the highlighted box in panel E and F. Arrows, sensory neurons; Arrowheads, neurite projections of the sensory neurons; Open arrowheads, bristle neurites. Scale bars: 10 μm.

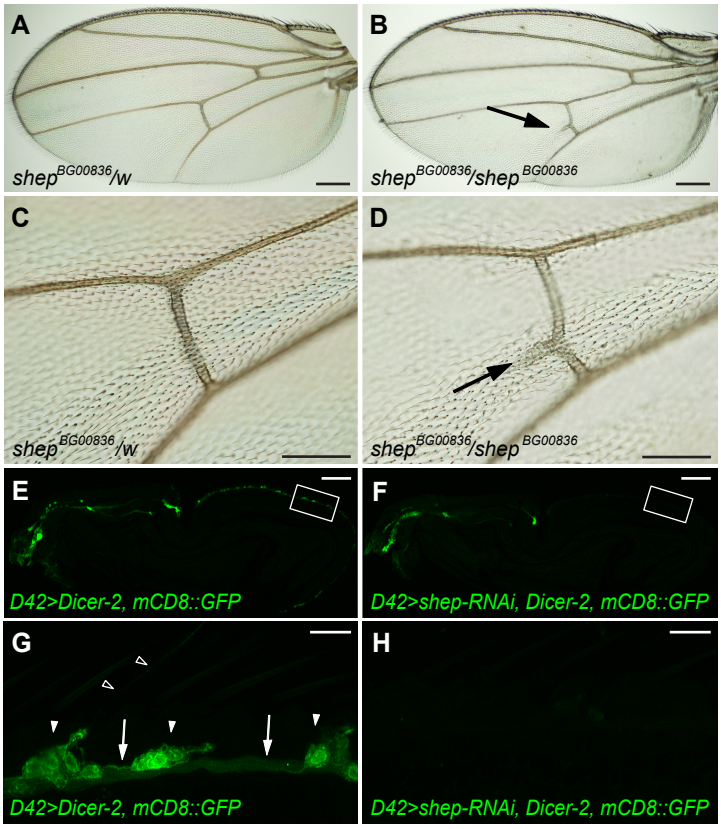
A
shep^BG00836/w
B
shep^BG00836/shep^BG00836
C
shep^BG00836/w
D
shep^BG00836/shep^BG00836
E
D42>Dicer-2, mCD8::GFP
F
D42>shep-RNAi, Dicer-2, mCD8::GFP
G
D42>Dicer-2, mCD8::GFP
H
D42>shep-RNAi, Dicer-2, mCD8::GFP

Figure 12. Embryonic *shep* mRNA and SHEP protein expression patterns. (A-B) Ectopic expression of *shep* in stage 11-12 *engrailed-Gal4/UAS-shep* embryos was detected by *in situ* hybridization (A) and immunostaining (B) with an anti-SHEP antiserum. (C-F) Expression of *shep* was detected in oocytes (arrows in panels C-D) in the ovaries of P14 stage pharate adult females and in syncytial blastoderm embryos (panels E-F) by *in situ* hybridization (blue) and immunostaining with antibodies to SHEP (gray). (G-N) Expression of *shep* in early embryonic stages detected by *in situ* hybridization. Each top-bottom pair of images shows signals from the same embryo with dark field and köhler illumination. Zygotic *shep* was first detected at stage 7 in the pro-cephalic neurogenic region (arrow, panel K). (O-V) In later embryonic stages, the expression of *shep* expanded to include the entire central and peripheral nervous systems. Each top-bottom pair of images are lateral (top) and ventral (bottom) views of the same embryos. Arrows, putative mesectoderm; open arrowheads, ventral neurogenic region; arrowheads, peripheral nervous system. (W) Anti-SHEP immunostaining produced labeling in the CNS, PNS (arrows), and the antennomaxillary complex and labral sensory complex (arrowhead). (X) Control *in situ* hybridization with the sense probe in an *Oregon R* embryo. The embryonic stage is indicated in the lower right corner of each panel. Scale bars: (C, D), 25 μm; (all other panels), 50 μm.

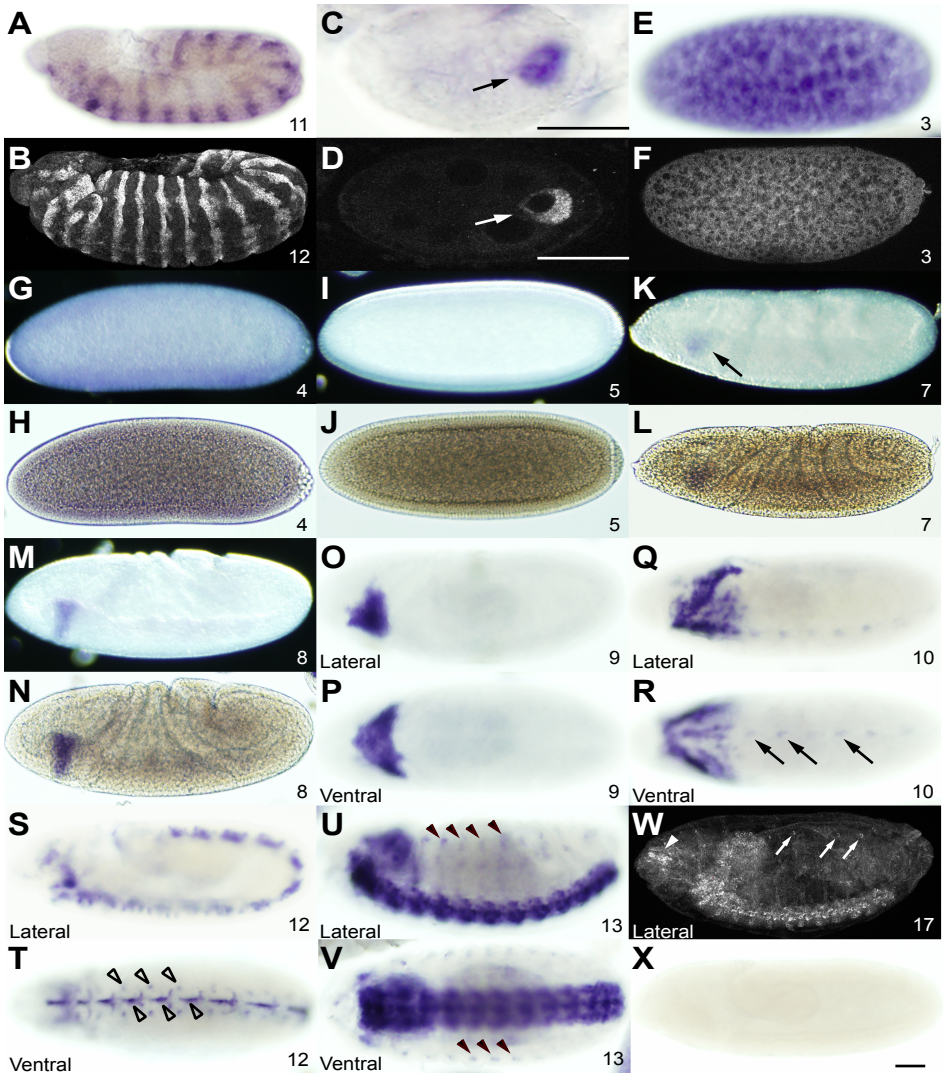
A
11
C
E
3
B
12
D
F
3
G
4
I
5
K
7
H
4
J
5
L
7
M
8
O
Lateral
9
Q
Lateral
10
N
8
P
Ventral
9
R
Ventral
10
S
Lateral
12
U
Lateral
13
W
Lateral
17
T
Ventral
12
V
Ventral
13
X

Figure 13. Loss of *shep* led to reduced levels of multiple presynaptic markers in the larval and pharate adult CNS. (A-B) Anti-nc82 immunostaining for the active zone protein Bruchpilot in wandering 3rd instar *elav>shep-RNAi, Dicer-2* larvae displayed lower signal intensity (panel B) than in *elav>Dicer-2* control larvae (panel A). (C-F) Immunostaining in P14 pharate adult CNS for Synapsin and Choline acetyltransferase (ChAT) revealed lower levels of both presynaptic markers in *shep* RNAi animals (D, F) than in *elav>Dicer-2* controls (C, E). Scale bars: 200 μm. G) Quantification of neuropil area for the anti-nc82 immunostaining in wandering 3rd instar larvae. The ventral nerve cord neuropil area (dashed lines, panels A and B) was unchanged in *elav>shep-RNAi, Dicer-2* animals at the wandering 3rd instar stage (P=0.143, Student's *t*-test).

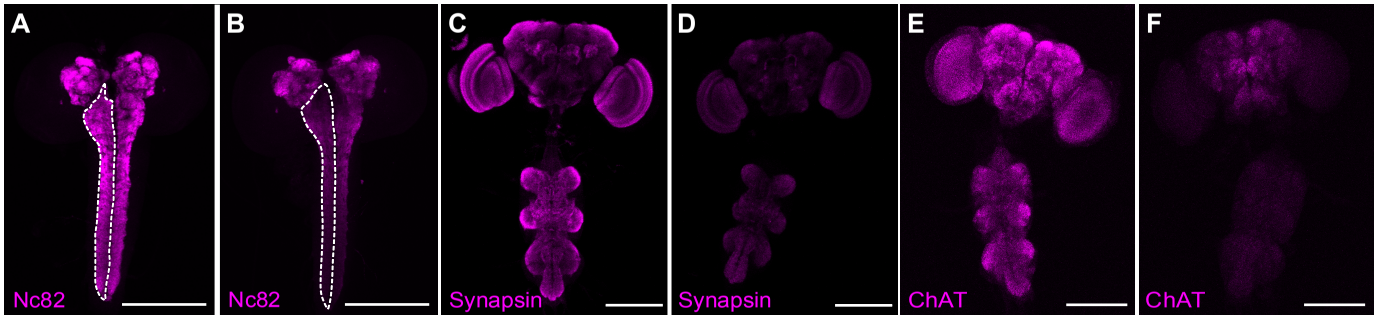
A
B
C
D
E
F
Nc82
Nc82
Synapsin
Synapsin
ChAT
ChAT
elav>Dicer-2
elav>shep-RNAi, Dicer-2
elav>Dicer-2
elav>shep-RNAi, Dicer-2
elav>Dicer-2
elav>shep-RNAi, Dicer-2

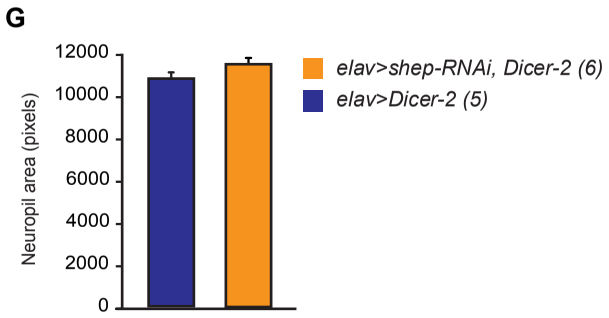
G
12000
10000
8000
6000
4000
2000
0
Neuropil area (pixels)
elav>shep-RNAi, Dicer-2 (6)
elav>Dicer-2 (5)

Figure 14. Loss of *shep* resulted in reduced life span. (A) Pan-neuronal *shep* RNAi led to shorter life span. The running percentage of surviving adults was plotted for *elav>shep-RNAi, Dicer-2* and *elav>Dicer-2* adult flies on regular food. (B-D) Reduced starvation resistance was detected in multiple *shep* mutants. Cumulative survival under starvation conditions was calculated (see methods) for $shep^{BG00836}$>*shep-RNAi*, $shep^{BG00836}$ homozygotes, $shep^{BG00836}$/$shep^{ED210}$ mutants, and $shep^{BG00836}$/$shep^{ED210}$, *UAS-shep* rescue flies. In each panel, the *shep* loss-of-function genotype is labeled in orange. The results for *shep* heterozygotes are shown in blue and magenta, and the results for flies rescued with *UAS-shep* are shown in green. Sample sizes are listed in parentheses following each genotype.

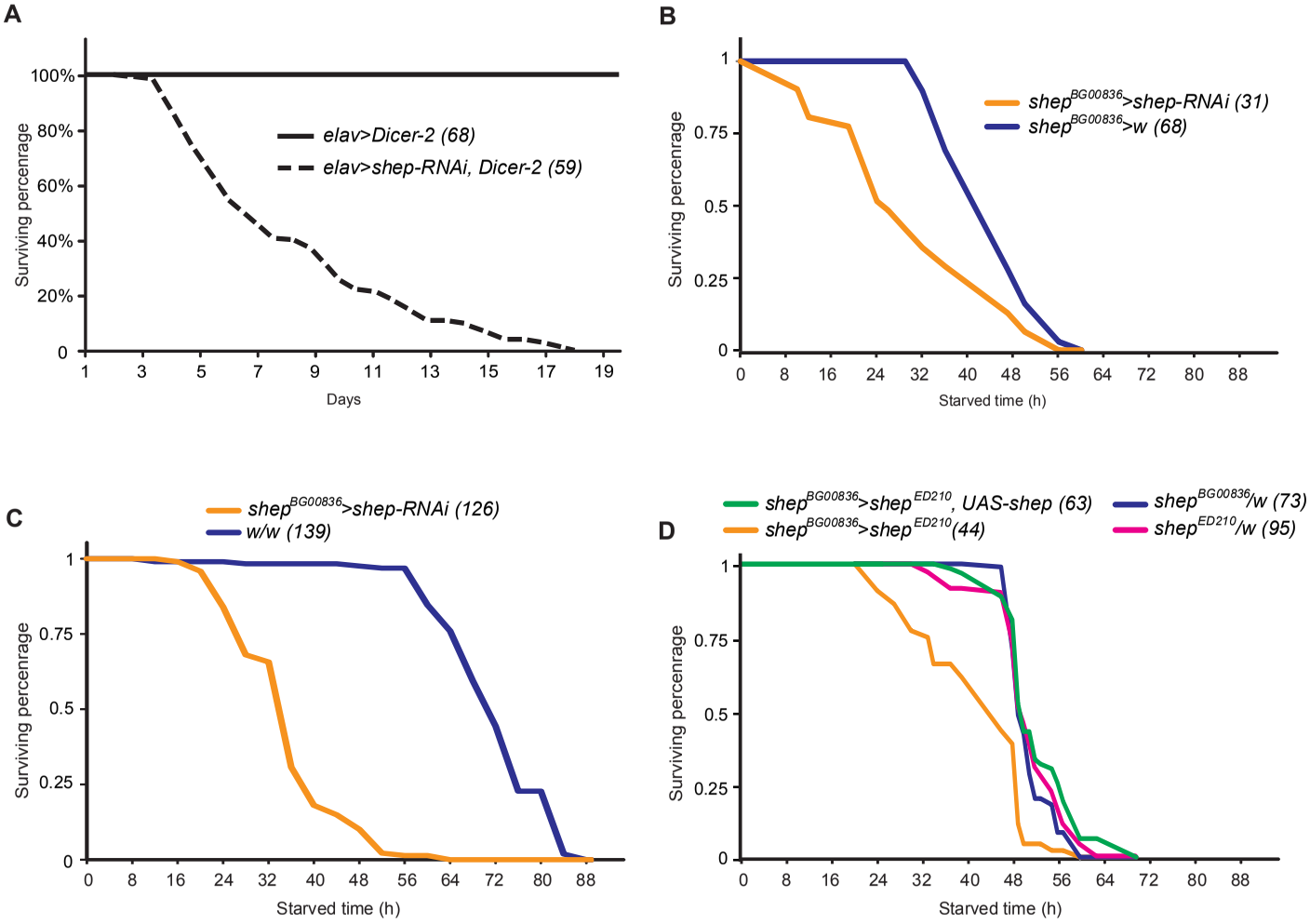
A
100%
80%
60%
40%
20%
0
Surviving percenrage
elav>Dicer-2 (68)
elav>shep-RNAi, Dicer-2 (59)
1 3 5 7 9 11 13 15 17 19
Days
B
1
0.75
0.5
0.25
0
Surviving percenrage
shepBG00836>shep-RNAi (31)
shepBG00836>w (68)
0 8 16 24 32 40 48 56 64 72 80 88
Starved time (h)
C
shepBG00836>shep-RNAi (126)
w/w (139)
1
0.75
0.5
0.25
0
Surviving percenrage
0 8 16 24 32 40 48 56 64 72 80 88
Starved time (h)
D
shepBG00836>shepED210, UAS-shep (63)
shepBG00836>shepED210(44)
shepBG00836/w (73)
shepED210/w (95)
1
0.75
0.5
0.25
0
Surviving percenrage
0 8 16 24 32 40 48 56 64 72 80 88
Starved time (h)

Figure 15. Pan-neuronal loss of *shep* produced larvae that remained near the center of apple-juice plates during locomotor behavior assays. (A) Apple juice-agarose plates were placed on a grid of concentric circles that defined four zones from the center to the periphery. (B) Representative 10-minute crawling trails for *elav>Dicer-2* and *elav>shep-RNAi, Dicer-2* wandering 3rd instar larvae. (C) The percentage of time spent by *elav> Dicer-2* and *elav>shep-RNAi, Dicer-2* larvae in each of the four concentric zones. The number of animals for each genotype is indicated in parentheses. **P*<0.05; Separate Student's *t*-tests with Bonferroni correction were performed for each zone.

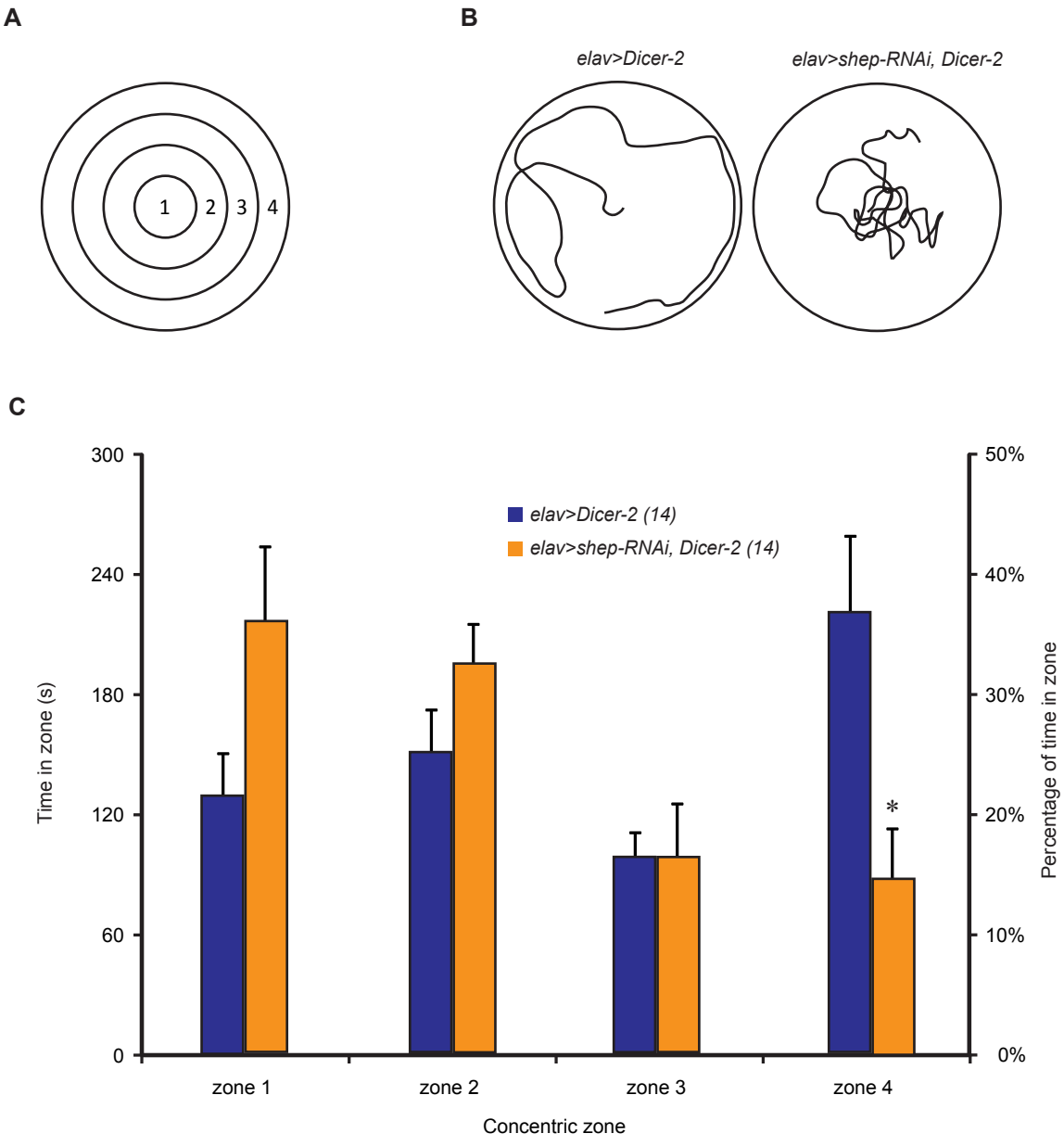
A
1
2
3
4
B
elav>Dicer-2
elav>shep-RNAi, Dicer-2
C
elav>Dicer-2 (14)
elav>shep-RNAi, Dicer-2 (14)
Time in zone (s)
Percentage of time in zone
300
240
180
120
60
0
50%
40%
30%
20%
10%
0%
*
zone 1
zone 2
zone 3
zone 4
Concentric zone

Figure 16. Loss of SHEP resulted in smaller bursicon neurons in P14 stage pharate adults but not in wandering 3rd instar larvae. (A-E) Anti-SHEP immunostaining of *shep* loss-of-function mutants at the P14 pharate adult stage. Lower SHEP levels were observed in all of the *shep* mutant backgrounds, but *elav>shep-RNAi, Dicer-2* displayed the greatest reduction of SHEP levels in the CNS. (F) In P14 stage pharate adults, I observed reduced bursicon neuron soma areas in hypomorphic *shep* mutant backgrounds, which included $shep^{Exel6103}/shep^{Exel6104}$, $shep^{BG00836}$ homozygotes, and *ccap>shep-RNAi*. (G) Bursicon neuron soma areas were unaffected in wandering 3rd larval instar *shep* mutants. The mutant backgrounds included *ccap>shep-RNAi, Dicer-2*, which was the strongest *shep* loss-of-function genotype, as judged by the impacts on branching in the peripheral axon arbor (Figure 17). The number of animals for each genotype is indicated in parentheses. **P*<0.05, ***P*<0.01, ****P*<0.001, Student's *t*-test. Scale bar: 200 μm.

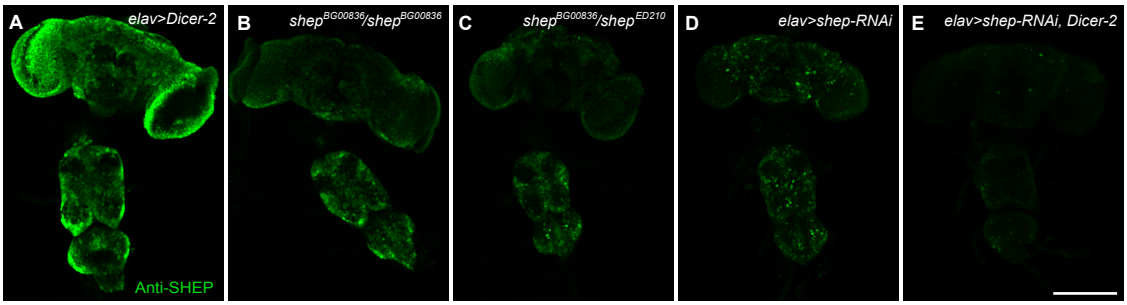
A
elav>Dicer-2
Anti-SHEP
B
shep^BG00836/shep^BG00836
C
shep^BG00836/shep^ED210
D
elav>shep-RNAi
E
elav>shep-RNAi, Dicer-2

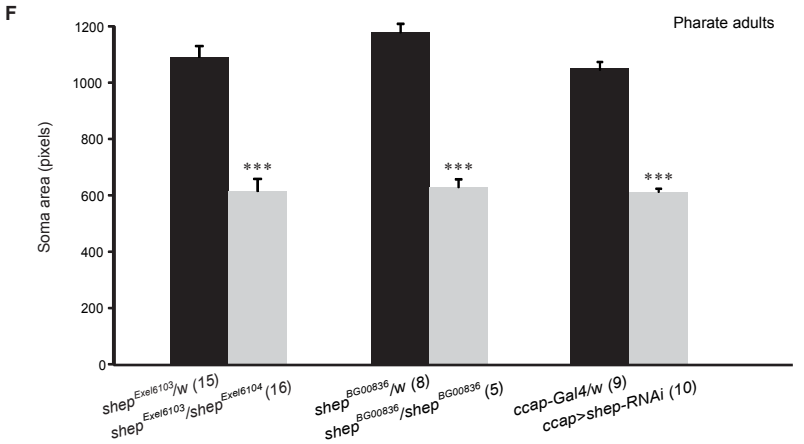
F
Pharate adults
Soma area (pixels)
1200
1000
800
600
400
200
0
***
***
***
shep^Exel6103/w (15)
shep^Exel6103/shep^Exel6104 (16)
shep^BG00836/w (8)
shep^BG00836/shep^BG00836 (5)
ccap-Gal4/w (9)
ccap>shep-RNAi (10)

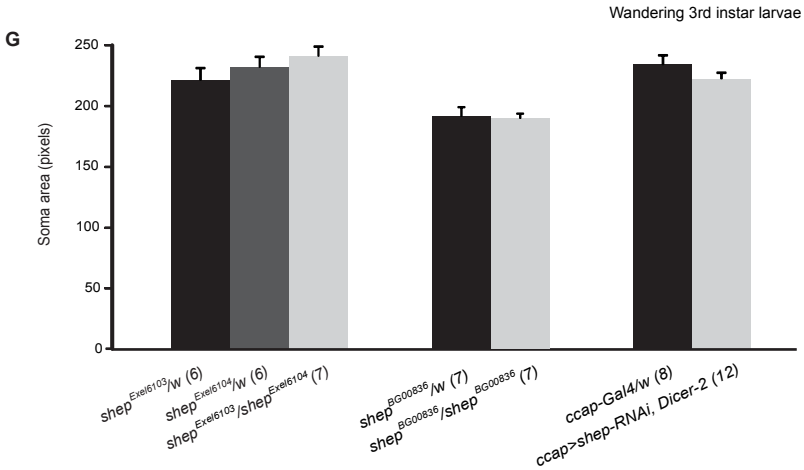
G
Wandering 3rd instar larvae
Soma area (pixels)
250
200
150
100
50
0
shep^Exel6103/w (6)
shep^Exel6104/w (6)
shep^Exel6103/shep^Exel6104 (7)
shep^BG00836/w (7)
shep^BG00836/shep^BG00836 (7)
ccap-Gal4/w (8)
ccap>shep-RNAi, Dicer-2 (12)

Figure 17. Bursicon neuron peripheral axon projections and synaptic terminals were visualized by anti-BURS immunostaining or genetic labeling with the membrane-localized fusion protein, mCD8::GFP. (A-C) Peripheral axons in the abdominal nerves of a *ccap>shep-RNAi, Dicer-2, mCD8::GFP* P14 stage pharate adult. Although the anti-BURS immunostaining (magenta) is more restricted to boutons than the mCD8::GFP labeling (green), each axon in the nerve can be clearly resolved at lower magnification (panels A-C), which captures most of the peripheral axon arbor, and at higher magnification (insets; region of the abdominal nerve trunk indicated by the white boxes in panels A-C). Within the abdominal nerve trunk, there is much less bursicon accumulation than in the distal boutons, but anti-BURS immunostaining still permits the visualization of each axon. Arrows, boutons; arrowheads, axons. Scale bars: A-C, 100 μm; insets, 5 μm. (D-F) Labeling of the bursicon neuron terminals on muscles 12-13 of the 2nd abdominal segment with mCD8::GFP (green) and anti-BURS immunostaining (magenta) in *ccap>shep-RNAi, Dicer-2, mCD8::GFP* wandering 3rd instar larvae. Arrows, boutons. Scale bar: 10 μm.

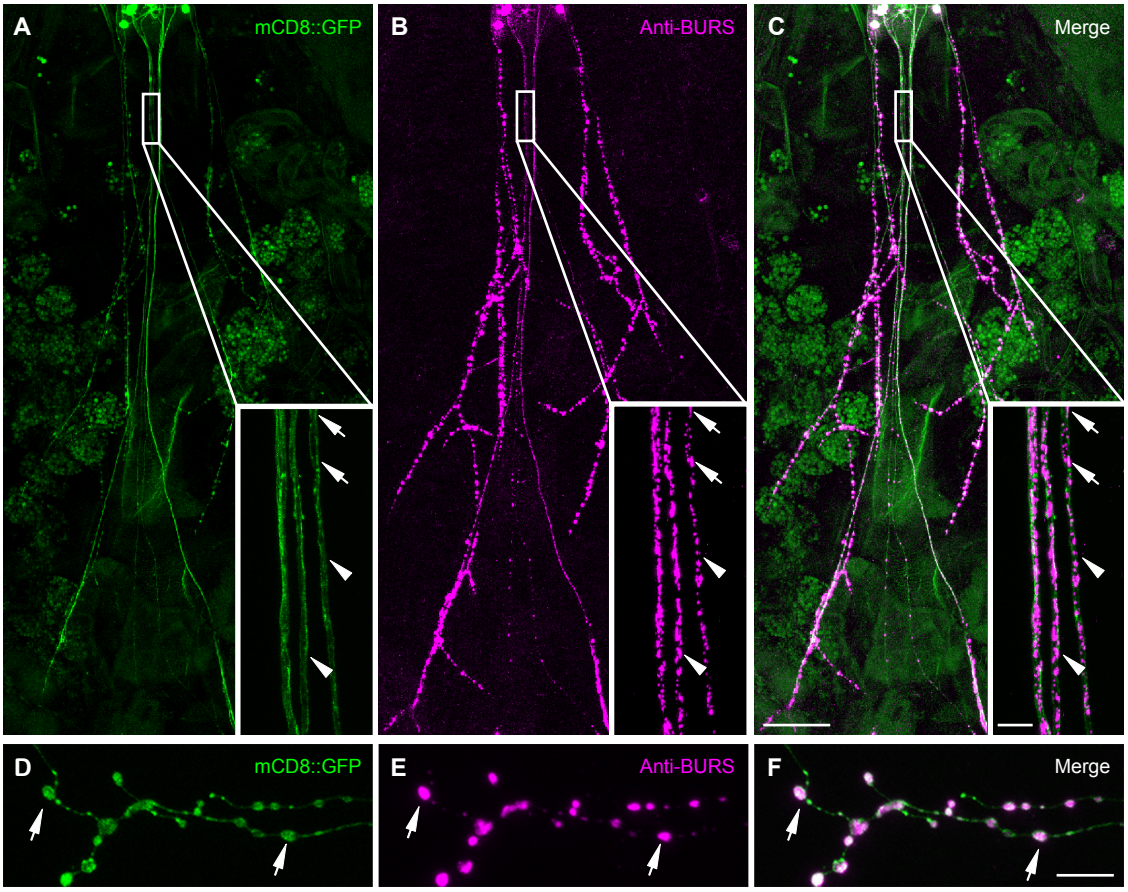
A
mCD8::GFP
B
Anti-BURS
C
Merge
D
mCD8::GFP
E
Anti-BURS
F
Merge

Figure 18. *shep* promoted outgrowth of the peripheral projections of the bursicon neurons during metamorphosis. (A-C) Sholl analysis on the peripheral projections of P14 stage pharate adult bursicon neurons. For this analysis, I counted the number of axon intersections with nested, concentric rings, each with a 50 μm increase in radius from the next smallest ring. Sample sizes are listed in parentheses following each genotype. (D-I) In wandering 3rd instar larvae, the morphology of the neuromuscular junctions (NMJ) of the hypomorphic mutants $shep^{Exel6103}/shep^{Exel6104}$ (E), $shep^{BG00836}/shep^{ED210}$ (G), and *ccap>shep-RNAi, Dicer-2* (I) was similar to the morphology of the respective hemizygous controls (D, F, and H). (J-L) Binned counts of wandering 3rd instar larval NMJ boutons within size classes for *shep* loss-of-function animals. Sample sizes are listed in parentheses. Two-way ANOVAs, P=0.452479 (panel J), P=0.597591 (panel K), and P=0.271019 (panel L). Scale bars: 100 μm.

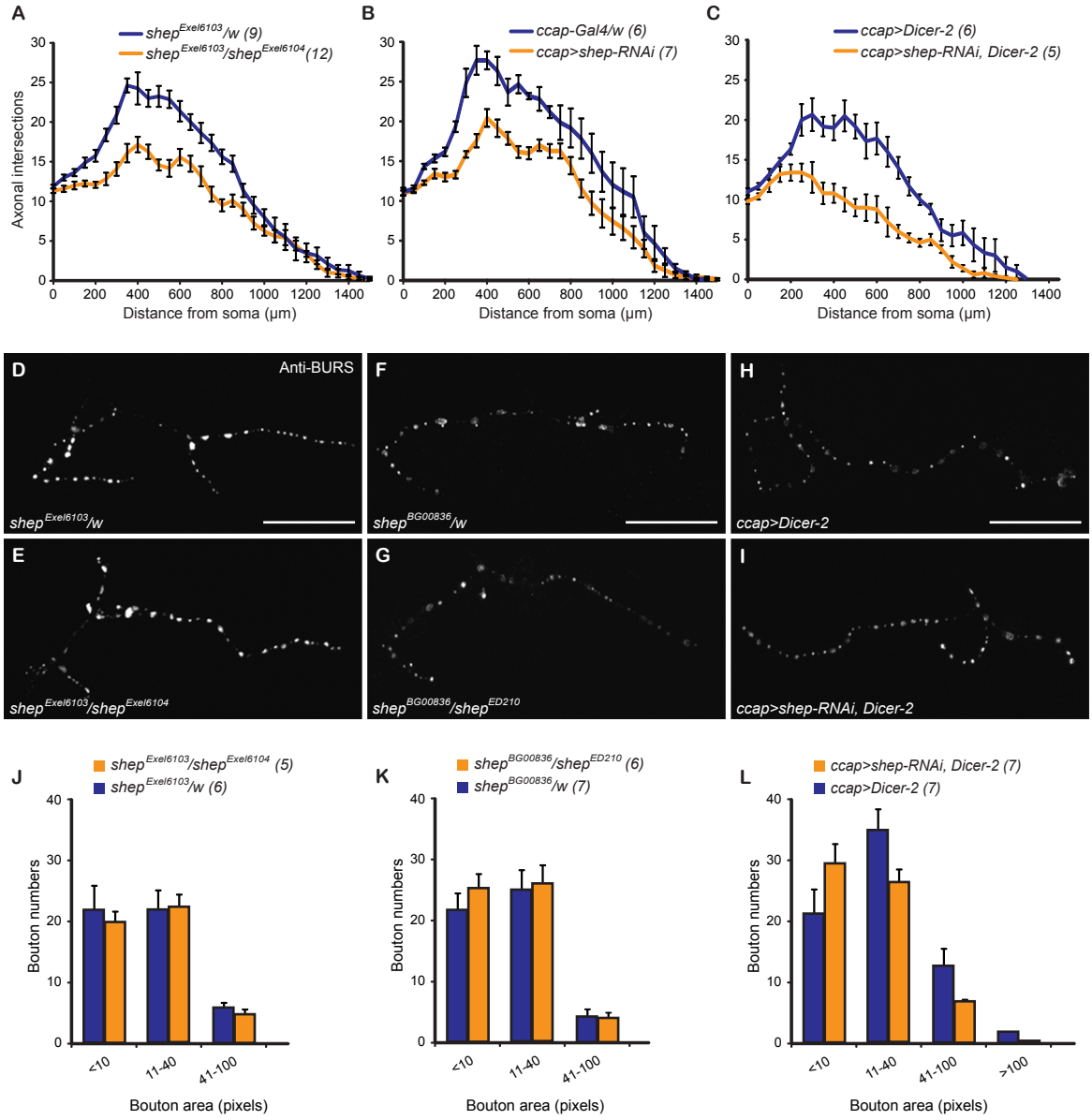
A
shep Exel6103 /w (9)
shep Exel6103 /shep Exel6104 (12)
Axonal intersections
Distance from soma (µm)
B
ccap-Gal4/w (6)
ccap>shep-RNAi (7)
Distance from soma (µm)
C
ccap>Dicer-2 (6)
ccap>shep-RNAi, Dicer-2 (5)
Distance from soma (µm)
D
Anti-BURS
shep Exel6103 /w
F
shep BG00836 /w
H
ccap>Dicer-2
E
shep Exel6103 /shep Exel6104
G
shep BG00836 /shep ED210
I
ccap>shep-RNAi, Dicer-2
J
shep Exel6103 /shep Exel6104 (5)
shep Exel6103 /w (6)
Bouton numbers
<10
11-40
41-100
Bouton area (pixels)
K
shep BG00836 /shep ED210 (6)
shep BG00836 /w (7)
Bouton numbers
<10
11-40
41-100
Bouton area (pixels)
L
ccap>shep-RNAi, Dicer-2 (7)
ccap>Dicer-2 (7)
Bouton numbers
<10
11-40
41-100
>100
Bouton area (pixels)

Videos

Video 1. Mounting of an *Oregon R* female by an *Oregon R* virgin male. The male mounted the female shortly after copulation started, and the female extended her wings to accept the male.

Video 2. Kicking of an *Oregon R* male by a $shep^{BG00836}/shep^{ED210}$ virgin female after the onset of copulation. The female continued to kick the male during copulation and did not extend her wings to accept mounting by the male.

Video 3. Three-leg grooming by a $shep^{BG00836}/shep^{ED210}$ female immediately after copulation was completed. The predominant grooming pattern involved only the legs, with the two metathoracic legs rubbed together with one of the mesothoracic legs (Figure 5). Correspondingly, the proportion of time spent grooming the wings and abdomen was reduced.

Video 4. Two-leg grooming of an *Oregon R* female immediately after copulation. Grooming of the wings and abdomen was performed with the two metathoracic legs.

Video 5. Expulsion of what appears to be seminal fluid and the mating plug by a $shep^{BG00836}/shep^{ED210}$ female immediately after copulation. The mated $shep^{BG00836}/shep^{ED210}$ female groomed with three legs and then expelled material after ovipositor extrusion. There is a one-minute pause in the video, during which the fluid was first visible after repetitive ovipositor extrusion.

Chapter III: A deficiency screen for modifiers of *alan shepard* (*shep*) function during nervous system metamorphosis

Abstract

The *alan shepard* (*shep*) gene promotes neuronal outgrowth during metamorphic remodeling in *Drosophila.* The SHEP protein contains RNA recognition motifs, binds to DNA, and interacts with *gypsy* insulators. SHEP has also been implicated through genetic or RNA interference (RNAi) screens in gravitaxis, fat storage, starvation resistance, and cell size determination. To shed light on the molecular mechanisms by which SHEP regulates metamorphic outgrowth of neurons, I conducted a genetic modifier screen for *shep* suppressors. I screened a total of 702 deficiencies that covered 86% of the euchromatic genes for suppression of the wing expansion defects caused by loss of *shep*. I isolated 33 deficiencies as candidate suppressors. From this set, I identified 12 deficiencies that partially suppressed the morphological defects seen in *shep* mutant bursicon neurons. RNAi tests and crosses with mutant alleles for individual genes led to the identification of *Daughters against dpp* (*Dad*) and *Olig family* (*Oli*) as *shep* suppressor genes, and both rescued neurites of the bursicon neuron in the subesophageal ganglia. *Oli* encodes a transcription factor with unknown downstream targets. *Dad* encodes an inhibitory Smad protein that inhibits phosphorylation of R-Smad by activated Bone morphogenetic protein (BMP) receptors, thus implicating BMP signaling in the control of neurite outgrowth from the bursicon neurons during metamorphosis. In addition, I found that the *su(Hw)* gene, which encodes a *gypsy* insulator protein that is known to interact with SHEP, suppressed the wing expansion defects causes by loss of *shep*, although I did not observe rescue of bursicon neuron outgrowth by *su(Hw)*. These findings highlight novel genetic

interactions that are important for controlling neurite growth in mature, terminally differentiated neurons.

Introduction

The nervous systems of holometabolous insects, such as *Drosophila melanogaster*, undergo dramatic structural and functional remodeling during metamorphosis (WEEKS 2003; WILLIAMS and TRUMAN 2005b). In addition, there are many *Drosophila* tools available for the precise manipulation and analysis of metamorphosing neurons, which serve as powerful models for understanding the mechanisms by which mature neurons can be structurally remodeled (WATTS *et al.* 2003; ZHU *et al.* 2003; WILLIAMS and TRUMAN 2005a; AWASAKI *et al.* 2006; ZHAO *et al.* 2008; DURA *et al.* 2009; KIRILLY *et al.* 2009). The *alan shepard (shep)* gene has been investigated for its critical role during metamorphic neuronal remodeling and loss of *shep* leads to adult-specific defects in many neurons (CHEN *et al.* 2014). In addition, *shep* has been identified in multiple genetic screens for factors involved in gravitaxis (ARMSTRONG *et al.* 2006), regulation of fat storage (REIS *et al.* 2010), starvation resistance (HARBISON *et al.* 2004), and cell size determination (BJORKLUND *et al.* 2006). SHEP proteins bind the insulator proteins Suppressor of Hairy wing [SU(HW)] and Modifier of mdg4 [MOD(MDG4)] to suppress DNA insulator activity specifically in the nervous system (MATZAT *et al.* 2012). The vertebrate orthologs of *shep*, which belong to the MSSP (*c-myc* single strand binding protein) family, also regulate a variety of biological processes, including DNA replication, gene expression, cell transformation, and apoptosis, by binding to

DNA, RNA, or proteins (KIMURA *et al.* 1998a; NIKI *et al.* 2000a; NIKI *et al.* 2000c; NOMURA *et al.* 2005a).

Here, I have taken a modifier screening approach to identify candidate molecular mechanisms by which *shep* functions to regulate neuronal remodeling. In the absence of *a priori* models regarding a gene's function, this approach can reveal strong molecular interactions that are critical to a given process (WARD *et al.* 2003; KAPLOW *et al.* 2007; KUCHERENKO *et al.* 2008). The method is most effective when it is based on obvious phenotypes that are sensitive to genetic modification. Wing expansion is one such phenotype (Dahong Chen, Tingting Gu, Tao Zhao, and Randall Hewes, unpublished observations; MA *et al.* 2012), and it is also linked to the function of neurons, the bursicon cells, that undergo metamorphic remodeling (ZHAO *et al.* 2008). Under the conditions used for this modifier screen, bursicon neuron-targeted *shep* RNAi led to a intermediate wing expansion and neuronal remodeling phenotypes that could be either enhanced or suppressed by introduction of genetic modifiers. By crossing 702 deficiency strains to a *shep* RNAi strain, I screened ~86% of the *Drosophila melanogaster* euchromatic genes and identified 33 regions containing candidate suppressors. Further cellular analysis of 17 unique regions narrowed the set to 12 deficiencies that suppressed defects in neurite morphology or soma growth observed in the bursicon neurons. By mapping with RNAi to individual loci, I successfully identified two suppressor genes, *Dad* and *Oli*, both of which were confirmed as suppressors through crosses with independent mutant alleles. *Dad* encodes an inhibitory Smad protein (KAMIYA *et al.* 2008b), thus implicating BMP signaling in the

remodeling process. I also identified another gene, *su(Hw)*, that suppressed the *shep* RNAi wing expansion defects, but not the bursicon neuron cellular defects. Taken together, these findings shed light on the molecular mechanisms by which SHEP regulates postembryonic, structural plasticity of neurons.

Materials and methods

Stocks: *Drosophila melanogaster* stocks and crosses were cultured on standard cornmeal–yeast–agarose media at 25° unless otherwise noted. I obtained Exelixis, DrosDel, and BSC deficiency strains for the X, 2nd, and 3rd chromosomes from the Bloomington *Drosophila* Stock Center (BDSC). A total of 777 deficiencies were selected from the larger set of Exelixis, DrosDel, and BSC lines available from the BDSC with the goal of obtaining maximum coverage of the genome, minimal overlap among the deficiencies, and deficiencies that deleted on average 20 genes. A total of 702 deficiencies were tested in the screen after 75 were discarded due to problems such as possible stock contamination (e.g., unexpected variation in eye color), difficulty with rebalancing certain stocks, and crosses that resulted in very few progeny. With a mean length of 224 kbp, the 702 deficiencies each deleted and/or affected an average of 21 genes. Based on the deficiency breakpoints and gene locations (COOK *et al.* 2012), I calculated that these deficiencies covered 86% of the euchromatic genes in the genome.

Most RNAi strains were obtained from the Vienna *Drosophila* RNAi Center (VDRC). The RNAi strains for *mod(mdg4)* and *su(Hw)*, together with alleles for the *su(Hw)* gene, were generous gifts from Elissa Lei (National Institute of Diabetes and Digestive and

Kidney Diseases, Bethesda, MD) (MATZAT *et al.* 2012). The other strains used included *386-Gal4* (*w*;; P{GawB}386Y*; FBti0020938) (BANTIGNIES *et al.* 2000), *tub-Gal80^{ts}* (*w*;; P{tubP-GAL80ts}2*; FBst0007017) (FERRIS *et al.* 2006), *bur-Gal4* (*w; bursicon-Gal4[P16]*) (PEABODY *et al.* 2008), *UAS-Dcr-2* (*w[1118]; P{UAS-Dcr-2, w*[+]}; FBst0024650) *UAS-shep-RNAi* (*w[1118]; P{GD5125}v37863*; FBti0092714), and *ccap-Gal4* (*y* w*;P{ccap-Gal4.P}16*; FBti0037998) (PARK *et al.* 2003).

Screen crosses and scoring: Prior to screening, all deficiencies on the 2nd chromosome were rebalanced with *CyO, Act-GFP* (FBst0004533) in order to select against *Act-GFP* instead of *Curly* (*Cy*) in crosses with wing expansion defects among the progeny. In addition, some deficiencies on the 3rd chromosome were rebalanced with *TM6B, Tb^{1}* in order to replace balancers that had lost the (*Tubby*) *Tb* marker or balancers that contained (*Serrate*) *Ser*, which I could not score in flies with folded wings.

For deficiencies on the 2nd and 3rd chromosomes and RNAi strains, five males were crossed with sixteen *w*/w^{1118}, UAS-shep-RNAi*, *UAS-Dcr-2; 386-Gal4, tub-Gal80ts* (*386>shep-RNAi, Dcr-2, tub-Gal80^{ts}*) virgin females and kept at 30° on regular food. On day 4 after the cross, the parents were removed, and the progeny were scored on days 10, 12, and 14. For deficiencies on the X chromosome, 20 virgin females from each deficiency stock were crossed to five *386>shep-RNAi, Dcr-2, tub-Gal80^{ts}* males. Along with every round of crosses, I included a control cross of *386>shep-RNAi, Dcr-2, tub-Gal80^{ts}* to the isogenic *w^{1118}* background stock that was used to create the DrosDel deficiencies. After several months, I detected phenotypic drift in the wing expansion

phenotype in the control crosses (see *Results*). I used the test stock until I observed a statistically significant difference in wing expansion rates in two consecutive crosses ($P<0.05$; Fisher's exact test), as compared to the wing expansion scores for the first test cross. I then established a new *386>shep-RNAi, Dcr-2, tub-Gal80^{ts}* stock for further screening.

The progeny of each cross were anesthetized on a CO_2 plate and scored for wing expansion (*Results*). If a fly had two wings with different degrees of expansion, the wing with the more severe phenotype was scored. When we were uncertain if flies were virgin (the *shep* RNAi flies with unexpanded wings also displayed delayed cuticular tanning), they were held until the next day for scoring. Crosses producing fewer than 20 progeny of the test genotype were discarded, and these crosses were then repeated (often in multiple vials to achieve greater numbers). The wing expansion performance for all crosses was ranked based on the percentage of fully expanded (and then partially expanded) wings among the progeny, and test crosses were repeated for another two rounds for the strongest 50 suppressor deficiencies.

Immunostaining and imaging: Immunostaining was performed as previously described (HEWES *et al.* 2003). I used antibodies against Bursicon α-subunit (anti-BURS) (1:5000, PFA/PA) (LUAN *et al.* 2006) to determine cellular phenotypes of bursicon neurons. Secondary antibodies conjugated with Cy3 or ALEXA 488 from goat and mouse were each used at a 1:500 dilution. Cells and projections were imaged as confocal z-series scans with an Olympus (Center Valley, PA) FluoView FV500

confocal microscope, and a Leica (Mannheim, Germany) SP8 scanning multiphoton microscope. Identical settings were used in parallel for all of the samples in each experiment. For the B_{AG} neurons at the P14 pharate adult stage, I measured the average soma area of the six most anterior neurons in the abdominal ganglia of each preparation as previously described (CHEN *et al.* 2014). Axonal branches of the B_{AG} neurons were counted in Adobe Illustrator by Sholl analysis (MILOSEVIC and RISTANOVIC 2007) after overlaying a grid of nested, concentric circles, each with a radius 50 μm larger than the previous circle, over the image. The area covered by the ventral portion of the B_{SEG} arbor within the subesophageal ganglia (Figure 2J, magenta; Video 1) was imaged as maximum-intensity z-series projections and was measured by first setting an image threshold pixel intensity of 40 in Fiji and then counting all above-threshold pixels (SCHINDELIN *et al.* 2012). The 3D tracing was made of z-series scans with the filament function in Imaris (South Windsor, CT).

Results

Loss of *shep* in CNS peptidergic neurons resulted in defective wing expansion and altered cellular morphology: *shep* has been shown to regulate neuronal remodeling during metamorphosis, and loss of *shep* led to defects in a neuropeptide-regulated behavior, wing expansion (CHEN *et al.* 2014). Because pan-neuronal loss of *shep* results in strong pupal lethality and severe locomotor defects in adult escapers (CHEN *et al.* 2014), I used the *386-Gal4* insertion (BANTIGNIES *et al.* 2000; TAGHERT *et al.* 2001) to drive expression of *UAS-shep-RNAi* and *UAS-Dcr-2* (*386>shep-RNAi, Dcr-2*) in a pattern restricted to peptidergic neurons. To prevent phenotypic drift in wing expansion

rates that can occur in stocks with peptidergic neuron Gal4 drivers (Tingting Gu, Tao Zhao, and Randall S. Hewes, personal communication), I also included a temperature sensitive *Gal4* inhibitor, *tub-Gal80^{ts}*, in the test stock, *386>shep-RNAi, Dcr-2, tub-Gal80^{ts}*. This test stock grew and bred normally, with normal wing expansion, when homozygous and reared at 25°. When the *386>shep-RNAi, Dcr-2, tub-Gal80^{ts}* flies were crossed at 30° to the isogenic *w^{1118}* background stock that was used to create the DrosDel deficiencies (hereafter referred to as the isogenic *w^{1118}* "Control A" stock), the heterozygous progeny displayed 16% fully expanded wings, 40% partially expanded wings, and 44% unexpanded wings (Figure 1, A-C). Thus, the progeny of crosses with the test stock provided a sensitized background to select for suppressors or enhancers of the wing expansion phenotype.

Adult cuticle tanning and wing expansion requires the bursicon neurons (LUAN *et al.* 2006; PEABODY *et al.* 2008), and disruption of the remodeling of these neurons during metamorphosis often results in disruption of these post-eclosion events (ZHAO *et al.* 2008; GU *et al.* 2014). We have previously shown that *shep* loss-of-function manipulations lead to reduced growth and neurite branching of the bursicon neurons (CHEN *et al.* 2014), which are a subgroup of neurons covered by the *386-Gal4* driver (Figure 9, A-C). Thus, I examined the progeny of crosses with *386>shep-RNAi, Dcr-2, tub-Gal80^{ts}* for temperature-dependent defects in bursicon neuron growth by anti-BURS immunostaining. At the P14 pharate adult stage, the bursicon neurons in the abdominal ganglia (B_{AG} cells) and the subesophageal ganglia (B_{SEG} cells) (PEABODY *et al.* 2008) in progeny from crosses of the Control A stock to *386>shep-RNAi, Dcr-2, tub-Gal80^{ts}*

displayed smaller soma areas (Figure 2, A-F and L). In addition, the B_{SEG} cells had a less profuse CNS arbor (Figure 2, A-C and K), and the B_{AG} cells had fewer neurite projections in the peripheral axon arbor (Figure 2, G-I and M). By contrast, bursicon cell morphologies were normal in the same crosses at 25° (Figure 2, C, F, I and K-M).

Deficiency screen for *shep* modifiers: A modifier screen was conducted with 702 deficiency strains from the DrosDel (RYDER *et al.* 2004), Exelixis (PARKS *et al.* 2004), and BSC (COOK *et al.* 2012) collections that covered 86% of the genes in the euchromatic genome. These deficiencies were crossed to the *386>shep-RNAi, Dcr-2, tub-Gal80^{ts}* strain at 30°. Deficiencies that deleted *shep*-interacting factors were expected to modify (by either enhancing or suppressing) the wing expansion defects seen in the progeny of crosses to the *386>shep-RNAi, Dcr-2, tub-Gal80^{ts}* strain. A total of 69 crosses resulted in pupal lethality, and these deficiencies were classified as enhancers (Table 2). Among these, 34 deficiencies produced head eversion defects (PARK *et al.* 2003), late pupal lethality (after stage P12 with wing pigmentation), and/or eclosion defects when crossed with the *386>shep-RNAi, Dcr-2, tub-Gal80^{ts}* strain at 30° (Figure 1, E-G; Table 2). The remaining 35 deficiencies caused lethality that occurred prior to pupariation.

For all other crosses in which adult progeny emerged, I scored the degree of wing expansion as expanded wings (EXW; Figure 1A), partially expanded wings (PEW), and unexpanded wings (UEW) (Figure 1). Wings were scored as UEW when the distal tip of the wing was opened less than 90° relative to the long (proximal to distal) axis of the

wing (Figure 1C). All intermediate degrees of wing expansion were scored as PEW (Figure 1B). I plotted the wing expansion scores, ranked based on the proportion of progeny with EXW, and secondarily based on the proportion of PEW animals, for the 633 deficiencies that produced adult progeny (Figure 7).

In spite of our inclusion of the *tub-Gal80^{ts}* inhibitor in the test stock, I detected phenotypic drift (manifest as higher percentages of PEW and EXW progeny) after about eight months (Figure 8). Therefore, I stopped using the first test stock and created a new one with the same genotype that restored the prior wing expansion rates observed in crosses to the Control A stock (Figure 8). In order to control in the screen for phenotypic drift as it started to emerge, I obtained the line of best fit (highest R^2 value, together with 75%, 90%, or 99% confidence intervals), using the cubic method in SPSS for all of the control crosses (first and second test stocks crossed to Control A) plotted for EXW and separately for UEW as a function of time (in days) after the creation of the test stock (Figure 3). Although many of the same deficiencies were located outside of these confidence intervals in the EXW and UEW plots, and were therefore candidate modifiers, the resolution of suppressors was better with the EXW-based plot due to the larger possible range of scores.

For our subsequent analysis, I concentrated on suppressors, since I expected them to be less prone than enhancers to producing false positive interactions. Among the 25 deficiencies with the highest EXW percentages (52%-92% versus 16% in the crosses to the isogenic *w^{1118}* "Control A" stock; Figure 7), 24 had EXW scores above the 99%

confidence interval in Figure 3. In the plot of UEW scores, 24 of these 25 deficiencies were located below the curve fit line, and they included 5 of the 9 deficiencies with UEW scores below the 90% confidence interval. Thus, while the resolution of suppressors appeared less reliable with the plot of UEW scores, the UEW and EXW scores were inversely correlated. Based on these findings, I classified all deficiencies with EXW scores that were located above the 99% confidence interval as candidate suppressors. From among these, I selected the 24 with the highest EXW scores (magenta and green dots in Figure 3) for further analysis to order to identify the individual genes responsible for the genetic interactions.

To narrow down the search regions, I first tested deficiencies that overlapped with or were nested within the 24 candidate suppressor deficiencies. I eliminated three deficiencies, *Df(1)ED6720*, *Df(3L)BSC671* and *Df(2R)BSC813*, for which I had overlapping or nested deficiencies that covered the entire candidate region and yet failed to display suppression. In addition, one of the deficiencies, *Df(3R)BSC505*, deletes *pasha*, an important co-factor for pri-miRNA cleavage during microRNA synthesis (HAN *et al.* 2006). Thus, I eliminated *Df(3R)BSC505* due to its potential effect on RNAi efficacy. Three of the remaining deficiencies, *Df(3R)BSC874*, *Df(3R)Exel6176* and *Df(3L)BSC449*, overlap or are nested within other members of this set of 20 candidate suppressors (Table 1). Therefore, this narrowed our analysis down to 17 regions for further mapping of candidate suppressors (Table 1). This set was represented in the initial screen by one deficiency from the DrosDel collection (from the isogenic w^{1118} Control A background w^{1118}, FBst0005905) (RYDER *et al.* 2004) and 16

deficiencies from the Exelixis and BSC collections (which shared a different isogenic w^{1118} background, FBst0006326) (PARKS *et al.* 2004; COOK *et al.* 2012). Using overlapping and/or nested deficiencies, we were able to narrow down the list of candidate suppressors for each of the 17 regions to 1-20 genes (Table 1).

Interestingly, I found that the *TM6B, Tb*^{1} balancer fully suppressed the wing expansion defects in crosses to the *386>shep-RNAi, Dcr-2, tub-Gal80*^{ts} strain, while the *TM6C, Sb*^{1}*, cu*^{1} balancer did not (data not shown). This did not affect the scoring of wing expansion in the deficiency modifier screen, because we were able to select against *Tb*, but it did suggest the presence of a suppressor on the *TM6B* chromosome. I did not attempt to map the *TM6B* suppressor, but it is notable that an inversion breakpoint found in *TM6B* but not *TM6C* was covered by *Df(3L)BSC671*, one of the suppressor deficiencies isolated in the screen.

We have previously identified several genes that produce wing expansion defects when misexpressed in the *386-Gal4* pattern but not the more restricted *ccap-Gal4* pattern, which contains the bursicon neurons (ZHAO *et al.* 2008). Therefore, some suppressors may reflect interactions within other non-bursicon neurons that regulate wing expansion. In order to test whether the deficiency suppressors of the wing expansion phenotype also suppressed the bursicon neuron cellular phenotype, I performed anti-BURS immunostaining on *burs>UAS-shep-RNAi, Dcr-2* animals that were crossed to the 17 suppressor deficiencies. With 12 of the 17 deficiencies, I observed rescue of the B_{SEG} cell neurite projections to the thoracic ganglia (Figure 4, A-C) and/or restoration

of the B_{AG} neuron soma areas (Figure 4, D-G and Table 1). None of the 17 deficiencies rescued the number of peripheral bursicon axonal branches (data not shown).

I expected to find some deficiencies that non-specifically produced suppression by reducing the efficacy of transgene expression in the bursicon neurons (e.g., by interfering with Gal4 expression). In addition, we were less interested in deficiencies that impacted bursicon neuron growth independently of *shep* (i.e., in a *shep* wild type background). To rule out deficiencies with such nonspecific genetic interactions, I monitored soma areas and the expression levels of a membrane-tagged GFP reporter for the most anterior pair of B_{AG} neurons (Figure 10, panel C arrowheads) in *ccap>mCD8::GFP/deficiency* animals [bursicon neurons are a subset of the Crustacean cardioactive peptide (CCAP) neurons and are therefore targeted by the *ccap-Gal4* driver; Figure 10, A-C]. None of the 12 suppressor deficiencies led to changes in GFP levels (Figure 10D), which would have reflected changes in efficacy of the Gal4-UAS expression system. In addition, none of these deficiencies altered bursicon neuron cellular morphologies by themselves (Figure 10E). These results suggest that the suppressor deficiencies rescued the wing expansion performance and cellular phenotypes by interacting specifically with *shep*.

RNAi-based modifier screen for *shep* suppressor genes: In order to map the genetic interactions uncovered by the above deficiencies to single loci, I performed RNAi for genes directly adjacent to or deleted by nine of the 12 suppressor deficiencies. I selected the nine deficiencies based on the candidate genes in these regions and the

availability of reagents: *Df(3L)BSC579, Df(3L)BSC816, Df(3L)BSC250, Df(1)Exel6233, Df(3R)Exel6164, Df(3L)BSC613, Df(3L)BSC553,* and *Df(2L)Exel9044* (Table 1).

For the RNAi, I tested three different stock collections: GD and KK strains from the VDRC (DIETZL *et al.* 2007) and *attP2* lines from the Transgenic RNAi Project (TRiP) (NI *et al.* 2009). I encountered genetic interactions with the backgrounds for two of the three strains, *GD* and *attP2*. The GD strains could not be used for RNAi mapping of suppressors, because the GD genetic background stock as well as 49 GD RNAi strains all produced strong lethality when they were crossed with the *386>shep-RNAi, Dcr-2, tub-Gal80^{ts}* stock at 30°. The *attP2* TRiP lines were also unusable, although these crosses suggested the presence of another *shep* suppressor. I tested six TRiP lines with an *attP2* docking site, and the background strain with the empty *attP2* docking site (FBst0036303) (NI *et al.* 2009), and all seven produced 100% suppression of the wing expansion defects in crosses to the *shep* RNAi strain. Therefore, I tested whether the *Mocs1* gene, which contains the *attP2* docking site insertion, was a *shep* suppressor by crossing the *386>shep-RNAi, Dcr-2, tub-Gal80^{ts}* strain to a *UAS-Mocs1-RNAi*, which was created with an *attP40* landing site. I found that *UAS-Mocs1-RNAi*, and the *attP40* landing site alone (FBst0036304), did not alter the wing expansion rates observed with the *shep* RNAi (data not shown). These results suggest that the *attP2*-based TRiP lines suppress *shep* through unidentified factors (not *Mocs1*) in the genetic background.

Crosses of the *386>shep-RNAi, Dcr-2, tub-Gal80^{ts}* strain at 30° with the KK genetic background stock (VDRC ID 60100) resulted in viable progeny with strong wing

expansion defects (50% UEW, 20% PEW, and 30% EXW) (Figure 5A), and I did not observe wing expansion defects in crosses at 30° of the 60100 genetic background strain to a control stock without *shep* RNAi (*386>Dcr-2, tub-Gal80^{ts}*). Therefore, I performed all subsequent RNAi tests for candidate modifier genes with KK strains.

I tested RNAi strains for 45 genes that are deleted or potentially affected by the nine suppressor deficiencies. While seven strains led to lethality in crosses to the test stock (Table 3), eight strains—targeting *CG10565*, *Dad* (*Daughters against dpp*), *Oli* (*Olig family*), *dm* (*diminutive*), *CG13305*, *Tim17a1*, *Cpr66D* (*Cuticular protein 66D*), and *CG2469*—provided statistically significant suppression of wing expansion defects in crosses to the *386>shep-RNAi, Dcr-2, tub-Gal80^{ts}* strain at 30° (Figure 5A). In control crosses with the *60100* KK background strain, only 17% of the progeny had fully expanded wings. I focused on the strongest four suppressors, *CG10565, Dad*, *Oli*, and *dm*, as the best candidates for cellular-level analysis, and all four were verified to show strong and statistically significant (P<0.01) wing expansion rescue (51-73% EXW) in three repeated crosses to the *386>shep-RNAi, Dcr-2, tub-Gal80^{ts}* stock.

The B_{SEG} neurons have been shown to play an essential command role in the neuroendocrine circuit controlling wing expansion, whereas the B_{AG} neurons are activated downstream of the B_{SEG} neurons to secrete bursicon into the blood to control associated changes in that adult cuticle (LUAN *et al.* 2006; PEABODY *et al.* 2008). To test whether these four suppressor RNAi strains rescued the wing expansion defects by development of the bursicon neurons, I examined the soma areas and projections of the

B_{AG} and B_{SEG} neurons of the progeny from the same crosses referred above. Interestingly, the suppression was largely detected in the B_{SEG}. The four strains carrying *Dad-RNAi, dm-RNAi*, *Oli-RNAi* or *CG10565-RNAi* vectors all restored B_{SEG} neurite projections in the subesophageal ganglia (Figure 5, B-D and I). However, none of the four RNAi lines to *CG10565*, *Dad*, *Oli*, and *dm* rescued branching in the peripheral axon arbor (data not shown), and only the RNAi to *Dad* restored B_{AG} neuron soma areas (Figure 5, E-G, I and J). Thus, loss of *CG10565*, *Dad*, *Oli*, and *dm* suppressed the effects of *shep* knock-downs on wing expansion, and for all of these genes, the effects were associated with rescue of adult B_{SEG} neurites in the subesophageal ganglia.

I performed four additional control experiments in order to validate the candidate suppressors. First, I tested whether the suppression caused by RNAi for *Dad*, *Oli*, and *dm* could be phenocopied with independent loss-of-function alleles for each gene (no independent alleles were available for *CG10565*). I crossed the test stock *386>shep-RNAi, Dcr-2, tub-Gal80^{ts}* to *Dad^{212}* (OGISO *et al.* 2011), *dm^{2}* (MAINES et al. 2004), *dm^{4}* (PIERCE et al. 2004), *Oli$^{\Delta 9}$* (OYALLON *et al.* 2012) and their respective genetic background strains, and I analyzed the wing expansion rates of the progeny that were raised at 30°. *Dad^{212}*, *dm^{4}*, and *Oli$^{\Delta 9}$* contain small deletions and are likely molecular null alleles, and *dm^{2}* is the result of a point mutation and is a strong, homozygous lethal allele. Crosses of the test stock to *Dad^{212}* and *Oli$^{\Delta 9}$* produced strong suppression of the wing expansion defects, with 50% EXW (n=26) and 91% EXW (n=32) among the heterozygous progeny, respectively (Figure 6A). Control crosses with a *yw* strain used

previously as a control for *Dad*^{212} (OGISO *et al.* 2011) and an *Oli*$^{\Delta 9}$ genetic background strain *y*^{1}*w*^{67c23} (TOBA *et al.* 1999) both produced progeny with 100% UEW rates. In P14 stage pharate adults from the cross between *Oli*$^{\Delta 9}$ and the *386>shep-RNAi, Dcr-2, tub-Gal80*^{ts} test stock, I observed partial restoration of soma areas and neurite arbors in both the B_{AG} and B_{SEG} neurons (Figure 6, B-D). These results confirmed that the suppression of *shep* observed with *Oli* was likely due to loss of *Oli* rather than off-target effects of the RNAi. The progeny of a cross between *Dad*^{212} and the *386>shep-RNAi, Dcr-2, tub-Gal80*^{ts} test stock also displayed rescue of wing expansion (Figure 6A). There was also a trend suggesting that *Dad*^{212} had a positive effect on the soma areas of B_{AG} neurons, although this trend was not statistically significant (P=0.0957) (Figure 6D). This may simply reflect stronger knock-down of *Dad* expression by the *Dad* RNAi, which led to suppression of both the wing expansion defects and cellular defects of bursicon neurons, than by the heterozygous *Dad*^{212} allele. Alternatively, the *Dad*^{212} allele might have suppressed the wing expansion defects by altering the expression level of bursicon peptides (VEVERYTSA and ALLAN 2011). In contrast, crosses of the test stock with *dm*^{2} and *dm*^{4} produced progeny with similar wing expansion rates to the control cross with the genetic background for *dm*^{4} (*w*; *Iso2A*; *Iso3A*) (PIERCE *et al.* 2004), and *dm*^{4} failed to suppress the cellular phenotypes observed in the bursicon neurons (data not shown). I eliminated *dm* from further consideration, since these results suggested that the suppression seen with the *dm* RNAi resulted from off-target effects or a second-site mutation carried by the RNAi strain. However, I cannot rule out *dm* as a suppressor of *shep*, since RNAi may produce a stronger knock-down than is possible with a heterozygous null allele.

Notably, a second, cryptic docking site was recently identified in the genetic background strain for the KK RNAi collection (GREEN *et al.* 2014). Since the newly described docking site is located in the 5' UTR of *tiptop*, the insertion of UAS sites in this region may lead to misexpression of *tiptop*, which in turn can produce wing expansion defects (DENHOLM *et al.* 2013). I cannot exclude the possibility that *tiptop* misexpression may have altered wing expansion rates produced in crosses with our candidate suppressors, but in this case, the suppressors likely needed to be stronger in order to overcome the combined effects of *tiptop* misexpression and *shep* RNAi. Moreover, once I independently validated the suppressors with other alleles, I eliminated this potential confound.

In a second set of control experiments, I tested whether the candidate suppressors altered the morphology of neurite arbors and soma areas of the B_{SEG} and/or B_{AG} neurons in the absence of *shep* RNAi. Crosses of *386>Dcr-2, tub-Gal80^{ts}* animals to the genotypes that produced the strongest suppression (*Dad* RNAi; *Oli$^{\Delta 9}$* allele) at 30° produced progeny flies with normal wing expansion and the cellular morphology of the B_{AG} and B_{SEG} neurons (Figure 11). Crosses of *386>Dcr-2, tub-Gal80^{ts}* animals to the *CG10565* RNAi strain produced smaller B_{AG} neuron soma areas, and fewer B_{AG} neuron peripheral branches (Figure 11). However, *CG10565* RNAi did not alter the morphology of the B_{SEG} neurites (Figure 11A), where the genetic interaction between *CG10565* RNAi and *shep* RNAi was detected. The latter result suggests that *CG10565* may be a true suppressor of *shep*, although that conclusion is tempered by the other

effects of *CG10565* RNAi alone on the B_{AG} and B_{SEG} neurons, and I did not investigate *CG10565* further.

For the third control, I will need to test whether *Oli* and *Dad* suppressed the *shep* RNAi phenotype simply by reducing Gal4-UAS transgene expression, measured indirectly by assessing the impacts of these genotypes on levels of Gal4-dependent mCD8::GFP expression (fluorescence). With *UAS-mCD8::GFP*, *UAS-Dcr-2* expressed under the control of a *ccap-Gal4* driver at 30°, I expect that the levels of mCD8::GFP fluorescence in the B_{SEG} and B_{AG} somata will be the same with *shep* RNAi alone and with *shep* RNAi together with *Dad* RNAi or $Oli^{\Delta 9}$. These control experiments are in progress.

In the final control, I will examine whether the changes in neurite arbors observed with anti-BURS immunostaining are also observed with the mCD8::GFP membrane tag. This will involve anti-BURS immunostaining of the bursicon neurons in heterozygous *ccap>shep-RNAi, Dcr-2, mCD8::GFP* animals, with or without $Oli^{\Delta 9}$ or *Dad* RNAi, that were raised at 30°. These experiments are in progress, but I expect, based on other similar controls that I have performed for other gene manipulations in the bursicon neurons (CHEN *et al.* 2014), that the resolution of gross neurite morphology will be equivalent with these two markers. This will confirm that the changes in the B_{SEG} arbor measured with anti-BURS immunostaining reflected changes in neurites and not changes in bursicon synthesis or trafficking within the neurons. Even with some of these controls pending, I have multiple independent lines of evidence to identify *Dad*

and *Oli* as suppressors of the wing expansion defects and cellular phenotypes resulting from the loss of *shep* function.

Suppression of wing expansion defects by *su(Hw)*: The insulator component proteins SU(HW) and MOD(MDG4) have been studied for their interactions with SHEP, which negatively and specifically regulates *gypsy* insulator activities in the nervous system (MATZAT *et al.* 2012). In order to test whether the interactions between insulator proteins and SHEP affect wing expansion, I crossed the test stock *386>shep-RNAi, Dcr-2, tub-Gal80^{ts}* with *UAS-su(Hw)-RNAi* (P{GD4493}v10724; FBti0091830) and *UAS-mod(mdg4)-RNAi* (P{GD16547}v52268; FBti0086701) at 30°, and found that only *su(Hw)* RNAi suppressed the wing expansion defects (Figure 5H). I tested *shep* modification with three other *su(Hw)* mutant alleles, *su(Hw)^{V}* (FBal0032826) (HARRISON et al. 1992), *su(Hw)^{V}* together with *su(Hw)^{tHa}* (FBal0046546) (HARRISON et al. 1992), and *su(Hw)^{2}* (FBal0016319) (PARKHURST et al. 1988). The *su(Hw)^{2}* mutation is an insertion allele, *su(Hw)^{V}* is a small deletion of *su(Hw)* and the neighboring RNA polymerase II 15kD subunit (RpII15) gene, and *su(Hw)^{tHa}* contains a genomic fragment including *RpII15* and *su(Hw)* without a zinc finger domain essential for SU(HW) function. For two of the three *su(Hw)* alleles, I found suppression of wing expansion defects (Figure 5H). Conversely, I observed enhancement of the *shep* loss-of-function phenotype when I crossed *386>shep-RNAi, Dcr-2, tub-Gal80^{ts}* with *UAS-su(Hw)* at 30°. The overexpression of *su(Hw)* together with *shep* RNAi led to 30% pupal lethality (n=104), with 45% of these pupae also displaying defective head eversion, which is a phenotype associated with earlier disruptions of bursicon neurons and other peptidergic

cells in the *386-Gal4* pattern (ZHAO *et al.* 2008). Crosses with *386>shep-RNAi, Dcr-2, tub-Gal80^{ts}* to the 60100 genetic background strain produced only 4% lethality (n=75). Taken together, these data suggested that *su(Hw)* and *shep* act antagonistically (directly or indirectly) to regulate ecdysis and post-ecdysis behaviors.

In spite of the ability of *su(Hw)* alleles to suppress the wing expansion defects seen with *shep* RNAi, I did not detect rescue of the B_{AG} and B_{SEG} neuron soma areas or neurite arbors (data not shown). Given the fact that other, non-bursicon neurons in the *386-Gal4* pattern have been implicated as important for regulating the wing expansion program (ZHAO *et al.* 2008), it appears likely that *su(Hw)* interacted with *shep* in some of these other neurons to suppress the wing expansion defects. Since these neurons have not yet been identified, we were not able to test this hypothesis.

In addition to the regulation of bursicon neuron development, we have also shown that loss of *shep* leads to reduced neuropil areas and reduced expression of synaptic markers (CHEN *et al.* 2014). To test for suppression of this phenotype by *su(Hw)*, I crossed *elav>shep-RNAi*, *Dcr-2*, *mCD8::GFP* animals to *su(Hw)*^{2}, or su*(Hw)*^{V} together with *su(Hw)*^{tHa}, or the genetic background stock for these *su(Hw)* alleles (*y*^{2}*wct*^{6}). Progeny of these crosses replicated the suppression of the wing expansion defects seen with the more restricted, *386-Gal4* pattern of expression (Figure 5H). *shep* RNAi also reduces the intensity of anti-synapsin (3C11) immunostaining and the sizes of neuropils in the adult CNS (CHEN *et al.* 2014), but these phenotypes were not suppressed by the *su(Hw)* alleles (data not shown). Therefore, for the three *shep* suppressors analyzed in this

study, we have identified cellular correlates for two, *Oli* and *Dad*, while cellular correlates for *su(Hw)* remain to be defined.

Discussion

In order to identify *shep*-interacting factors and signaling pathways that contribute to the control of metamorphic neuronal remodeling, I screened 702 deficiencies located on X, 2nd, and 3rd chromosomes for genetic modification of the wing expansion defects and cellular defects caused by the loss of *shep* function in peptidergic neurons. These deficiencies together covered 86% of the euchromatic genes in the genome. I focused on suppressor deficiencies because of the expected lower incidence of false positive and the greater sensitivity in our assay for suppressors. Using regression analysis of wing expansion rates, I identified 33 suppressor deficiencies beyond the 99% confidence interval for the control crosses. After preliminary mapping experiments with the 24 strongest suppressor deficiencies in this set, we were left with 17 regions (represented by 20 deficiencies from our screen) containing candidate suppressor genes. Deficiencies for 12 of these regions also suppressed aspects of the *shep* loss-of-function phenotype in the bursicon neurons. Based on the candidate genes in these regions and the availability of reagents (RNAi lines or other mutations), I selected nine of the deleted regions for mapping to single genes.

I successfully mapped four of the suppressor activities to individual loci: *dm*, *Oli*, *CG10565*, and *Dad* (Table 1). RNAi-mediated down-regulation of each of these genes produced partial suppression of wing expansion defects and cellular defects in the

bursicon neurons resulting from the loss of *shep*. In addition, I analyzed a fifth gene, *su(Hw)*, which encodes a component of *gypsy* chromatin insulator complexes and has been shown previously to interact with *shep* (MATZAT et al. 2012). *su(Hw)* did not suppress cellular defects in the bursicon neurons, but it did suppress the wing expansion defects and lethality resulting from pan-neuronal loss of *shep*. These findings expanded our understanding of *shep* through the identification of novel genetic interactions with other genes and by linking chromatin insulator activity to *shep* regulation of neuronal remodeling during metamorphic development.

Suppressors may interact with *shep* in one of three ways, each of which is not mutually exclusive. First, the suppressor genes could directly inhibit SHEP expression or function. Because SHEP promotes bursicon cell neurite branching and soma growth (CHEN *et al.* 2014), the removal of direct suppressors would lead to increased branching and growth. Second, the suppressor genes may encode factors that normally repress neurite/soma growth by the bursicon neurons during metamorphosis, and the expression or function of the suppressor genes may in turn be inhibited by SHEP. The known epistatic relationships for genes in the SHEP/MSSP family suggest that *su(Hw)* may fall into this category (see below). Third, *shep* may promote growth independently of growth inhibition by the suppressor genes. In this case, the effects of mutations in both *shep* and a suppressor would be additive, with the net effect being restoration of more normal growth.

***Olig family (Oli)*:** The vertebrate Olig family of basic Helix–Loop–Helix (bHLH) transcription factors have important functions during generation and differentiation of motorneurons, such as regulation of the axon targeting of cortical neurons and survival of spinal cord neurons during neuronal development (LEE and PFAFF 2003; LEE *et al.* 2004; JOSHI *et al.* 2008; ROSS *et al.* 2010; ROSS *et al.* 2012). In *Drosophila*, neuronal development requires tight regulation of the timing and/or expression level of *Oli*, the only member of the Olig family. *Oli* is widely expressed in differentiated neurons at intermediate embryonic stages, and it is down-regulated during late embryogenesis. Changes in this expression profile, either through loss or constitutive over-expression of *Oli*, result in defects in larval motorneuron axon pathfinding and muscle targeting, and altered locomotor behavior in larvae and adults (OYALLON *et al.* 2012). Our results show that *Oli* also interacts with *shep* to regulate the development of peptidergic neurons. Interestingly, zygotic SHEP is not detected until late embryonic stage 17 (CHEN *et al.* 2014) when *Oli* expression is down-regulated (GRAVELEY *et al.* 2011; OYALLON *et al.* 2012). Based on this negative correlation and our finding that *shep* and *Oli* have opposing functions during metamorphic remodeling of bursicon neurons, it will be important to determine whether either SHEP or Oli inhibits the expression or function of the other.

***shep* and BMP signaling:** Bone morphogenetic proteins (BMPs) are a group of growth factors that regulate the differentiation and proliferation of neural cells (LIU and NISWANDER 2005) and other tissues (BLEUMING *et al.* 2007; MILANO *et al.* 2007; RAFTERY and UMULIS 2012). Retrograde BMP signaling occurs in larval neurons that

express CCAP, MiP, and bursicon neuropeptides and become the most anterior 7-8 B_{AG} neurons in the P14 pharate adult stage (VEVERYTSA and ALLAN 2011; VEVERYTSA and ALLAN 2012). The loss of retrograde BMP signaling in these neurons leads to reduced expression of all three peptides and ecdysis defects (VEVERYTSA and ALLAN 2011). In addition to the regulation of neuropeptide expression, BMP signaling plays important roles in neurite growth and fasciculation (Fu *et al.* 2006; Hegarty *et al.* 2014), and synaptic growth (Aberle *et al.* 2002) and stability (EATON and DAVIS 2005).

BMPs bind to type II membrane receptors, which recruit and phosphorylate type I receptors. The activated type I receptors then phosphorylate receptor regulated Smad (R-Smad); R-Smad in turn dimerizes with common Smad (co-Smad), and these complexes enter nuclei as transcription factors to regulate various genes (LIU and NISWANDER 2005). So far, three type I receptors (Tkv, Sax and Babo), two R-Smads (Mad and dSmad2/Smox), and one Co-Smad (Medea) have been identified in *Drosophila* (RAFTERY 2006; KAMIYA *et al.* 2008b). The *Dad* gene encodes inhibitory Smad proteins (I-Smad) that physically interact with the BMP type I receptors, Sax and Tkv, and inhibit BMP signaling by interfering with Mad phosphorylation and dimerization with Medea (INOUE *et al.* 1998; KAMIYA *et al.* 2008a). The ability of *Dad* loss-of-function manipulations (*Dad* RNAi or *Dad* alleles) to suppress the defects in B_{AG} soma growth and B_{SEG} neurite growth suggests that BMP signaling may promote neurite outgrowth through interactions with SHEP. Given the known role of BMP signaling in regulation of bursicon neuropeptide expression, the loss of *Dad* could also suppress the wing expansion defects seen in *shep* mutants by restoring (upregulating)

bursicon expression. This seems unlikely, as the intensity of anti-BURS immunostaining in the bursicon neurons was increased by *shep* RNAi (Figure 2E), but it remains possible given that the *shep* RNAi also reduces soma size, which could obscure any reduction in total bursicon expression by concentrating the remaining bursicon in a smaller area. Finally, *Dad* could serve as a suppressor of the *shep* wing expansion phenotype by regulating levels of neuropeptides in other cells included in the *386-Gal4* expression pattern.

SHEP interaction with the *gypsy* insulator protein, SU(HW): Insulators are DNA sequences that recruit various insulator proteins to interfere with enhancer-promoter interactions and/or the spreading of heterochromatin (NEGRE *et al.* 2010; BARKESS and WEST 2012; MATZAT *et al.* 2012; SCHWARTZ *et al.* 2012). SHEP is known to bind SU(HW) and MOD(MDG4) proteins, which are essential components of *gypsy* insulator complexes, and *shep* negatively regulates *gypsy* insulator activity specifically in the nervous system (GHOSH *et al.* 2001; MATZAT *et al.* 2012). Consistent with these known interactions of *gypsy* insulator proteins with SHEP, I detected suppression of *shep* wing expansion defects with *su(Hw)* RNAi and *su(Hw)* loss-of-function alleles. However, I did not observe suppression by *mod(mdg4)* RNAi (Figure 5H). This did not rule out the possibility of involvement of *gypsy* insulators in this phenotype, because the *su(Hw)* RNAi and *mod(mdg4)* RNAi may have had different efficacies [i.e., the *mod(mdg4)* RNAi may have been too weak to reveal an interaction]. Alternatively, SHEP and SU(HW) might interact with each other to affect the activities of other non-*gypsy* insulators that may not require MOD(MDG4). Consistent with this

interpretation, about 5% of SHEP DNA binding sites co-localize with those of SU(HW) but not MOD(MDG4), and only about 2.5% of SHEP DNA binding sites also recruit SU(HW) and MOD(MDG4) together (MATZAT *et al.* 2012).

Future directions: Here, and in the previous chapter, I have shown that SHEP regulates neurite branching and soma growth during the metamorphic remodeling of peptidergic neurons (CHEN *et al.* 2014). Our analysis of neuropil sizes and soma growth in other neurons revealed SHEP to be a broad regulator of metamorphic growth of many neuronal cell types, consistent with the wide range of behavioral defects that we and others have observed (ARMSTRONG *et al.* 2006; CHEN *et al.* 2014). Here, I identified novel genetic interactions between SHEP and other factors, some of which are known to regulate nervous system development (OYALLON *et al.* 2012) or to bind directly to SHEP in the nervous system, potentially to regulate DNA insulator activities (MATZAT *et al.* 2012). These findings shed new light on the molecular mechanisms—which include direct interactions with RNA, DNA, and other proteins (MATZAT *et al.* 2012)—by which SHEP controls neuronal growth during metamorphosis. Given the diversity of these interacting factors (which include transcription factors, insulator proteins, and intracellular signaling molecules), these findings raise more questions than they answer, and additional studies will need to explore the exact nature of these interactions and the cross-talk among them.

Table 1. The 17 suppressor deficiencies obtained in the *shep* modifier screen.

Deficiency	Flybase ID	Overlapping/nested deficiencies tested	B_{AG} rescue	B_{SEG} rescue	Deleted or immediately flanking protein-encoding gene(s)[1]
Df(3R)Exel6164	FBst0007643	*Df(3R)Exel7315, Df(3R)Exel7316*	Y	Y	***MBD*, *svp*, *CG10013*, *CG10038*, *CG10041*, *CG4115*, *Tim17a1*, *CG18548***, *CG10091*, *CG4066, GstD9, GstD1, GstD10*
Df(1)Exel6233	FBst0007707	*Df(1)Exel6712*	N	Y	***dm***
Df(2L)Exel9044	FBst0007836	N/A	Y	Y	***CG6412*, *Oli*, *CG6870*, *syntalpha*, *CG15143*, *CG15144*, *CG15145*, *CG7094***, *Dhc*
Df(3L)BSC250	FBst0023150	*Df(3L)BSC363, Df(3L)BSC431, Df(3L)BSC311, Df(3L)BSC289*	Y	Y	***CG9149*, *CG2277*, *CG2469*, *CG9186*, *CG9153*, *Myo61F*, *CG9184*, *mtacp1***, *msd1*
Df(3L)BSC553	FBst0025116	*Df(3L)BSC449*	Y	N	***Sin*, *siz*, *CG12984*, *CG10584*, *CG10585*, *CG10581*, *CG33284*, *CG10566*, *CG10565***, *CG43072*, *CG43938*, *ko*, *skd*, *CG33285*, *Ac78C, asparagine-synthetase*

Df(3L)BSC613	FBst0025688	*Df(3L)Exel6117*	Y	Y	***CG10948, CG42709, CG32110, CG42588***, *CG10973*, *CG32113*, *Hip1*, *CG32106*, *CG10969*, *CG17666*, *Atg1*, *Sap130*, *CG10754*, *CG10960*
Df(3L)BSC816	FBst0027577	*Df(3L)BSC612, Df(3L)ED4110*	Y	Y	***Cpr66D***, ***pex7***, ***CG13305***, ***Zasp66***, *Arr2, hairy*
Df(3R)BSC748	FBst0026846	*Df(3R)Exel6176*	Y	N	***Dad***
Df(3L)Exel6084	FBst0007563	*Df(3L)BSC121, Df(3L)BSC128, Df(3L)BSC125, Df(3L)BSC126, Df(3L)ED4177*	Y	N	***Kaz1***, ***DIP2***, *pyx*, *E(bx)*, *mthl14*, *CG13877*, *CG33229*, *CG34453*, *CG42846*, *thoc7*, *CG34454*, *CG16940*, *CG34263*, *mRpL17*, *Tudor-SN*, *wac*, *miple*, *miple2*, *CG32845*, *CG7028*
Df(3L)BSC579	FBst0025413	*Df(3L)BSC559, Df(3L)BSC560, Df(3L)BSC649*	Y	Y	*Nplp3*, *CG13041*, *CG13060*, *CG42718*, *CG13059*, *CG13062*
Df(3R)Exel6215	FBst0007693	*Df(3R)BSC503, Df(3R)BSC504, Df(3R)Exel6216, Df(3R)Exel7378*	Y	Y	*Tmod*, *CG34155*
Df(1)BSC760	FBst0026857	N/A	Y	Y	*Para*, *CG9903*, *CG9902*, *Arp2*, *Pp28-14D*, *CanA-14F*, *CG13014*, *Cap*, *UBc7, CG9784*, *Nup153*,

					mbt, *CG9782*, *rok*, *CG9777*, *Cnx14D*
Df(3R)Exel6210	FBst0007688	*Df(3R)BSC567, Df(3R)BSC789, Df(3R)BSC806, Df(3R)BSC322, Df(3R)Exel6209, Df(3R)BSC874*	N	N	*CG1646*, *wdn*, *CG1523*, *CG1647*, *CheB98a*
Df(3L)BSC116	FBst0008973	*Df(3L)BSC385, Df(3L)Exel6090*	N	N	*CG1317*, *CG8993*, *mRpL23*, *CG9004, CG15877, CG45186, CG42787, CG32298, CG32299,*
Df(3L)BSC389	FBst0024413	*Df(3L)BSC157*	N/A	N/A	*ergic53*, *rhea*, *CG6638*, *CG43078*
Df(3R)BSC476	FBst0024980	*Df(3R)Exel6264, Df(3R)Exel6153*	N	N	*Alpha-Man-II*, *ps*, *GstZ1*, *GstZ2*, *CG16779*, *CG8147*, *RhoL*, *CG8149*, *rump*, *Ras85D*, *Rlb1*, *mRpL47*
Df(1)ED7289	FBst0029732	*Df(1)BSC310*	N	N	*CG5599*, *Rab3-GEF*, *CG9072*, *Cyp4s3*, *drd*

The column labeled "B_{AG} rescue" indicates whether the B_{AG} soma size defects caused by *shep* RNAi were partially or completely suppressed. The "B_{SEG} rescue" column indicates whether B_{SEG} arbor in the ventral nerve cord was partially or completely restored. Individual genes

partially or completely deleted by each deficiency, together with flanking genes located within 3 kb of the deficiency breakpoints (underlined), are listed.

[1]Bold, genes tested by RNAi.

Figure legends

Figure 1. Wing expansion defects and lethality produced by loss of *shep* in peptidergic neurons. (A-C) Three wing expansion categories for modifier screen scoring. Flat wings were scored as fully expanded wings (EXW, panel A). Wings with the distal tip opened less than 90° relative to the long axis of the wing (white dashed line, panel C) were scored as unexpanded wings (UEW). All wings that opened larger than 90° (white dashed line, panel B) but were not flattened were scored as PEW. (D) Pupa with normal head eversion. Wings and legs were extended toward posterior end. (E) Pupa with head eversion defects: the head remained entirely within the thorax, and the wings and legs were not extended as far toward the posterior end. (F) Pupa that displayed late pupal lethality, marked by pigmentation of the eyes and wings (later than stage 12) (BAINBRIDGE and BOWNES 1981b) and subsequent desiccation of the animal after death. (G) Flies with eclosion defects. Some flies initiated eclosion, often freeing their prothoracic legs, but then died after failing to completely exit the pupal case. Arrows, distal tips of metathoracic legs.

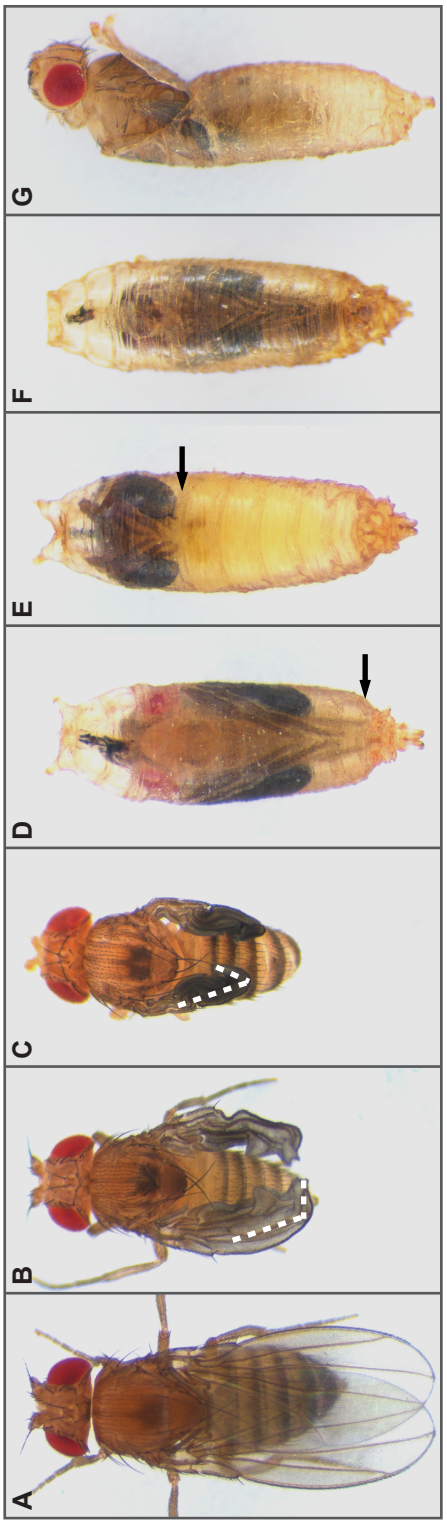
G
F
E
D
C
B
A

Figure 2. Loss of *shep* in peptidergic neurons reduced soma area and neurite branching of bursicon neurons at the P14 pharate adult stage. (A-C) Anti-BURS immunostaining showed the effects of *shep* RNAi on neurites of the B_{SEG} neurons in the subesophageal ganglia. The *386>shep-RNAi, Dcr-2, tub-Gal80^{ts}* animals displayed reduced neurite branching at 30° (panel B), the restrictive temperature for Gal80ts, but not at 25° (panel C), the permissive temperature. Scale bar: 100 μm. (D-F) Reduced soma areas were observed in the B_{AG} neurons of the *386>shep-RNAi, Dcr-2, tub-Gal80^{ts}* animals at 30°, but not in non-RNAi controls (panel D) or at 25° (panel F). Scale bar: 100 μm. (G-I) Branching of the B_{AG} neuron peripheral axon arbors for the same genotypes as in panels A-C and D-F. Anti-BURS immunostaining of a *386>Dcr-2, tub-Gal80^{ts}* control pharate adult at 30° (panel G) and a *386>shep-RNAi, Dcr-2, tub-Gal80^{ts}* pharate adult at 25° (panel I) revealed normal B_{AG} neuron peripheral axon arbors. In contrast, I observed reduced branching in the peripheral arbor of a *386>shep-RNAi, Dcr-2, tub-Gal80^{ts}* pharate adult at 30° (panel H). Scale bar: 200 μm. (J) A 3D tracing (projected to 2D) showing the organization of the B_{SEG} neurite arbors in brain (cyan) and subesophageal ganglia (magenta). Maximum intensity projection images of the ventral portion of the B_{SEG} neurite arbor (magenta) were used for B_{SEG} neurite area quantification. d, dorsal; p, posterior; r, right. (K) Quantification of the area covered by the magenta portion of the B_{SEG} arbor for the genotypes shown in panels A-C. I performed a one-way ANOVA [P<0.0000001; ***, P<0.001, Tukey HSD (honest significant difference) *post hoc* test]. Sample sizes were the same as in panel L. (L) Quantification of B_{SEG} and B_{AG} neuron soma areas for P14 pharate adults. One-way ANOVAs were done for the B_{SEG} and B_{AG} somata separately (P< 0.000001; Tukey

HSD *post hoc*, ***P<0.001; sample sizes in parentheses). (M) Sholl analysis of branches in the B_{AG} peripheral axon arbors. The space between each of the concentric rings used to count intersecting axons was 50 μm.

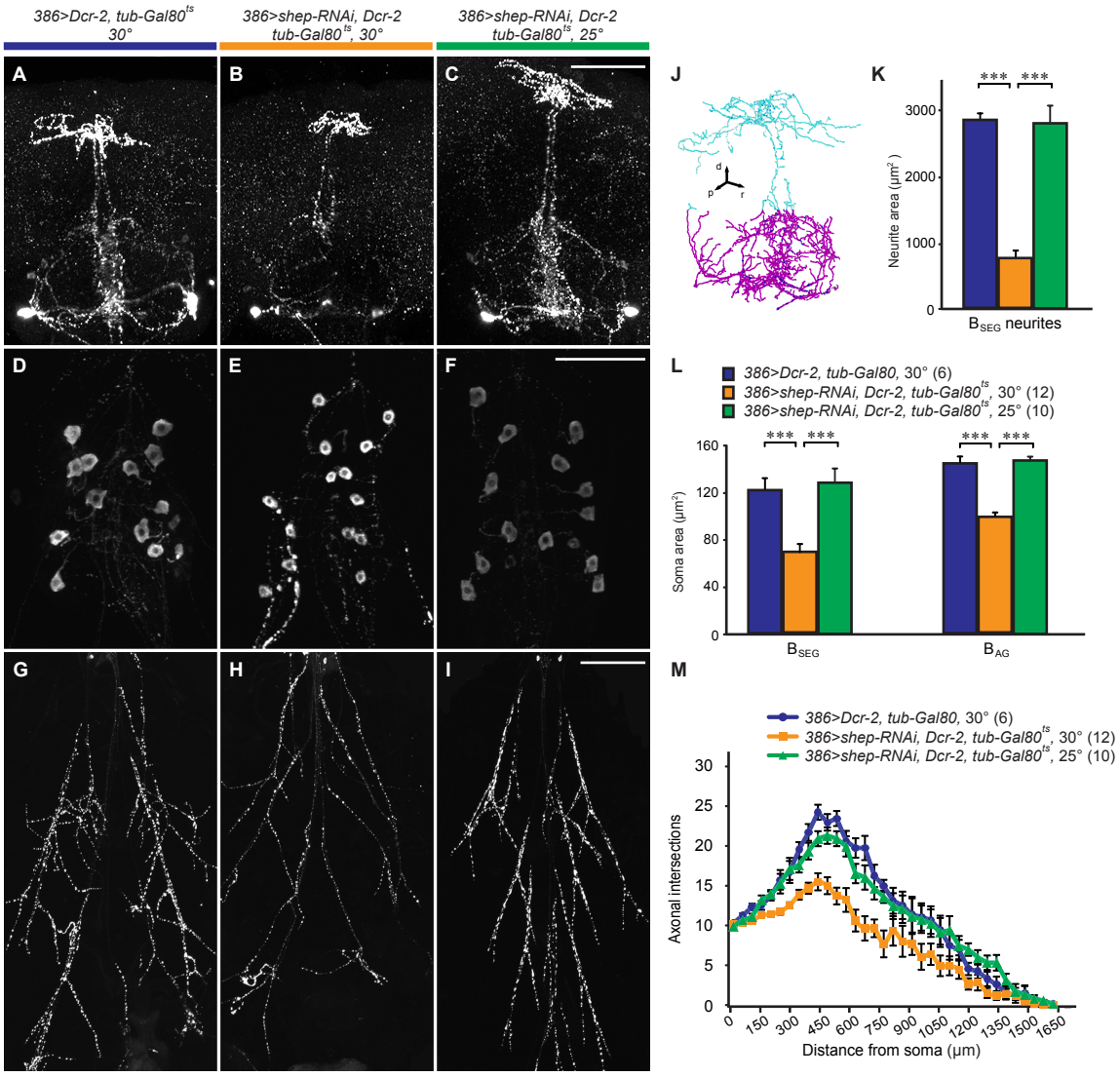
386>Dcr-2, tub-Gal80ts 30°
386>shep-RNAi, Dcr-2 tub-Gal80ts, 30°
386>shep-RNAi, Dcr-2 tub-Gal80ts, 25°
A
B
C
D
E
F
G
H
I
J
d
p
r
K
***
***
3000
2000
1000
0
Neurite area (µm2)
BSEG neurites
L
386>Dcr-2, tub-Gal80, 30° (6)
386>shep-RNAi, Dcr-2, tub-Gal80ts, 30° (12)
386>shep-RNAi, Dcr-2, tub-Gal80ts, 25° (10)
***
***
***
***
160
120
80
40
0
Soma area (µm2)
BSEG
BAG
M
386>Dcr-2, tub-Gal80, 30° (6)
386>shep-RNAi, Dcr-2, tub-Gal80ts, 30° (12)
386>shep-RNAi, Dcr-2, tub-Gal80ts, 25° (10)
30
25
20
15
10
5
0
Axonal intersections
0
150
300
450
600
750
900
1050
1200
1350
1500
1650
Distance from soma (µm)

Figure 3. Plots of wing expansion scores for all deficiencies that produced adult progeny in the test crosses. (A) Percentage of EXW progeny for all deficiencies. Black-filled circles, EXW scores for control crosses (the test stock crossed to the Control A stock) as a function of time (in days) after the test stock was created; Open circles, percentage of EXW progeny in the test crosses (*386>shep-RNAi, Dcr-2, tub-Gal80^{ts}* test stock crossed to individual deficiencies); Magenta-filled and green-filled circles, EXW percentages for suppressor deficiencies that were selected for further analysis; Green-filled circles, EXW percentages for suppressor deficiencies that were mapped to individual genes for tests of cellular rescue; Orange-filled circle, EXW percentage for a deficiency that deleted the *su(Hw)* gene. (B) A similar plot of UEW scores for all deficiencies.

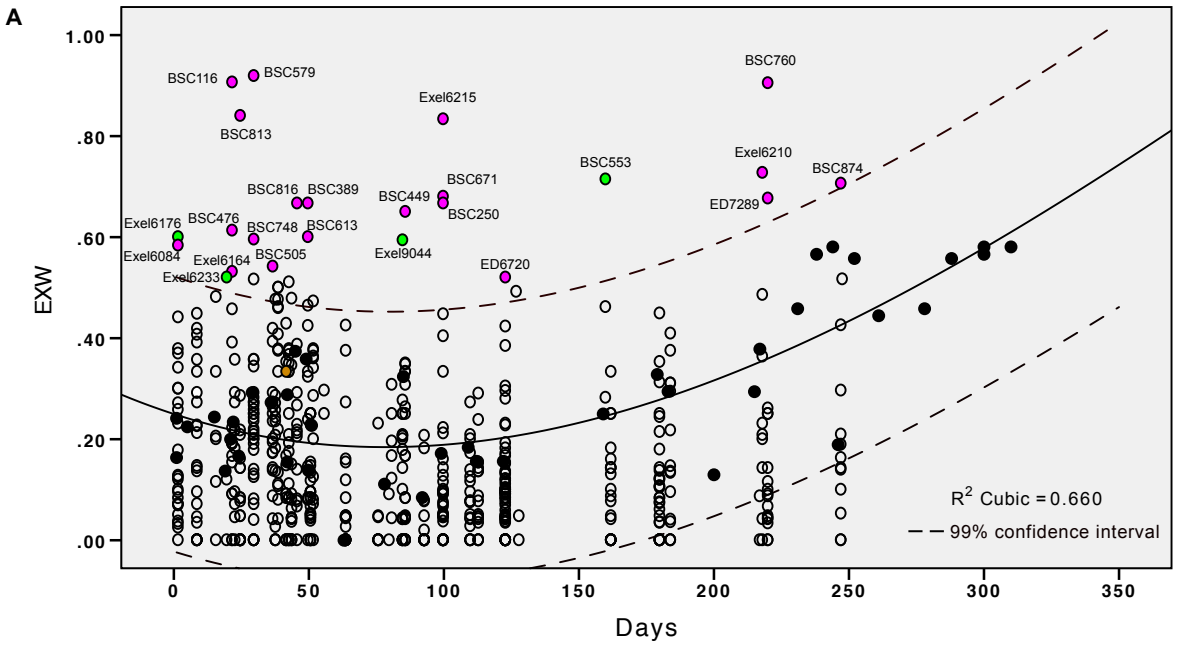
A
EXW
Days
R² Cubic = 0.660
99% confidence interval
BSC116
BSC579
BSC813
Exel6215
BSC760
BSC553
Exel6210
BSC874
BSC671
BSC816
BSC389
BSC449
BSC250
ED7289
Exel6176
BSC476
BSC748
BSC613
Exel6084
Exel6164
BSC505
Exel9044
ED6720
Exel6233

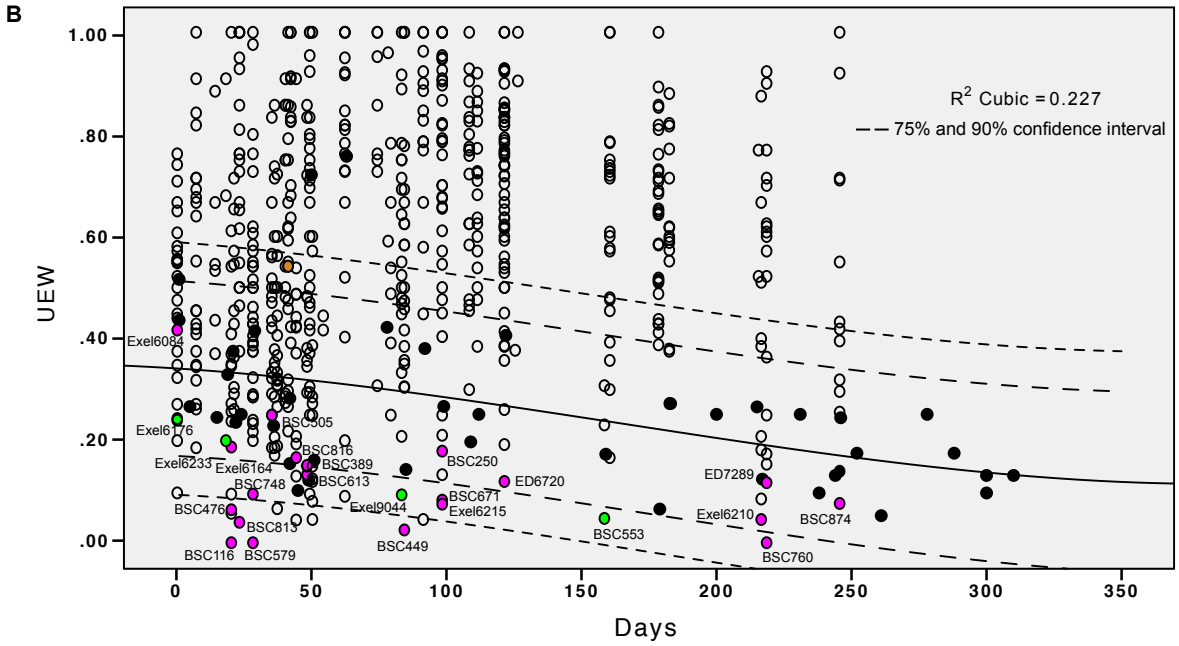
B
UEW
Days
R² Cubic = 0.227
75% and 90% confidence interval
Exel6084
Exel6176
BSC505
BSC816
Exel6233
Exel6164
BSC389
BSC250
ED6720
ED7289
BSC748
BSC613
BSC671
BSC476
Exel9044
Exel6215
Exel6210
BSC874
BSC813
BSC553
BSC116
BSC579
BSC449
BSC760

Figure 4. Suppression of bursicon neuron phenotypes by selected deficiencies. (A-B) Anti-BURS immunostaining detected projections in the thoracic ganglia (panel A) that originated from B_{SEG} neurons in *burs>Dcr-2* animals. These projections were mostly absent in *burs>shep-RNAi, Dcr-2* animals (panel B). Scale bar: 100 μm. (C) Counts of B_{SEG} neuron projections in the thoracic ganglia of progeny from crosses with *burs>shep-RNAi, Dcr-2* to suppressor deficiencies. Phenotypes of the B_{SEG} projections were divided into three categories (orange, yellow, or green), depending on whether none, one, or both B_{SEG} neurites were detected by anti-BURS immunostaining in the thoracic ganglia. (D-F) Rescue of B_{AG} soma areas by suppressor deficiencies. The soma area was reduced in *burs>shep-RNAi, Dcr-2* animals at the P14 pharate adult stage (panel E), and this defect was rescued by crossing *burs>shep-RNAi, Dcr-2* to suppressor deficiencies (as shown for *Df(3R)BSC748* in panel F). Scale bar: 100 μm. (G) Quantification of the mean B_{AG} soma areas in test crosses with 17 suppressor deficiencies. The B_{AG} neuron soma areas were smaller in *burs>shep-RNAi, Dcr-2* P14 pharate adults (orange column) than in the control, *burs>Dcr-2* animals (blue column). A total of 11 of the 17 suppressor deficiencies produced significant rescue of the soma areas (green columns). I performed a one-way ANOVA, $P<0.000001$; (*) $P<0.05$, (**) $P<0.01$, (***) $P<0.001$, Tukey *post hoc* test.

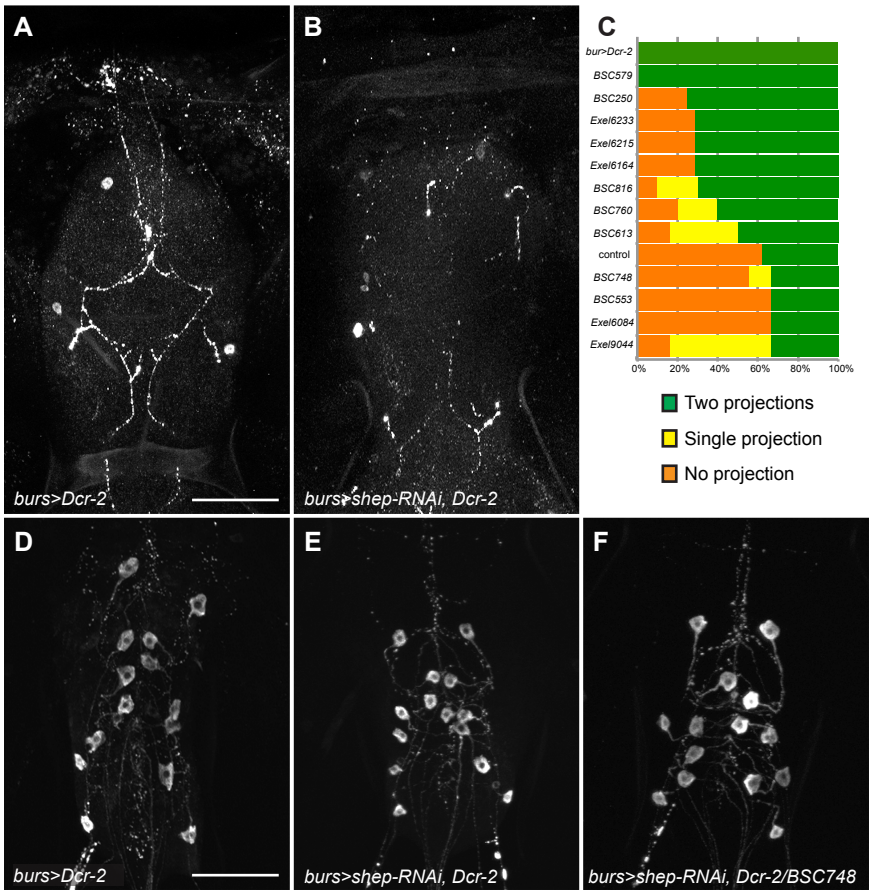
A
B
C
D
E
F
burs>Dcr-2
burs>shep-RNAi, Dcr-2
bur>Dcr-2
BSC579
BSC250
Exel6233
Exel6215
Exel6164
BSC816
BSC760
BSC613
control
BSC748
BSC553
Exel6084
Exel9044
0%
20%
40%
60%
80%
100%
Two projections
Single projection
No projection
burs>Dcr-2
burs>shep-RNAi, Dcr-2
burs>shep-RNAi, Dcr-2/BSC748

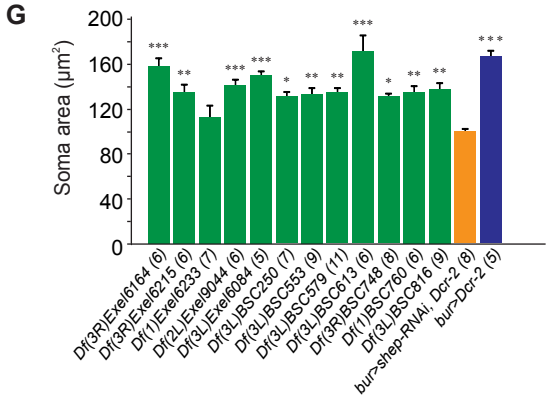
G
Soma area (μm²)
200
160
120
80
40
0
Df(3R)Exel6164 (6)
Df(3R)Exel6215 (6)
Df(1)Exel6233 (7)
Df(2L)Exel9044 (6)
Df(3L)Exel6084 (5)
Df(3L)BSC250 (7)
Df(3L)BSC553 (9)
Df(3L)BSC579 (11)
Df(3L)BSC613 (6)
Df(3R)BSC748 (8)
Df(1)BSC760 (6)
Df(3L)BSC816 (9)
bur>shep-RNAi, Dcr-2 (8)
bur>Dcr-2 (5)

Figure 5. Mapping of candidate *shep* suppressor genes by RNAi. (A) Wing expansion rates obtained in crosses of the *shep* RNAi test stock (*386>shep-RNAi, Dcr-2, tub-Gal80^{ts}*) to RNAi for genes contained within nine selected suppressor deficiencies. The histogram shows a plot of wing expansion scores for each of these crosses. (*) $P<0.05$, (**) $P<0.01$, (***) $P<0.001$ (Fisher's exact test with Bonferroni correction). (B-D) RNAi-mediated rescue of the B_{SEG} neurites. Loss of *shep* led to a reduced B_{SEG} neurite arbor in the subesophageal ganglia (panel C), and loss of suppressor genes partially or completely restored this arbor. Panel D shows rescue of the B_{SEG} neurons by *Oli* RNAi. (E-G) RNAi of suppressor genes rescued B_{AG} neuron soma areas. Loss of *shep* in *burs>shep-RNAi, Dcr-2* animals led to smaller B_{AG} neurons soma areas (panel F) than in control *burs>Dcr-2* animals (E). This defect was rescued by *Dad* RNAi (panel G). Scale bar: 100 μm. (H) Suppression of the wing expansion defects by the *su(Hw)* gene. The mutant alleles, *su(Hw)^{V}* with or without *su(Hw)^{tHa}*, and *su(Hw)* RNAi suppressed the wing expansion defects when crossed to the *386>shep-RNAi, Dcr-2, tub-Gal80^{ts}* test stock. This suppression of the wing expansion defects was also detected for two *su(Hw)* alleles, *su(Hw)^{2}* and *su(Hw)^{V}* with *su(Hw)^{tHa}* when they were crossed to *elav>shep-RNAi, Dcr-2* animals. Data were analyzed with Fisher's exact test with Bonferroni correction at (*) $P<0.05$, (**) $P<0.01$, (***) $P<0.001$. (I) Loss of suppressor genes rescued B_{SEG} neurons neurite areas at 30°. The *386>shep-RNAi, Dcr-2, tub-Gal80^{ts}* animals showed significantly fewer B_{SEG} neurites (orange) than the *386>Dcr-2, tub-Gal80^{ts}* control animals (blue). Introduction of RNAi for four suppressor genes into the *386>shep-RNAi, Dcr-2, tub-Gal80^{ts}* animals produced partial to complete (*CG10565* RNAi) rescue. The data (sample sizes in parentheses) were

analyzed with a One-way ANOVA (P=0.000001) with Tukey HSD *post hoc* tests compared to the control genotype (orange) or between genotypes indicated with a bracket; (*) P<0.05, (**) P<0.01, (***) P<0.001. (I) Quantification of B_{AG} neuron soma areas with or without *Dad-RNAi*. One-way ANOVA, P< 0.000001; Tukey HSD *post hoc* (***) P<0.001. Scale bar: 100 μm.

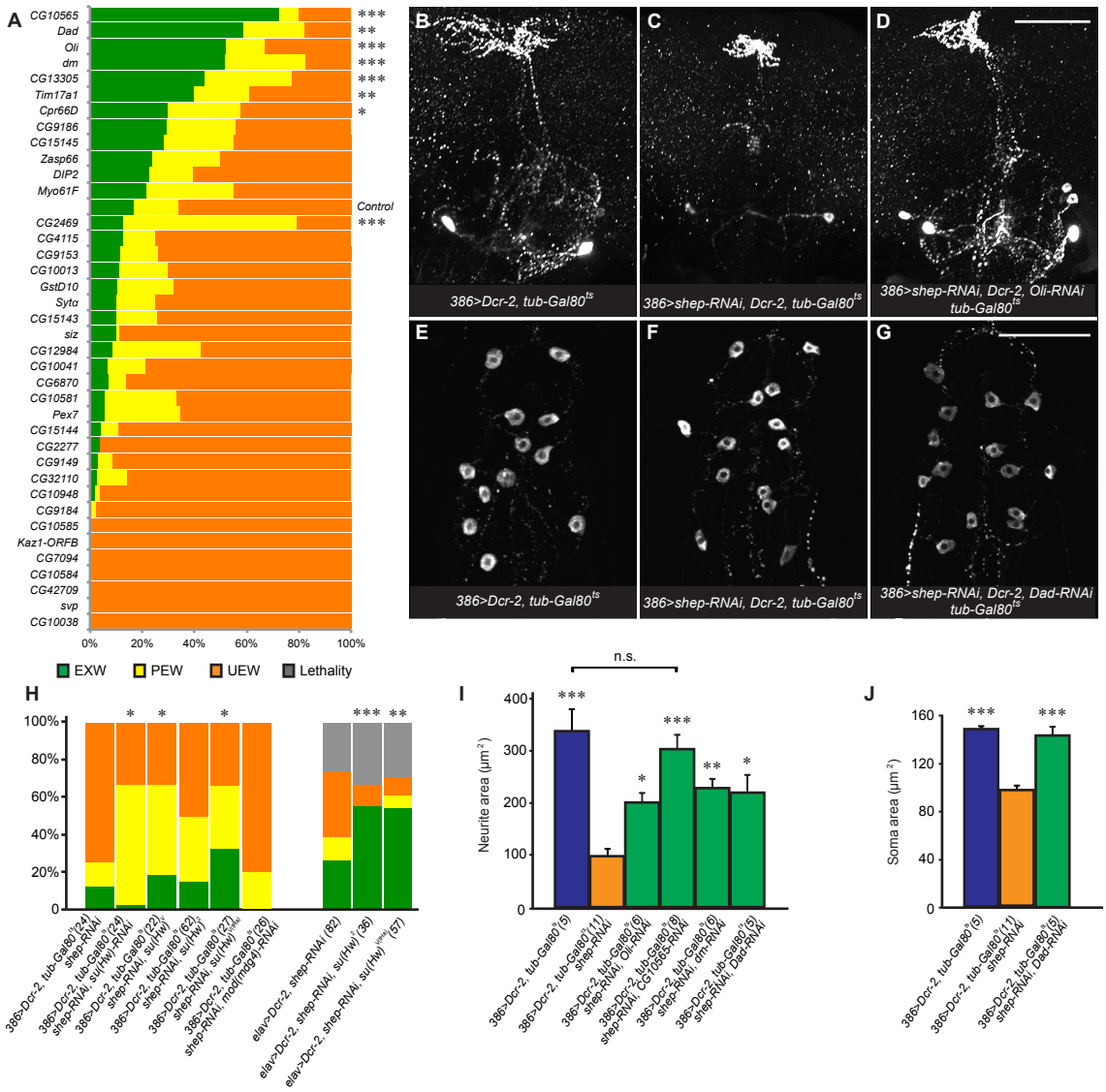
A
CG10565
Dad
Oli
dm
CG13305
Tim17a1
Cpr66D
CG9186
CG15145
Zasp66
DIP2
Myo61F
Control
CG2469
CG4115
CG9153
CG10013
GstD10
Sytα
CG15143
siz
CG12984
CG10041
CG6870
CG10581
Pex7
CG15144
CG2277
CG9149
CG32110
CG10948
CG9184
CG10585
Kaz1-ORFB
CG7094
CG10584
CG42709
svp
CG10038
***
**
***
***
***
**
*
***
0%
20%
40%
60%
80%
100%
EXW
PEW
UEW
Lethality
B
386>Dcr-2, tub-Gal80ts
C
386>shep-RNAi, Dcr-2, tub-Gal80ts
D
386>shep-RNAi, Dcr-2, Oli-RNAi tub-Gal80ts
E
386>Dcr-2, tub-Gal80ts
F
386>shep-RNAi, Dcr-2, tub-Gal80ts
G
386>shep-RNAi, Dcr-2, Dad-RNAi tub-Gal80ts
H
100%
80%
60%
40%
20%
0
I
n.s.
Neurite area (μm2)
400
300
200
100
0
J
Soma area (μm2)
160
120
80
40
0

Figure 6. Suppression of the wing expansion defects and bursicon cellular defects by *Dad* and *Oli* alleles. (A) Heterozygous *Oli* and *Dad* alleles suppressed the wing expansion defects caused by *shep* RNAi. Wing expansion scores for the genotypes shown were analyzed with the Fisher's exact test with Bonferroni correction, (***) $P<0.001$. EXW, expanded wings; PEW, partially expanded wings; UEW, unexpanded wings. (B) The $Oli^{\Delta 9}$ mutant allele partially restored the cellular defects of seen in bursicon neurons with *shep* RNAi. (*) $P<0.05$, (**) $P<0.01$, (***) $P<0.001$ [One-way ANOVA (P=0.000017, 0.00005, and 0.00217 for B_{AG}, B_{SEG} and B_{SEG} neurites, respectively) with Tukey HSD *post hoc*]. (C) Sholl analysis of B_{AG} peripheral axon arbors. When crossed to the *386>shep-RNAi, Dcr-2, tub-Gal80^{ts}* test stock, the $Oli^{\Delta 9}$ mutant allele partially rescued B_{AG} peripheral axon branching defects caused by loss of *shep*. (D) The Dad^{212} mutant positively affected the soma area of the B_{AG} cells in *shep* mutants. Crossing the *386>shep-RNAi, Dcr-2, tub-Gal80^{ts}* test stock to a *yw* genetic background produced weaker cellular phenotypes in the B_{AG} cells. With Dad^{212}, the soma area was larger, although this effect was not statistically significant (P=0.0957).

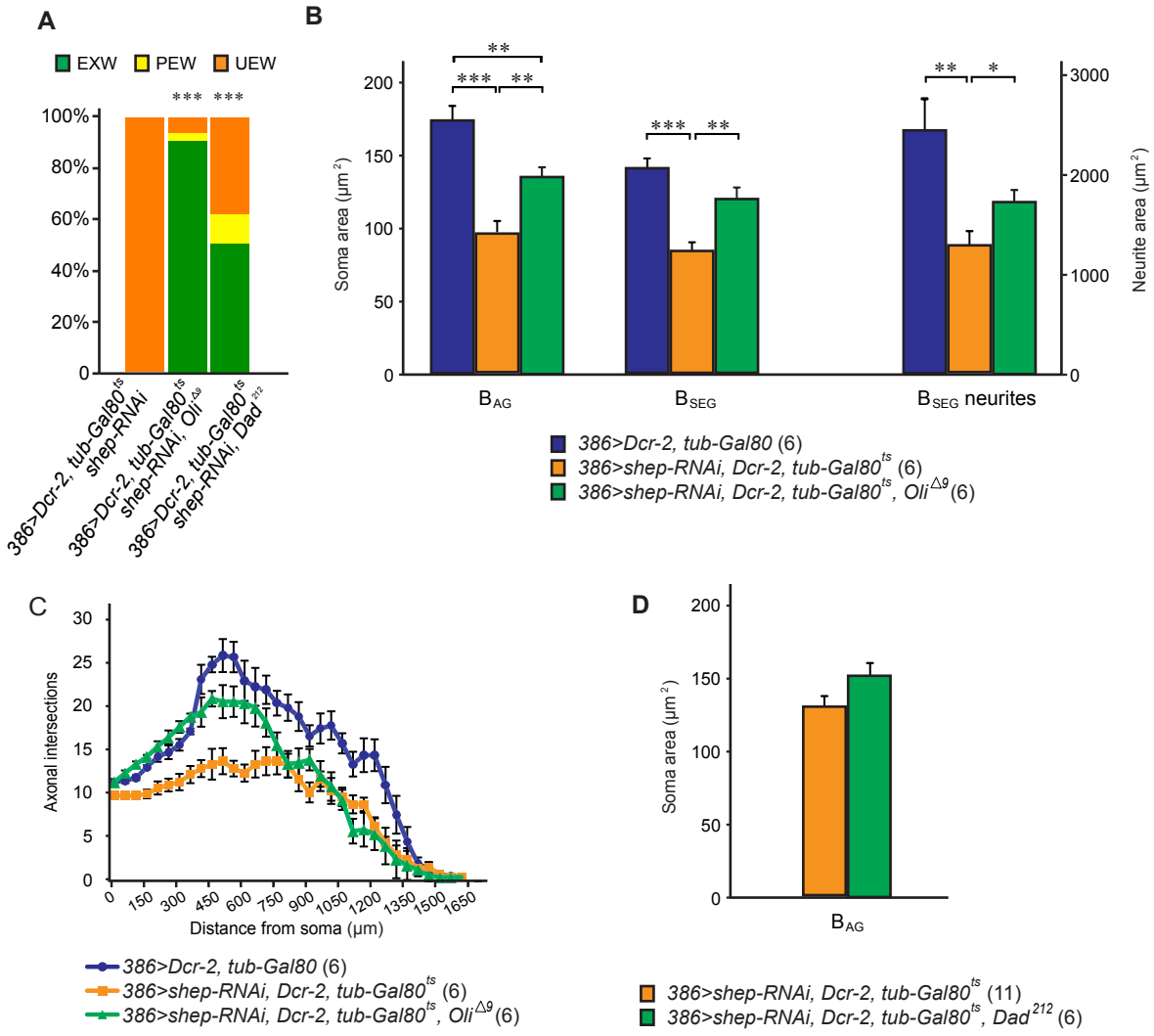
A
EXW
PEW
UEW
*** ***
100%
80%
60%
40%
20%
0
386>Dcr-2, tub-Gal80ts shep-RNAi
386>Dcr-2, tub-Gal80ts shep-RNAi, Oli△9
386>Dcr-2, tub-Gal80ts shep-RNAi, Dad212
B
**
*** **
*** **
** *
Soma area (µm2)
Neurite area (µm2)
200
150
100
50
0
3000
2000
1000
0
BAG
BSEG
BSEG neurites
386>Dcr-2, tub-Gal80 (6)
386>shep-RNAi, Dcr-2, tub-Gal80ts (6)
386>shep-RNAi, Dcr-2, tub-Gal80ts, Oli△9 (6)
C
Axonal intersections
30
25
20
15
10
5
0
0 150 300 450 600 750 900 1050 1200 1350 1500 1650
Distance from soma (µm)
386>Dcr-2, tub-Gal80 (6)
386>shep-RNAi, Dcr-2, tub-Gal80ts (6)
386>shep-RNAi, Dcr-2, tub-Gal80ts, Oli△9 (6)
D
Soma area (µm2)
200
150
100
50
0
BAG
386>shep-RNAi, Dcr-2, tub-Gal80ts (11)
386>shep-RNAi, Dcr-2, tub-Gal80ts, Dad212 (6)

Figure 7. Wing expansion percentages for test crosses with deficiencies. Wing expansion rates were quantified and plotted for progeny of test crosses between *386>shep-RNAi, Dcr-2, tub-Gal80ts* flies and then 632 deficiencies that generated adult progeny. The rates were ranked based on EXW and then PEW scores.

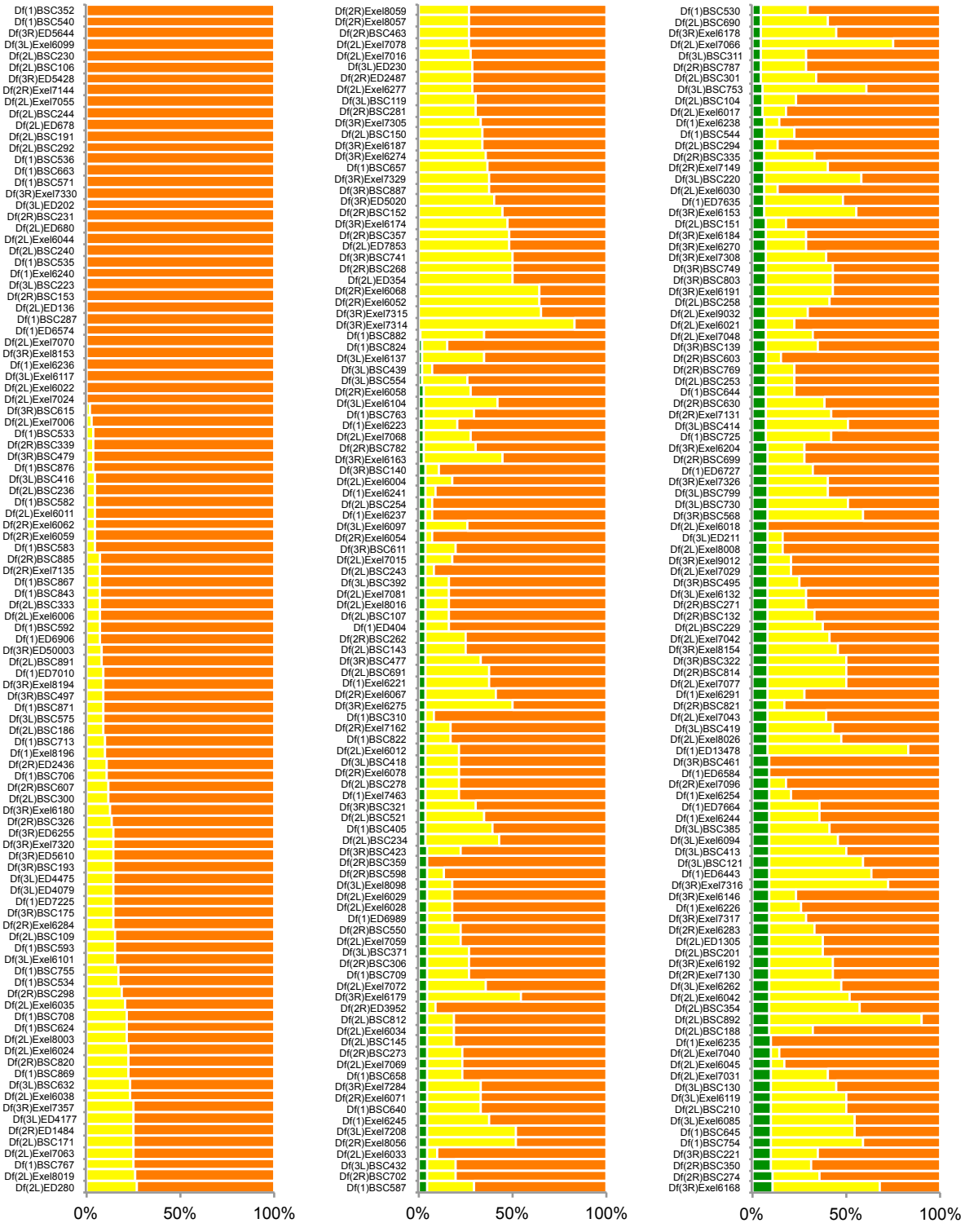
Df(1)BSC352
Df(1)BSC540
Df(3R)ED5644
Df(3L)Exel6099
Df(2L)BSC230
Df(2L)BSC106
Df(3R)ED5428
Df(2R)Exel7144
Df(2L)Exel7055
Df(2L)BSC244
Df(2L)ED678
Df(2L)BSC191
Df(2L)BSC292
Df(1)BSC536
Df(1)BSC663
Df(1)BSC571
Df(3R)Exel7330
Df(3L)ED202
Df(2R)BSC231
Df(2L)ED680
Df(2L)Exel6044
Df(2L)BSC240
Df(1)BSC535
Df(1)Exel6240
Df(3L)BSC223
Df(2R)BSC153
Df(2L)ED136
Df(1)BSC287
Df(1)ED6574
Df(2L)Exel7070
Df(3R)Exel8153
Df(1)Exel6236
Df(3L)Exel6117
Df(2L)Exel6022
Df(2L)Exel7024
Df(3R)BSC615
Df(2L)Exel7006
Df(1)BSC533
Df(2R)BSC339
Df(3R)BSC479
Df(1)BSC876
Df(3L)BSC416
Df(2L)BSC236
Df(1)BSC582
Df(2L)Exel6011
Df(2R)Exel6062
Df(2R)Exel6059
Df(1)BSC583
Df(2R)BSC885
Df(2R)Exel7135
Df(1)BSC867
Df(1)BSC843
Df(2L)BSC333
Df(2L)Exel6006
Df(1)BSC592
Df(1)ED6906
Df(3R)ED50003
Df(2L)BSC891
Df(1)ED7010
Df(3R)Exel8194
Df(3R)BSC497
Df(1)BSC871
Df(3L)BSC575
Df(2L)BSC186
Df(1)BSC713
Df(1)Exel8196
Df(2R)ED2436
Df(1)BSC706
Df(2R)BSC607
Df(2L)BSC300
Df(3R)Exel6180
Df(2R)BSC326
Df(3R)ED6255
Df(3R)Exel7320
Df(3R)ED5610
Df(3R)BSC193
Df(3L)ED4475
Df(3L)ED4079
Df(1)ED7225
Df(3R)BSC175
Df(2R)Exel6284
Df(2L)BSC109
Df(1)BSC593
Df(3L)Exel6101
Df(1)BSC755
Df(1)BSC534
Df(2R)BSC298
Df(2L)Exel6035
Df(1)BSC708
Df(1)BSC624
Df(2L)Exel8003
Df(2L)Exel6024
Df(2R)BSC820
Df(1)BSC869
Df(3L)BSC632
Df(2L)Exel6038
Df(3R)Exel7357
Df(3L)ED4177
Df(2R)ED1484
Df(2L)BSC171
Df(2L)Exel7063
Df(1)BSC767
Df(2L)Exel8019
Df(2L)ED280
0%
50%
100%
Df(2R)Exel8059
Df(2R)Exel8057
Df(2R)BSC463
Df(2L)Exel7078
Df(2L)Exel7016
Df(3L)ED230
Df(2R)ED2487
Df(2L)Exel6277
Df(3L)BSC119
Df(2R)BSC281
Df(3R)Exel7305
Df(2L)BSC150
Df(3R)Exel6187
Df(3R)Exel6274
Df(1)BSC657
Df(3R)Exel7329
Df(3R)BSC887
Df(3R)ED5020
Df(2R)BSC152
Df(3R)Exel6174
Df(2R)BSC357
Df(2L)ED7853
Df(3R)BSC741
Df(2R)BSC268
Df(2L)ED354
Df(2R)Exel6068
Df(2R)Exel6052
Df(3R)Exel7315
Df(3R)Exel7314
Df(1)BSC882
Df(1)BSC824
Df(3L)Exel6137
Df(3L)BSC439
Df(3L)BSC554
Df(2R)Exel6058
Df(3L)Exel6104
Df(1)BSC763
Df(1)Exel6223
Df(2L)Exel7068
Df(2R)BSC782
Df(3R)Exel6163
Df(3R)BSC140
Df(2L)Exel6004
Df(1)Exel6241
Df(2L)BSC254
Df(1)Exel6237
Df(3L)Exel6097
Df(2R)Exel6054
Df(3R)BSC611
Df(2L)Exel7015
Df(2L)BSC243
Df(3L)BSC392
Df(2L)Exel7081
Df(2L)Exel8016
Df(2L)BSC107
Df(1)ED404
Df(2R)BSC262
Df(2L)BSC143
Df(3R)BSC477
Df(2L)BSC691
Df(1)Exel6221
Df(2R)Exel6067
Df(3R)Exel6275
Df(1)BSC310
Df(2R)Exel7162
Df(1)BSC822
Df(2L)Exel6012
Df(3L)BSC418
Df(2R)Exel6078
Df(2L)BSC278
Df(1)Exel7463
Df(3R)BSC321
Df(2L)BSC521
Df(1)BSC405
Df(2L)BSC234
Df(3R)BSC423
Df(2R)BSC359
Df(2R)BSC598
Df(3L)Exel8098
Df(2L)Exel6029
Df(2L)Exel6028
Df(1)ED6989
Df(2R)BSC550
Df(2L)Exel7059
Df(3L)BSC371
Df(2R)BSC306
Df(1)BSC709
Df(2L)Exel7072
Df(3R)Exel6179
Df(2R)ED3952
Df(2L)BSC812
Df(2L)Exel6034
Df(2L)BSC145
Df(2R)BSC273
Df(2L)Exel7069
Df(1)BSC658
Df(3R)Exel7284
Df(2R)Exel6071
Df(1)BSC640
Df(1)Exel6245
Df(3L)Exel7208
Df(2R)Exel8056
Df(2L)Exel6033
Df(3L)BSC432
Df(2R)BSC702
Df(1)BSC587
0%
50%
100%
Df(1)BSC530
Df(2L)BSC690
Df(3R)Exel6178
Df(2L)Exel7066
Df(3L)BSC311
Df(2R)BSC787
Df(2L)BSC301
Df(3L)BSC753
Df(2L)BSC104
Df(2L)Exel6017
Df(1)Exel6238
Df(1)BSC544
Df(2L)BSC294
Df(2R)BSC335
Df(2R)Exel7149
Df(3L)BSC220
Df(2L)Exel6030
Df(1)ED7635
Df(3R)Exel6153
Df(2L)BSC151
Df(3R)Exel6184
Df(3R)Exel6270
Df(3R)Exel7308
Df(3R)BSC749
Df(3R)BSC803
Df(3R)Exel6191
Df(2L)BSC258
Df(2L)Exel9032
Df(2L)Exel6021
Df(2L)Exel7048
Df(3R)BSC139
Df(2R)BSC603
Df(2R)BSC769
Df(2L)BSC253
Df(1)BSC644
Df(2R)BSC630
Df(2R)Exel7131
Df(3L)BSC414
Df(1)BSC725
Df(3R)Exel6204
Df(2R)BSC699
Df(1)ED6727
Df(3R)Exel7326
Df(3L)BSC799
Df(3L)BSC730
Df(3R)BSC568
Df(2L)Exel6018
Df(3L)ED211
Df(2L)Exel8008
Df(3R)Exel9012
Df(2L)Exel7029
Df(3R)BSC495
Df(3L)Exel6132
Df(2R)BSC271
Df(2R)BSC132
Df(2L)BSC229
Df(2L)Exel7042
Df(3R)Exel8154
Df(3R)BSC322
Df(2R)BSC814
Df(2L)Exel7077
Df(1)Exel6291
Df(2R)BSC821
Df(2L)Exel7043
Df(3L)BSC419
Df(2L)Exel8026
Df(1)ED13478
Df(3R)BSC461
Df(1)ED6584
Df(2R)Exel7096
Df(1)Exel6254
Df(1)ED7664
Df(1)Exel6244
Df(3L)BSC385
Df(3L)Exel6094
Df(3L)BSC413
Df(3L)BSC121
Df(1)ED6443
Df(3R)Exel7316
Df(3R)Exel6146
Df(1)Exel6226
Df(3R)Exel7317
Df(2R)Exel6283
Df(2L)ED1305
Df(2L)BSC201
Df(3R)Exel6192
Df(2R)Exel7130
Df(3L)Exel6262
Df(2L)Exel6042
Df(2L)BSC354
Df(2L)BSC892
Df(2L)BSC188
Df(1)Exel6235
Df(2L)Exel7040
Df(2L)Exel6045
Df(2L)Exel7031
Df(3L)BSC130
Df(3L)Exel6119
Df(2L)BSC210
Df(3L)Exel6085
Df(1)BSC645
Df(1)BSC754
Df(3R)BSC221
Df(2R)BSC350
Df(2R)BSC274
Df(3R)Exel6168
0%
50%
100%

Df(3L)Exel6134
Df(2L)BSC202
Df(2L)BSC234
Df(3R)Exel8158
Df(2R)Exel6077
Df(1)BSC570
Df(2R)BSC858
Df(2L)ED369
Df(2L)Exel8036
Df(2L)Exel6047
Df(3R)BSC137
Df(1)ED6957
Df(3R)Exel6155
Df(2R)BSC829
Df(2R)Exel6057
Df(2R)BSC135
Df(2L)BSC689
Df(2L)BSC862
Df(3L)BSC673
Df(3R)Exel6141
Df(3R)BSC683
Df(2L)BSC407
Df(3L)Exel6128
Df(2L)Exel6041
Df(2L)Exel6005
Df(3L)BSC561
Df(2L)Exel8033
Df(3R)Exel7313
Df(2R)Exel6056
Df(3R)Exel6152
Df(2L)Exel6009
Df(2R)BSC608
Df(2R)Exel6070
Df(1)Exel6234
Df(3L)BSC675
Df(3L)Exel9002
Df(3R)BSC194
Df(3R)BSC881
Df(3L)BSC437
Df(2R)Exel7173
Df(3R)BSC506
Df(3L)BSC370
Df(3L)BSC431
Df(2R)BSC696
Df(2R)BSC161
Df(2L)BSC209
Df(2L)Exel8034
Df(3L)ED4288
Df(2L)ED611
Df(1)ED6521
Df(3R)Exel9025
Df(2L)BSC110
Df(2L)BSC692
Df(2L)Exel6003
Df(3L)BSC157
Df(3R)BSC174
Df(3L)BSC369
Df(3R)BSC634
Df(1)ED12432
Df(2R)Exel8047
Df(3L)Exel6096
Df(3R)Exel6154
Df(3L)BSC452
Df(1)BSC629
Df(2L)Exel7049
Df(2L)BSC296
Df(2R)BSC597
Df(1)Exel6231
Df(2R)ED50004
Df(2R)BSC856
Df(3L)Exel9057
Df(2R)BSC355
Df(3L)Exel6090
Df(2R)BSC260
Df(2L)BSC454
Df(3R)BSC789
Df(2R)BSC360
Df(2R)BSC308
Df(3R)BSC567
Df(3L)BSC126
Df(2R)Exel6069
Df(3L)BSC649
Df(2L)BSC200
Df(2R)BSC347
Df(3L)BSC555
Df(3L)BSC378
Df(3R)Exel7318
Df(3R)Exel6147
Df(2L)BSC165
Df(3L)BSC670
Df(2R)BSC265
Df(2L)Exel6046
Df(3R)Exel6182
Df(3L)BSC249
Df(2L)ED479
Df(2L)BSC215
Df(3L)BSC441
Df(3R)BSC788
Df(3L)BSC612
Df(3L)BSC128
Df(2R)BSC482
Df(3R)Exel6272
Df(3L)Exel6279
Df(3L)BSC839
Df(2L)Exel7038
Df(3R)BSC422
0%
50%
100%
Df(2R)Exel7150
Df(3R)Exel9013
Df(3R)BSC549
Df(3L)BSC450
Df(2R)BSC263
Df(3R)BSC502
Df(3L)BSC837
Df(2L)BSC251
Df(3L)BSC844
Df(3L)Exel7210
Df(2L)Exel8041
Df(2L)BSC291
Df(3L)BSC390
Df(2L)Exel6031
Df(3R)Exel7310
Df(2R)Exel7138
Df(3L)BSC734
Df(2L)ED1231
Df(3L)BSC445
Df(3L)BSC386
Df(3L)Exel6118
Df(3L)Exel6095
Df(3R)BSC793
Df(3R)BSC617
Df(2R)BSC361
Df(2R)BSC429
Df(2R)BSC303
Df(3R)Exel6195
Df(3R)Exel6189
Df(3L)BSC672
Df(3R)BSC124
Df(3R)BSC503
Df(3R)Exel7327
Df(1)ED6712
Df(3L)Exel6110
Df(1)Exel6239
Df(3R)Exel6264
Df(3L)BSC560
Df(2R)BSC356
Df(3L)Exel6083
Df(2R)BSC346
Df(3L)BSC446
Df(1)BSC662
Df(3L)BSC374
Df(3R)BSC686
Df(3L)BSC833
Df(2L)Exel6013
Df(3R)BSC467
Df(1)BSC623
Df(3L)BSC578
Df(3R)BSC636
Df(2R)Exel7092
Df(2R)BSC770
Df(2L)Exel6002
Df(3R)Exel8155
Df(3R)BSC806
Df(1)Exel6242
Df(3L)BSC736
Df(3L)BSC366
Df(3R)Exel6265
Df(2L)Exel7018
Df(1)ED6829
Df(2L)BSC239
Df(3L)Exel6105
Df(2R)Exel6072
Df(3R)Exel6185
Df(2R)ED2747
Df(2R)BSC889
Df(1)ED14021
Df(2R)BSC264
Df(3L)BSC224
Df(3R)Exel6143
Df(3L)BSC815
Df(1)ED7217
Df(3L)BSC733
Df(3R)BSC397
Df(3L)BSC817
Df(3L)BSC838
Df(3L)Exel6086
Df(3R)BSC847
Df(3R)ED10642
Df(3R)BSC650
Df(3R)BSC500
Df(2R)BSC400
Df(3R)Exel6269
Df(3R)Exel6183
Df(2R)Exel7123
Df(2L)BSC180
Df(2L)Exel6048
Df(3L)BSC835
Df(3R)Exel6169
Df(2R)BSC697
Df(3R)BSC547
Df(3R)BSC744
Df(2R)BSC606
Df(3R)BSC752
Df(3R)Exel6267
Df(3R)Exel6197
Df(3R)BSC510
Df(3L)BSC727
Df(2R)Exel6082
Df(2L)Exel7071
Df(1)Exel6227
Df(3R)Exel6216
Df(3R)Exel6203
Df(3L)Exel6087
0%
50%
100%
Df(1)Exel6255
Df(2L)Exel7034
Df(3L)Exel7253
Df(2R)BSC408
Df(2R)BSC279
Df(2R)BSC600
Df(3L)Exel9048
Df(3L)Exel9008
Df(3R)Exel6273
Df(3R)BSC318
Df(3R)Exel7378
Df(3L)BSC559
Df(3L)BSC375
Df(3R)Exel8143
Df(3R)BSC740
Df(3L)Exel6093
Df(2L)ED1317
Df(3L)BSC289
Df(3L)BSC181
Df(3R)Exel6209
Df(3R)BSC791
Df(1)Exel7468
Df(3L)Exel6130
Df(3R)Exel6276
Df(3L)BSC875
Df(2R)BSC383
Df(3L)BSC631
Df(3R)Exel6200
Df(3R)Exel6170
Df(3R)BSC499
Df(3R)BSC666
Df(3L)BSC674
Df(3L)BSC458
Df(3R)BSC620
Df(3R)Exel6202
Df(3R)Exel6198
Df(3L)BSC113
Df(3L)Exel6102
Df(2R)BSC307
Df(3L)Exel6103
Df(3L)BSC796
Df(3L)Exel6122
Df(3R)Exel6156
Df(3R)Exel6186
Df(3R)BSC507
Df(2L)ED206
Df(3R)BSC564
Df(3L)BSC125
Df(3L)Exel9004
Df(3R)BSC320
Df(3L)BSC363
Df(3L)Exel6089
Df(3R)Exel8162
Df(2R)BSC337
Df(3L)Exel6138
Df(3L)BSC391
Df(1)ED7153
Df(3R)BSC504
Df(2R)BSC883
Df(2R)BSC485
Df(3R)BSC486
Df(3L)Exel6112
Df(3R)Exel6173
Df(3R)Exel6196
Df(2L)Exel6007
Df(3R)Exel6167
Df(3R)Exel8178
Df(3R)Exel7328
Df(3L)Exel6116
Df(3R)BSC819
Df(3R)BSC681
Df(3L)Exel6098
Df(3L)BSC884
Df(1)ED7441
Df(3L)Exel8101
Df(3R)Exel9014
Df(3R)Exel6201
Df(3L)Exel6107
Df(3R)BSC618
Df(1)Exel6233
Df(3L)BSC379
Df(1)ED6720
Df(3L)BSC449
Df(2L)Exel9044
Df(3L)BSC117
Df(3R)Exel6164
Df(3R)BSC505
Df(3L)Exel6084
Df(3R)Exel6176
Df(3L)BSC613
Df(3R)BSC476
Df(3R)BSC748
Df(3L)BSC250
Df(3L)BSC816
Df(3L)BSC389
Df(1)ED7289
Df(3L)BSC671
Df(3R)BSC874
Df(3L)BSC553
Df(3R)Exel6210
Df(3R)Exel6215
Df(2R)BSC813
Df(1)BSC760
Df(3L)BSC116
Df(3L)BSC579
0%
50%
100%

Figure 8. Wing expansion rates in control crosses with two separately prepared stocks of the test stock, *386>shep-RNAi, Dcr-2, tub-Gal80ts*. The percentage of EXW adults obtained with the test stock 1 was plotted as a function of time with filled circles, and the scores obtained with test stock 2 were plotted with crosses. The day a test stock was used for the first time was set as day 1.

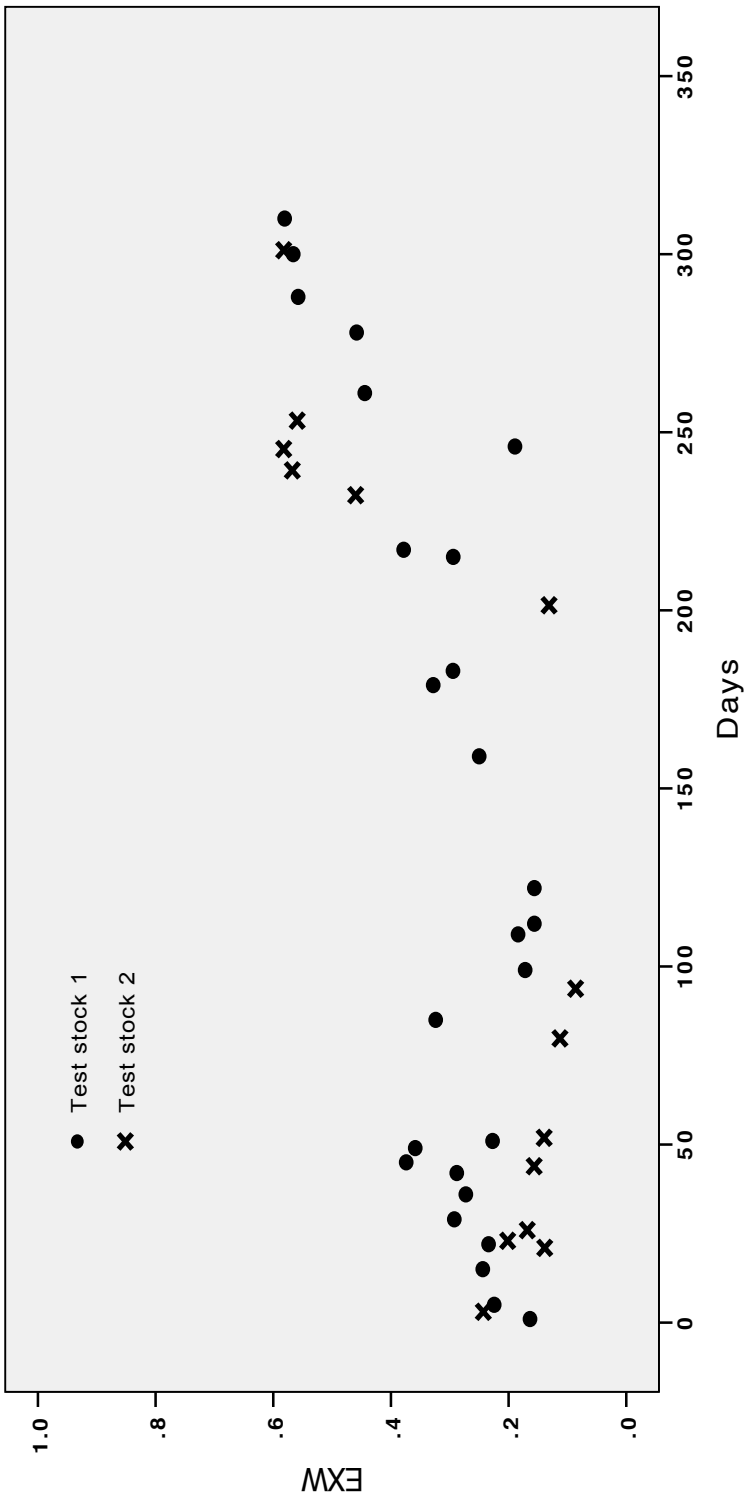
EXW
1.0
.8
.6
.4
.2
.0
0
50
100
150
200
250
300
350
Days
Test stock 1
Test stock 2

Figure 9. The bursicon neurons were a subgroup of neurons in the *386-Gal4* pattern. (A) *386-Gal4* was used to express *UAS-mCD8::GFP* in a P14 stage pharate adult CNS. (B) The same nervous system was labeled by anti-BURS immunostaining. (C) Merged image. Both the B_{SEG} (insets) and B_{AG} neurons (arrows) displayed co-localization of the mCD8::GFP reporter and BURS. Scale bars: 50 μm; insets, 3 μm.

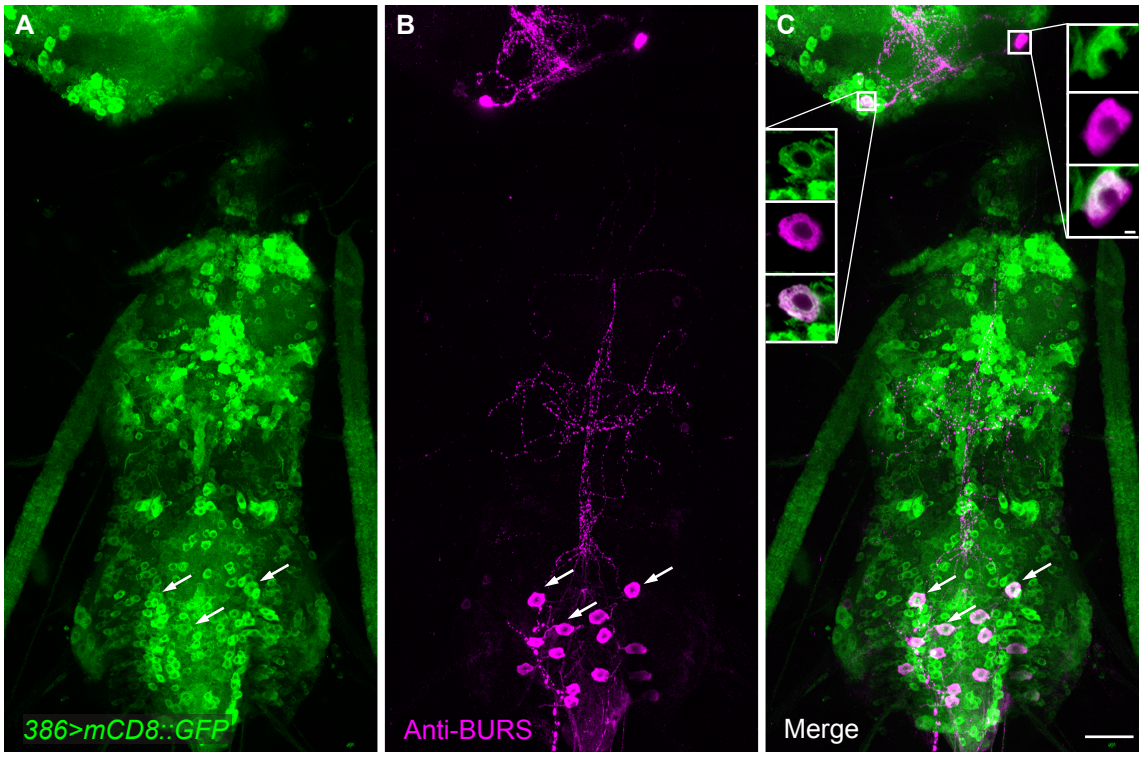
A
B
C
386>mCD8::GFP
Anti-BURS
Merge

Figure 10. Suppressor deficiencies did not affect growth or expression of a mCD8::GFP reporter in the B_{AG} neurons at the P14 pharate adult stage. (A-C) The B_{AG} neurons expressed bursicon peptides (panel B, anti-BURS immunostaining) that were co-localized with mCD8::GFP driven under control of the *ccap-Gal4* driver (panel A). Panel C shows the merged image. Scale bar: 100 μm. (D) Expression levels of mCD8::GFP, measured as soma fluorescence, in progeny of crosses of a *ccap>mCD8::GFP* strain to the suppressor deficiencies. (E) B_{AG} neuron soma areas resulting from the the same crosses as in (D). The most anterior pair of the B_{AG} neurons (arrowheads in panel C) were examined. None of the suppressor deficiencies affected mCD8::GFP expression levels or soma areas. One-way ANOVA, $P< 0.000001$; Tukey HSD *post hoc* (***) $P<0.001$.

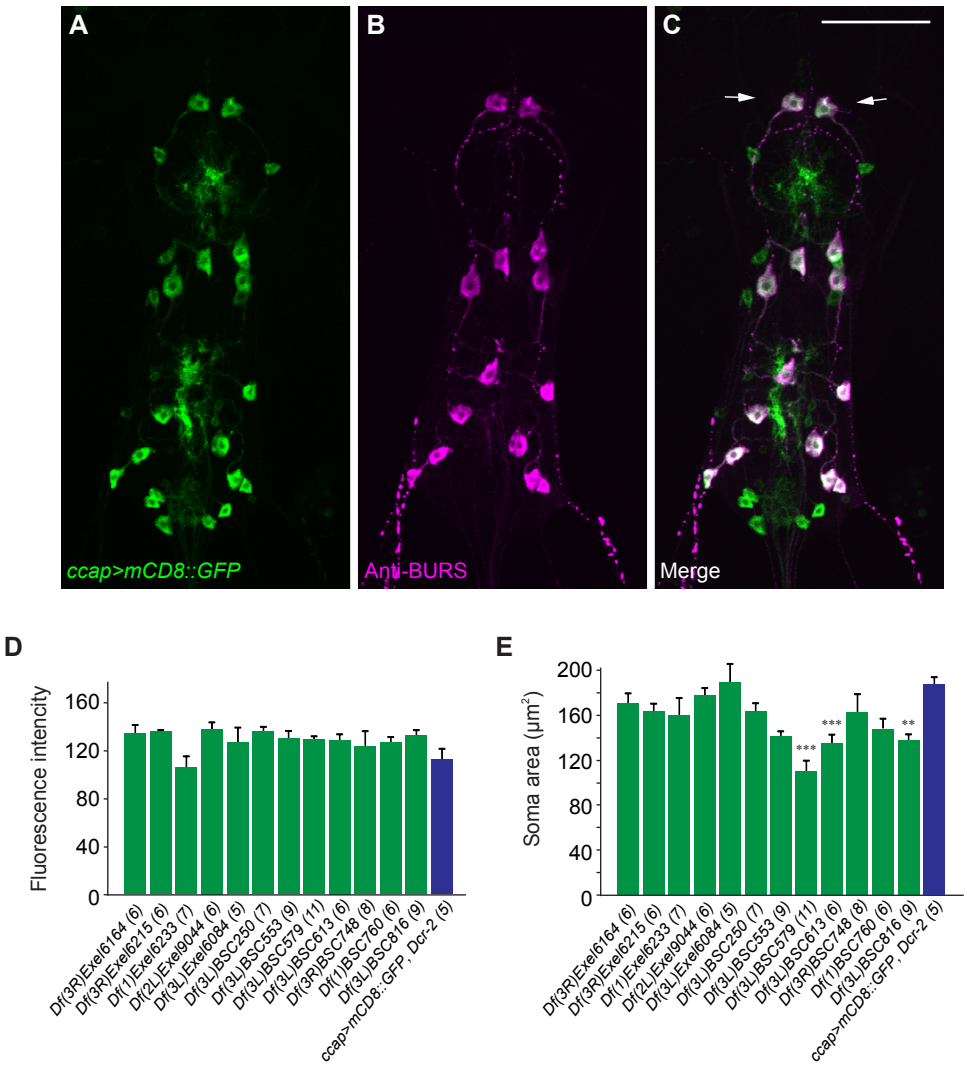
A
B
C
ccap>mCD8::GFP
Anti-BURS
Merge
D
Fluorescence intencity
0
40
80
120
160
Df(3R)Exel6164 (6)
Df(3R)Exel6215 (6)
Df(1)Exel6233 (7)
Df(2L)Exel9044 (6)
Df(3L)Exel6084 (5)
Df(3L)BSC250 (7)
Df(3L)BSC553 (9)
Df(3L)BSC579 (11)
Df(3L)BSC613 (6)
Df(3R)BSC748 (8)
Df(1)BSC760 (6)
Df(3L)BSC816 (9)
ccap>mCD8::GFP , Dcr-2 (5)
E
Soma area (μm²)
0
40
80
120
160
200
***
***
**
Df(3R)Exel6164 (6)
Df(3R)Exel6215 (6)
Df(1)Exel6233 (7)
Df(2L)Exel9044 (6)
Df(3L)Exel6084 (5)
Df(3L)BSC250 (7)
Df(3L)BSC553 (9)
Df(3L)BSC579 (11)
Df(3L)BSC613 (6)
Df(3R)BSC748 (8)
Df(1)BSC760 (6)
Df(3L)BSC816 (9)
ccap>mCD8::GFP , Dcr-2 (5)

Figure 11. The *Dad*, *CG10565*, and *Oli* suppressor genes did not independently affect bursicon neuron morphological features where the genetic interactions with *shep* were detected. (A) *Dad-RNAi* and *CG10565-RNAi* did not affect the B_{SEG} neurites and/or B_{AG} soma areas. Following a cross of *Dad-RNAi* and *386>Dcr-2, tub-Gal80^{ts}* flies, loss of *Dad* alone did not alter B_{SEG} neurite or B_{AG} soma areas. RNAi-mediated loss of *CG10565* resulted in smaller B_{AG} soma area, but the B_{SEG} neurite area was normal. ***, $P<0.001$ [one-way ANOVA ($P<0.000001$, B_{AG} soma area; $P=0.338$, B_{SEG} neurite area). (B) Loss of *CG10565* led to reduced branching in the B_{AG} peripheral axon arbor (Sholl analysis). (C) *Oli$^{\Delta 9}$* alone did not affect bursicon neuron morphology. Crosses of *Oli$^{\Delta 9}$* to *386>Dcr-2, tub-Gal80^{ts}* generated flies with normal B_{AG} and B_{SEG} soma areas, and B_{SEG} neurite areas (Student's *t*-test; $P=0.453544$, 0.509066, and 0.952419, respectively). (D) *Oli$^{\Delta 9}$* alone did not affect branching in the B_{AG} peripheral axon arbor (Sholl analysis). The numbers following the genotypes in (A-D) are sample sizes.

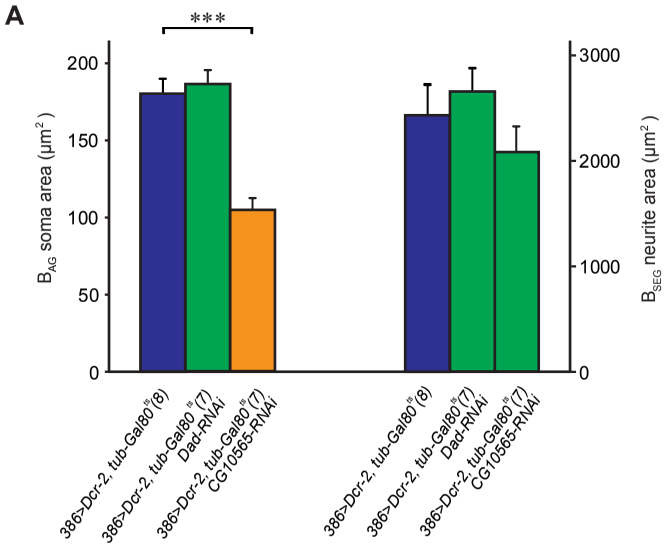
A
***
200
150
100
50
0
3000
2000
1000
0
B_AG soma area (µm²)
B_SEG neurite area (µm²)
386>Dcr-2, tub-Gal80ts (8)
386>Dcr-2, tub-Gal80ts (7), Dad-RNAi
386>Dcr-2, tub-Gal80ts (7), CG10565-RNAi

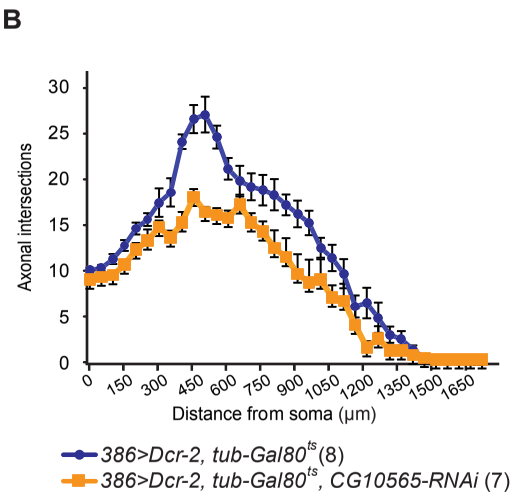
B
Axonal intersections
30
25
20
15
10
5
0
0 150 300 450 600 750 900 1050 1200 1350 1500 1650
Distance from soma (µm)
386>Dcr-2, tub-Gal80ts (8)
386>Dcr-2, tub-Gal80ts, CG10565-RNAi (7)

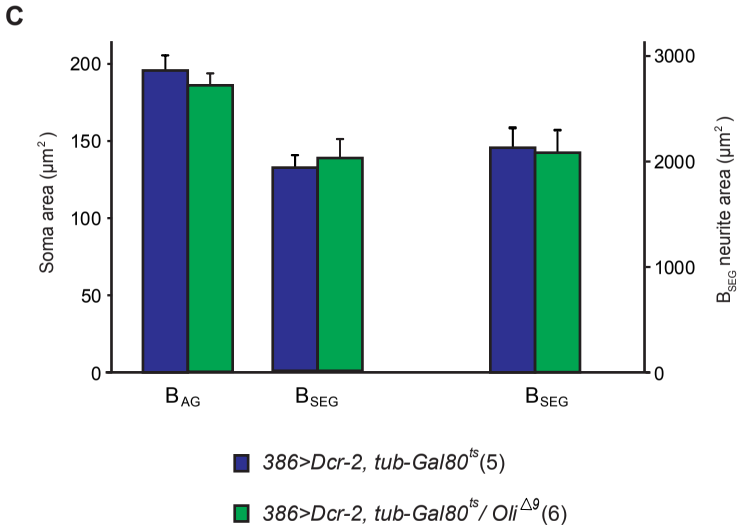
C
Soma area (µm²)
200
150
100
50
0
3000
2000
1000
0
B_SEG neurite area (µm²)
B_AG
B_SEG
B_SEG
386>Dcr-2, tub-Gal80ts (5)
386>Dcr-2, tub-Gal80ts / Oli^Δ9 (6)

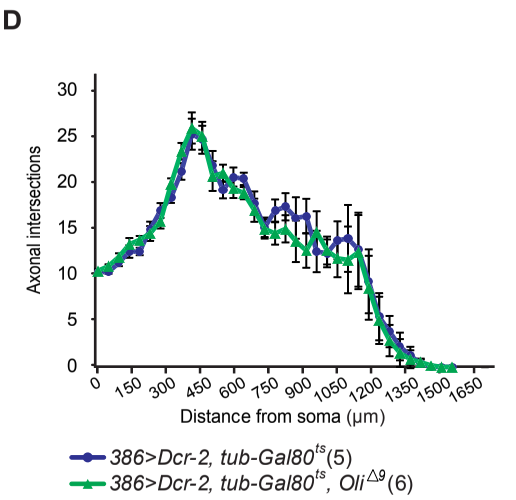
D
Axonal intersections
30
25
20
15
10
5
0
0 150 300 450 600 750 900 1050 1200 1350 1500 1650
Distance from soma (µm)
386>Dcr-2, tub-Gal80ts (5)
386>Dcr-2, tub-Gal80ts, Oli^Δ9 (6)

Table 2. Progeny lethality of crosses with the tester stock and deficiencies

Phenotype(s)	Deficiencies
Lethality before pupariation	*Df(1)ED7229, Df(1)ED7620, Df(2L)ED5878, Df(2L)ED19, Df(2L)ED6569, Df(2L)ED779, Df(2L)BSC768, Df(2R)Exel6064, Df(3L)ED224, Df(3R)ED5518, Df(1)BSC705, Df(2R)Exel6055, Df(3L)BSC443, Df(3L)ED220, Df(3R)ED5177, Df(3R)ED10893, Df(3L)ED225, Df(3L)ED4786, Df(3R)BSC633, Df(1)ED411, Df(1)BSC710, Df(2L)Exel6036, Df(2L)Exel6039, Df(3L)ED4293, Df(3R)ED6235, Df(1)BSC580, Df(2R)BSC639, Df(3R)BSC808, Df(2R)BSC880, Df(2L)ED1054, Df(3L)ED4529, Df(3R)ED5591,Df(3R)ED10845, Df(3R)ED6316, Df(3R)ED6361,*
Head eversion defect	*Df(3R)Exel6158, Df(2R)Exel6076*
Head eversion defect and late pupal lethality	*Df(3R)Exel6145, Df(3R)Exel6188, Df(3L)Exel6127, Df(3L)BSC800, Df(3R)ED6058, Df(3R)ED6346*
Late pupal lethality	*Df(2L)ED108, Df(2R)ED3923, Df(3L)ED4502, Df(3L)ED4543, Df(3R)ED6103, Df(3L)ED5017, Df(3R)ED5021, Df(3L)ED217, Df(3L)Exel6131, Df(3L)Exel6092, Df(3R)ED5147, Df(3R)ED5223, Df(3L)Exel6109, Df(3L)ED4789, Df(3L)ED4799, Df(3L)BSC797, Df(3R)Exel6181, Df(2R)ED3791, Df(3L)ED4414, Df(3L)ED4457, Df(3L)ED4978, Df(3R)ED5156, Df(3R)Exel6214,*
Late pupal lethality and eclosion defect	*Df(2L)Exel8038, Df(2R)ED2098*
Eclosion defect	*Df(3L)Exel6123*

Table 3. Progeny lethality produced by crosses with the tester strain to RNAi strains

Phenotype(s)	Targets of the VDRC RNAi strains
Head eversion defect and late pupal lethality	*CG10042*
Late pupal lethality	*CG42588*, *CG6412*, *CG10566*, *CG33284*, *mtacp1*, *Sin*

References

Aberle, H., A. P. Haghighi, R. D. Fetter, B. D. McCabe, T. R. Magalhaes *et al.*, 2002 wishful thinking encodes a BMP type II receptor that regulates synaptic growth in Drosophila. Neuron 33**:** 545-558.

Acampora, D., M. P. Postiglione, V. Avantaggiato, M. Di Bonito, F. M. Vaccarino *et al.*, 1999 Progressive impairment of developing neuroendocrine cell lineages in the hypothalamus of mice lacking the Orthopedia gene. Gene. Dev. 13**:** 2787-2800.

Adryan, B., G. Woerfel, I. Birch-Machin, S. Gao, M. Quick *et al.*, 2007 Genomic mapping of Suppressor of Hairy-wing binding sites in Drosophila. Genome Biol 8**:** R167.

Altschul, S. F., T. L. Madden, A. A. Schaffer, J. Zhang, Z. Zhang *et al.*, 1997 Gapped BLAST and PSI-BLAST: a new generation of protein database search programs. Nucleic Acids Res. 25**:** 3389-3402.

Altschul, S. F., J. C. Wootton, E. M. Gertz, R. Agarwala, A. Morgulis *et al.*, 2005 Protein database searches using compositionally adjusted substitution matrices. FEBS J. 272**:** 5101-5109.

Anderson, M. S., M. E. Halpern and H. Keshishian, 1988 Identification of the neuropeptide transmitter proctolin in Drosophila larvae: characterization of muscle fiber-specific neuromuscular endings. J Neurosci 8**:** 242-255.

Armstrong, J. D., M. J. Texada, R. Munjaal, D. A. Baker and K. M. Beckingham, 2006 Gravitaxis in Drosophila melanogaster: a forward genetic screen. Genes Brain Behav. 5**:** 222-239.

Awasaki, T., Y. L. Huang, M. B. O'Connor and T. Lee, 2011 Glia instruct developmental neuronal remodeling through TGF-beta signaling. Nature Neuroscience 14**:** 821-823.

Awasaki, T., R. Tatsumi, K. Takahashi, K. Arai, Y. Nakanishi *et al.*, 2006 Essential role of the apoptotic cell engulfment genes draper and ced-6 in programmed axon pruning during Drosophila metamorphosis. Neuron 50**:** 855-867.

Bainbridge, S. P., and M. Bownes, 1981a Staging the metamorphosis of *Drosophila melanogaster*. J. Embryol. Exp. Morph. 66**:** 57-80.

Bainbridge, S. P., and M. Bownes, 1981b Staging the Metamorphosis of Drosophila-Melanogaster. Journal of Embryology and Experimental Morphology 66**:** 57-80.

Balducci-Silano, P. L., K. Suzuki, M. Ohta, J. Saito, M. Ohmori *et al.*, 1998 Regulation of major histocompatibility (MHC) class II human leukocyte antigen-DR alpha gene expression in thyrocytes by single strand binding protein-1, a transcription

factor that also regulates thyrotropin receptor and MHC class I gene expression. Endocrinology 139**:** 2300-2313.

Bandziulis, R. J., M. S. Swanson and G. Dreyfuss, 1989 RNA-binding proteins as developmental regulators. Gene. Dev. 3**:** 431-437.

Bantignies, F., R. H. Goodman and S. M. Smolik, 2000 Functional interaction between the coactivator Drosophila CREB-binding protein and ASH1, a member of the trithorax group of chromatin modifiers. Mol. Cell. Biol. 20**:** 9317-9330.

Barkess, G., and A. G. West, 2012 Chromatin insulator elements: establishing barriers to set heterochromatin boundaries. Epigenomics 4**:** 67-80.

Berger, C., H. Harzer, T. R. Burkard, J. Steinmann, S. van der Horst *et al.*, 2012 FACS purification and transcriptome analysis of drosophila neural stem cells reveals a role for Klumpfuss in self-renewal. Cell Rep. 2**:** 407-418.

Bjorklund, M., M. Taipale, M. Varjosalo, J. Saharinen, J. Lahdenpera *et al.*, 2006 Identification of pathways regulating cell size and cell-cycle progression by RNAi. Nature 439**:** 1009-1013.

Bleuming, S. A., X. C. He, L. L. Kodach, F. J. ten Kate, G. J. Offerhaus *et al.*, 2007 Bone Morphogenetic Protein (BMP) signaling regulates fundic gland homeostasis and suppresses tumorigenesis at gastric epithelial transition zones in mice. European Journal of Gastroenterology & Hepatology 19**:** A49-A49.

Bohus, B., 1977 Pituitary neuropeptides, emotional behavior and cardiac responses. Prog Brain Res 47**:** 277-288.

Boulanger, A., C. Clouet-Redt, M. Farge, A. Flandre, T. Guignard *et al.*, 2011 ftz-f1 and Hr39 opposing roles on EcR expression during Drosophila mushroom body neuron remodeling. Nature Neuroscience 14**:** 37-U57.

Boulanger, A., and J. M. Dura, 2014 Nuclear receptors and Drosophila neuronal remodeling. Biochim Biophys Acta.

Brown, H. L. D., 2007 Steroid hormone receptor regulation of neuronal pruning and outgrowth in the Drosophila central nervous system. PhD thesis.

Brown, H. L. D., L. Cherbas, P. Cherbas and J. W. Truman, 2006 Use of time-lapse imaging and dominant negative receptors to dissect the steroid receptor control of neuronal remodeling in Drosophila. Development 133**:** 275-285.

Caldwell, H. K., H. J. Lee, A. H. Macbeth and W. S. Young, 3rd, 2008 Vasopressin: behavioral roles of an "original" neuropeptide. Prog Neurobiol 84**:** 1-24.

Chee, S. S., W. A. Espinoza, A. N. Iwaniuk, J. M. Pakan, C. Gutierrez-Ibanez *et al.*, 2013 Social status, breeding state, and GnRH soma size in convict cichlids (Cryptoheros nigrofasciatus). Behav Brain Res 237**:** 318-324.

Chen, D., C. Qu and R. S. Hewes, 2014 Neuronal Remodeling During Metamorphosis Is Regulated by the alan shepard (shep) Gene in Drosophila melanogaster. Genetics.

Chiang, A., R. Priya, M. Ramaswami, K. VijayRaghavan and V. Rodrigues, 2009 Neuronal activity and Wnt signaling act through Gsk3-beta to regulate axonal integrity in mature Drosophila olfactory sensory neurons. Development 136**:** 1273-1282.

Clynen, E., A. Reumer, G. Baggerman, I. Mertens and L. Schoofs, 2010 Neuropeptide biology in Drosophila. Adv Exp Med Biol 692**:** 192-210.

Cook, R. K., S. J. Christensen, J. A. Deal, R. A. Coburn, M. E. Deal *et al.*, 2012 The generation of chromosomal deletions to provide extensive coverage and subdivision of the Drosophila melanogaster genome. Genome Biol. 13**:** R21.

Cottrell, E. C., R. E. Campbell, S. K. Han and A. E. Herbison, 2006 Postnatal remodeling of dendritic structure and spine density in gonadotropin-releasing hormone neurons. Endocrinology 147**:** 3652-3661.

Crowley, W. F., Jr., M. Filicori, D. I. Spratt and N. F. Santoro, 1985 The physiology of gonadotropin-releasing hormone (GnRH) secretion in men and women. Recent Prog Horm Res 41**:** 473-531.

Crown, A., D. K. Clifton and R. A. Steiner, 2007 Neuropeptide signaling in the integration of metabolism and reproduction. Neuroendocrinology 86**:** 175-182.

Curt, A., H. J. A. Van Hedel, D. Klaus, V. Dietz and E.-S. S. Grp, 2008 Recovery from a spinal cord injury: Significance of compensation, neural plasticity, and repair. Journal of Neurotrauma 25**:** 677-685.

Database, N., http://www.neuropeptides.nl/.

de Pedro, N., M. J. Delgado and M. Alonso-Bedate, 1995 Central administration of beta-endorphin increases food intake in goldfish: pretreatment with the opioid antagonist naloxone. Regul Pept 55**:** 189-195.

Demerec, M., 1994 *Biology of Drosophila*. Cold Spring Harbor Laboratory Press, New York.

Deng, P. Y., and V. A. Klyachko, 2011 The diverse functions of short-term plasticity components in synaptic computations. Commun Integr Biol 4**:** 543-548.

Denholm, B., N. Hu, T. Fauquier, X. Caubit, L. Fasano *et al.*, 2013 The tiptop/teashirt genes regulate cell differentiation and renal physiology in Drosophila. Development 140**:** 1100-1110.

Deviche, P., and G. Schepers, 1984 Intracerebroventricular injection of ostrich beta-endorphin to satiated pigeons induces hyperphagia but not hyperdipsia. Peptides 5**:** 691-694.

Dewey, E. M., S. L. McNabb, J. Ewer, G. R. Kuo, C. L. Takanishi *et al.*, 2004 Identification of the gene encoding bursicon, an insect neuropeptide responsible for cuticle sclerotization and wing spreading. Curr. Biol. 14**:** 1208-1213.

Dierick, H. A., and R. J. Greenspan, 2007 Serotonin and neuropeptide F have opposite modulatory effects on fly aggression. Nature Genetics 39**:** 678-682.

Dietzl, G., D. Chen, F. Schnorrer, K. C. Su, Y. Barinova *et al.*, 2007 A genome-wide transgenic RNAi library for conditional gene inactivation in Drosophila. Nature 448**:** 151-156.

Du Vigneaud, V., Lawler, H.C., and Popenoe, E.A., 1953 Enzymatic cleavage of glycinamide from vasopressin and a proposed structure for this pressor-antidiuretic hormone of the posterior pituitary. J. Am. Chem. Soc. 75**:** 4880-4881.

Duffy, J. B., 2002 GAL4 system in Drosophila: a fly geneticist's Swiss army knife. Genesis 34**:** 1-15.

Dulcis, D., R. B. Levine and J. Ewer, 2005 Role of the neuropeptide CCAP in Drosophila cardiac function. Journal of Neurobiology 64**:** 259-274.

Dura, J. M., A. Boulanger, C. Clouet, T. Guignard and A. Flandre, 2009 Homologous nuclear receptors ftz-f1 and Hr39 have opposite role on ecdysone receptor expression during Drosophila mushroom body gamma axon pruning. Journal of Neurogenetics 23**:** S22-S23.

Eaton, B. A., and G. W. Davis, 2005 LIM Kinase1 controls synaptic stability downstream of the type IIBMP receptor. Neuron 47**:** 695-708.

Eccles, J. C., 1983 Calcium in Long-Term Potentiation as a Model for Memory. Neuroscience 10**:** 1071-1081.

Eipper, B. A., D. A. Stoffers and R. E. Mains, 1992 The Biosynthesis of Neuropeptides - Peptide Alpha-Amidation. Annual Review of Neuroscience 15**:** 57-85.

Ferris, J., H. Ge, L. Liu and G. Roman, 2006 G(o) signaling is required for Drosophila associative learning. Nat Neurosci 9**:** 1036-1040.

Fontana, J. R., and S. T. Crews, 2012 Transcriptome analysis of Drosophila CNS midline cells reveals diverse peptidergic properties and a role for castor in neuronal differentiation. Dev. Biol. 372**:** 131-142.

Fox, R. M., C. D. Hanlon and D. J. Andrew, 2010 The CrebA/Creb3-like transcription factors are major and direct regulators of secretory capacity. J. Cell. Biol. 191**:** 479-492.

Fu, M., B. P. Vohra, D. Wind and R. O. Heuckeroth, 2006 BMP signaling regulates murine enteric nervous system precursor migration, neurite fasciculation, and patterning via altered Ncam1 polysialic acid addition. Dev Biol 299**:** 137-150.

Ghosh, D., T. I. Gerasimova and V. G. Corces, 2001 Interactions between the Su(Hw) and Mod(mdg4) proteins required for gypsy insulator function. Embo Journal 20**:** 2518-2527.

Goncalves, J., S. Baptista, M. V. Olesen, C. Fontes-Ribeiro, J. O. Malva *et al.*, 2012 Methamphetamine-induced changes in the mice hippocampal neuropeptide Y system: implications for memory impairment. J. Neurochem. 123**:** 1041-1053.

Graveley, B. R., A. N. Brooks, J. W. Carlson, M. O. Duff, J. M. Landolin *et al.*, 2011 The developmental transcriptome of Drosophila melanogaster. Nature 471**:** 473-479.

Green, E. W., G. Fedele, F. Giorgini and C. P. Kyriacou, 2014 A Drosophila RNAi collection is subject to dominant phenotypic effects. Nat. Methods 11**:** 222-223.

Gu, T., T. Zhao and R. S. Hewes, 2014 Insulin signaling regulates neurite growth during metamorphic neuronal remodeling. Biol. Open 3**:** 81-93.

Hamanaka, Y., D. Park, P. Yin, S. P. Annangudi, T. N. Edwards *et al.*, 2010 Transcriptional orchestration of the regulated secretory pathway in neurons by the bHLH protein DIMM. Curr. Biol. 20**:** 9-18.

Han, J., Y. Lee, K. H. Yeom, J. W. Nam, I. Heo *et al.*, 2006 Molecular basis for the recognition of primary microRNAs by the Drosha-DGCR8 complex. Cell 125**:** 887-901.

Harbison, S. T., A. H. Yamamoto, J. J. Fanara, K. K. Norga and T. F. Mackay, 2004 Quantitative trait loci affecting starvation resistance in Drosophila melanogaster. Genetics 166**:** 1807-1823.

Harrison, D. A., M. A. Mortin and V. G. Corces, 1992 The RNA polymerase II 15-kilodalton subunit is essential for viability in Drosophila melanogaster. Mol Cell Biol 12**:** 928-935.

He, C., X. Cong, R. Zhang, D. Wu, C. An *et al.*, 2013 Regulation of circadian locomotor rhythm by neuropeptide Y-like system in Drosophila melanogaster. Insect Mol Biol 22**:** 376-388.

Hegarty, S. V., L. M. Collins, A. M. Gavin, S. L. Roche, S. L. Wyatt *et al.*, 2014 Canonical BMP-Smad signalling promotes neurite growth in rat midbrain dopaminergic neurons. Neuromolecular Med 16**:** 473-489.

Hens, J. J. H., M. De Wit, W. E. J. M. Ghijsen, A. G. M. Leenders, H. W. G. M. Boddeke *et al.*, 1998 Role of calcineurin in Ca2+-induced release of catecholamines and neuropeptides. Journal of Neurochemistry 71**:** 1978-1986.

Hewes, R. S., 2008 The buzz on fly neuronal remodeling. Trends in Endocrinology and Metabolism 19**:** 317-323.

Hewes, R. S., T. T. Gu, J. A. Brewster, C. J. Qu and T. Zhao, 2006 Regulation of secretory protein expression in mature cells by DIMM, a basic helix-loop-helix neuroendocrine differentiation factor. Journal of Neuroscience 26**:** 7860-7869.

Hewes, R. S., D. Park, S. A. Gauthier, A. M. Schaefer and P. H. Taghert, 2003 The bHLH protein Dimmed controls neuroendocrine cell differentiation in Drosophila. Development 130**:** 1771-1781.

Hewes, R. S., A. M. Schaefer and P. H. Taghert, 2000 The cryptocephal gene (ATF4) encodes multiple basic-leucine zipper proteins controlling molting and metamorphosis in *Drosophila*. Genetics 155**:** 1711-1723.

Hewes, R. S., E. C. Snowdeal, M. Saitoe and P. H. Taghert, 1998 Functional redundancy of FMRFamide-related peptides at the Drosophila larval neuromuscular junction. Journal of Neuroscience 18**:** 7138-7151.

Hodge, J. J., J. C. Choi, C. J. O'Kane and L. C. Griffith, 2005 Shaw potassium channel genes in *Drosophila*. J. Neurobiol. 63**:** 235-254.

Hoopfer, E. D., A. Penton, R. J. Watts and L. Q. Luo, 2008 Genomic analysis of Drosophila neuronal remodeling: A role for the RNA-binding protein boule as a negative regulator of axon pruning. Journal of Neuroscience 28**:** 6092-6103.

Horn, I., and E. Horn, 1982 The influence of ACTH fragments on habituation of the prey catching behaviour in the European toad (Bufo bufo L.). Physiol Behav 28**:** 497-500.

Huang, F., and Y. G. Chen, 2012 Regulation of TGF-beta receptor activity. Cell Biosci 2**:** 9.

Huang, X. Q., and W. Miller, 1991 A Time-Efficient, Linear-Space Local Similarity Algorithm. Adv. Appl. Math 12**:** 337-357.

Inoue, H., T. Imamura, Y. Ishidou, M. Takase, Y. Udagawa *et al.*, 1998 Interplay of signal mediators of decapentaplegic (Dpp): molecular characterization of mothers against dpp, Medea, and daughters against dpp. Mol Biol Cell 9**:** 2145-2156.

Jan, L. Y., and Y. N. Jan, 1982 Peptidergic transmission in sympathetic ganglia of the frog. J Physiol 327**:** 219-246.

Jette, L., R. Leger, K. Thibaudeau, C. Benquet, M. Robitaille *et al.*, 2005 Human growth hormone-releasing factor (hGRF)1-29-albumin bioconjugates activate the GRF receptor on the anterior pituitary in rats: identification of CJC-1295 as a long-lasting GRF analog. Endocrinology 146**:** 3052-3058.

Jiang, N., A. S. Kolhekar, P. S. Jacobs, R. E. Mains, B. A. Eipper *et al.*, 2000 PHM is required for normal developmental transitions and for biosynthesis of secretory peptides in Drosophila. Dev. Biol. 226**:** 118-136.

Joshi, P. S., B. J. Molyneaux, L. Feng, X. Xie, J. D. Macklis *et al.*, 2008 Bhlhb5 regulates the postmitotic acquisition of area identities in layers II-V of the developing neocortex. Neuron 60**:** 258-272.

Kamiya, Y., K. Miyazono and K. Miyazawa, 2008a Specificity of the inhibitory effects of Dad on TGF-beta family type I receptors, Thickveins, Saxophone, and Baboon in Drosophila. FEBS Lett 582**:** 2496-2500.

Kamiya, Y., K. Miyazono and K. Miyazawa, 2008b Specificity of the inhibitory effects of Dad on TGF-beta family type I receptors, Thickveins, Saxophone, and Baboon in Drosophila. Febs Letters 582**:** 2496-2500.

Kandel, E. R., 2012 The molecular biology of memory: cAMP, PKA, CRE, CREB-1, CREB-2, and CPEB. Molecular Brain 5.

Kaplow, M. E., L. J. Mannava, A. C. Pimentel, H. A. Fermin, V. J. Hyatt *et al.*, 2007 A genetic modifier screen identifies multiple genes that interact with Drosophila Rap/Fzr and suggests novel cellular roles. Journal of Neurogenetics 21**:** 105-151.

Karakozova, M., E. Savitskaya, L. Melnikova, A. Parshikov and P. Georgiev, 2004 The mod(mdg4) component of the Su(Hw) insulator inserted in the P transposon can repress its mobility in Drosophila melanogaster. Genetics 167**:** 1275-1280.

Kimura, K., H. Saga, K. Hayashi, H. Obata, Y. Chimori *et al.*, 1998a c-Myc gene single-strand binding protein-1, MSSP-1, suppresses transcription of alpha-smooth muscle actin gene in chicken visceral smooth muscle cells. Nucleic Acids Res 26**:** 2420-2425.

Kimura, K., H. Saga, K. Hayashi, H. Obata, Y. Chimori *et al.*, 1998b c-Myc gene single-strand binding protein-1, MSSP-1, suppresses transcription of alpha-

smooth muscle actin gene in chicken visceral smooth muscle cells. Nucleic Acids Res. 26**:** 2420-2425.

Kirilly, D., Y. Gu, Y. F. Huang, Z. H. Wu, A. Bashirullah *et al.*, 2009 A genetic pathway composed of Sox14 and Mical governs severing of dendrites during pruning. Nature Neuroscience 12**:** 1497-U1435.

Kirilly, D., J. J. L. Wong, E. K. H. Lim, Y. Wang, H. Zhang *et al.*, 2011 Intrinsic Epigenetic Factors Cooperate with the Steroid Hormone Ecdysone to Govern Dendrite Pruning in Drosophila. Neuron 72**:** 86-100.

Krupp, J. J., L. E. Yaich, R. J. Wessells and R. Bodmer, 2005 Identification of genetic loci that interact with cut during Drosophila wing-margin development. Genetics 170**:** 1775-1795.

Kucherenko, M. M., M. Pantoja, A. S. Yatsenko, H. R. Shcherbata, K. A. Fischer *et al.*, 2008 Genetic Modifier Screens Reveal New Components that Interact with the Drosophila Dystroglycan-Dystrophin Complex. Plos One 3.

Kuo, C. H., S. Ichida, K. Saito, T. Matsuda and H. Yoshida, 1978 Ascorbic-Acid, an Endogeneous Factor Required for Ca++- Sensitive Ach Release from Synaptic Vesicles. Japanese Journal of Pharmacology 28**:** P47-P47.

Kuo, C. T., L. Y. Jan and Y. N. Jan, 2005 Dendrite-specific remodeling of Drosophila sensory neurons requires matrix metalloproteases, ubiquitin-proteasome, and ecdysone signaling. Proceedings of the National Academy of Sciences of the United States of America 102**:** 15230-15235.

Lee, G., and J. H. Park, 2004 Hemolymph sugar homeostasis and starvation-induced hyperactivity affected by genetic manipulations of the adipokinetic hormone-encoding gene in Drosophila melanogaster. Genetics 167**:** 311-323.

Lee, S. K., L. W. Jurata, J. Funahashi, E. C. Ruiz and S. L. Pfaff, 2004 Analysis of embryonic motoneuron gene regulation: derepression of general activators function in concert with enhancer factors. Development 131**:** 3295-3306.

Lee, S. K., and S. L. Pfaff, 2003 Synchronization of neurogenesis and motor neuron specification by direct coupling of bHLH and homeodomain transcription factors. Neuron 38**:** 731-745.

Lee, T., A. Lee and L. Q. Luo, 1999 Development of the Drosophila mushroom bodies: sequential generation of three distinct types of neurons from a neuroblast. Development 126**:** 4065-4076.

Lee, T., S. Marticke, C. Sung, S. Robinow and L. Q. Luo, 2000 Cell-autonomous requirement of the USP/EcR-B ecdysone receptor for mushroom body neuronal remodeling in Drosophila. Neuron 28**:** 807-818.

Liu, A. M., and L. A. Niswander, 2005 Bone morphogenetic protein signalling and vertebrate nervous system development. Nature Reviews Neuroscience 6**:** 945-954.

Liu, Z. W., Y. Chen, D. Wang, S. Y. Wang and Y. Q. Zhang, 2010 Distinct Presynaptic and Postsynaptic Dismantling Processes of Drosophila Neuromuscular Junctions during Metamorphosis. Journal of Neuroscience 30**:** 11624-11634.

Lledo, P. M., G. O. Hjelmstad, S. Mukherji, T. R. Soderling, R. C. Malenka *et al.*, 1995 Calcium/calmodulin-dependent kinase II and long-term potentiation enhance synaptic transmission by the same mechanism. Proc Natl Acad Sci U S A 92**:** 11175-11179.

Lorković, Z. J., 2012 *RNA binding proteins*. Eurekah, Georgetown, Texas.

Loveall, B. J., and D. L. Deitcher, 2010 The essential role of bursicon during Drosophila development. BMC Dev. Biol. 10**:** 92.

Luan, H., W. C. Lemon, N. C. Peabody, J. B. Pohl, P. K. Zelensky *et al.*, 2006 Functional dissection of a neuronal network required for cuticle tanning and wing expansion in Drosophila. J. Neurosci. 26**:** 573-584.

Lukacsovich, T., Z. Asztalos, W. Awano, K. Baba, S. Kondo *et al.*, 2001 Dual-tagging gene trap of novel genes in *Drosophila melanogaster*. Genetics 157**:** 727-742.

Luquet, S., F. A. Perez, T. S. Hnasko and R. D. Palmiter, 2005 NPY/AgRP neurons are essential for feeding in adult mice but can be ablated in neonates. Science 310**:** 683-685.

Ma, Z., Z. Liu and X. Huang, 2012 Membrane phospholipid asymmetry counters the adverse effects of sterol overloading in the Golgi membrane of Drosophila. Genetics 190**:** 1299-1308.

MacDonald, P. E., M. Braun, J. Galvanovskis and P. Rorsman, 2006 Release of small transmitters through kiss-and-run fusion pores in rat pancreatic beta cells. Cell Metabolism 4**:** 283-290.

Magarinos, A. M., B. S. McEwen, M. Saboureau and P. Pevet, 2006 Rapid and reversible changes in intrahippocampal connectivity during the course of hibernation in European hamsters. Proc. Natl. Acad. Sci. U S A. 103**:** 18775-18780.

Maines, J. Z., L. M. Stevens, X. L. Tong and D. Stein, 2004 Drosophila dMyc is required for ovary cell growth and endoreplication. Development 131**:** 775-786.

Marchler-Bauer, A., J. B. Anderson, P. F. Cherukuri, C. DeWeese-Scott, L. Y. Geer *et al.*, 2005 CDD: a Conserved Domain Database for protein classification. Nucleic Acids Res. 33**:** D192-196.

Marin, E. C., R. J. Watts, N. K. Tanaka, K. Ito and L. Q. Luo, 2005 Developmentally programmed remodeling of the Drosophila olfactory circuit. Development 132**:** 725-737.

Maris, C., C. Dominguez and F. H. Allain, 2005 The RNA recognition motif, a plastic RNA-binding platform to regulate post-transcriptional gene expression. FEBS J. 272**:** 2118-2131.

Matzat, L. H., R. K. Dale, N. Moshkovich and E. P. Lei, 2012 Tissue-specific regulation of chromatin insulator function. PLoS Genet. 8**:** e1003069.

Mccarthy, H. D., P. E. Mckibbin, B. Holloway, R. Mayers and G. Williams, 1991 Hypothalamic Neuropeptide-Y Receptor Characteristics and Npy-Induced Feeding Responses in Lean and Obese Zucker Rats. Life Sciences 49**:** 1491-1497.

McCoy, A. N., and S. Y. Tan, 2014 Otto Loewi (1873-1961): Dreamer and Nobel laureate. Singapore Med J 55**:** 3-4.

McKay, L. D., N. J. Kenney, N. K. Edens, R. H. Williams and S. C. Woods, 1981 Intracerebroventricular beta-endorphin increases food intake of rats. Life Sci 29**:** 1429-1434.

Mckelvy, J. F., and J. D. White, 1987 Biosynthesis of Neuropeptides in the Rat Central-Nervous-System. Advances in Biochemical Psychopharmacology 43**:** 81-86.

McNeill, H., G. M. Craig and J. M. Bateman, 2008 Regulation of neurogenesis and epidermal growth factor receptor signaling by the insulin receptor/target of rapamycin pathway in Drosophila. Genetics 179**:** 843-853.

McShane, T. M., T. May, J. L. Miner and D. H. Keisler, 1992 Central actions of neuropeptide-Y may provide a neuromodulatory link between nutrition and reproduction. Biol. Reprod. 46**:** 1151-1157.

Melnikova, L., M. Gause and P. Georgiev, 2002 The gypsy insulators flanking yellow enhancers do not form a separate transcriptional domain in Drosophila melanogaster: The enhancers can activate an isolated yellow promoter. Genetics 160**:** 1549-1560.

Michaud, J. L., T. Rosenquist, N. R. May and C. M. Fan, 1998 Development of neuroendocrine lineages requires the bHLH-PAS transcription factor SIM1. Genes Dev. 12**:** 3264-3275.

Milano, F., J. W. P. M. Van Baal, N. S. Buttar, A. M. Rygiel, F. De Kort *et al.*, 2007 Bone morphogenetic protein 4 expressed in esophagitis induces a columnar phenotype in esophageal squamous cells. Gastroenterology 132**:** 2412-2421.

Milosevic, N. T., and D. Ristanovic, 2007 The Sholl analysis of neuronal cell images: semi-log or log-log method? J. Theor. Biol. 245**:** 130-140.

Misulovin, Z., Y. B. Schwartz, X. Y. Li, T. G. Kahn, M. Gause *et al.*, 2008 Association of cohesin and Nipped-B with transcriptionally active regions of the Drosophila melanogaster genome. Chromosoma 117**:** 89-102.

Morin, X., R. Daneman, M. Zavortink and W. Chia, 2001 A protein trap strategy to detect GFP-tagged proteins expressed from their endogenous loci in *Drosophila*. Proc. Natl. Acad. Sci. U S A 98**:** 15050-15055.

Nasmyth, K., 2005 How might cohesin hold sister chromatids together? Philosophical Transactions of the Royal Society B-Biological Sciences 360**:** 483-496.

Nassel, D. R., and A. M. Winther, 2010 Drosophila neuropeptides in regulation of physiology and behavior. Prog Neurobiol 92**:** 42-104.

Negre, N., C. D. Brown, P. K. Shah, P. Kheradpour, C. A. Morrison *et al.*, 2010 A comprehensive map of insulator elements for the Drosophila genome. PLoS Genet 6**:** e1000814.

Nephew, B. C., R. S. Bridges, D. F. Lovelock and E. M. Byrnes, 2009 Enhanced maternal aggression and associated changes in neuropeptide gene expression in multiparous rats. Behav. Neurosci. 123**:** 949-957.

Newcomb, R., E. Stuenkel and I. Cooke, 1985 Characterization, Biosynthesis, and Release of Neuropeptides from the X-Organ Sinus Gland System of the Crab, Cardisoma-Carnifex. American Zoologist 25**:** 157-171.

Ni, J. Q., L. P. Liu, R. Binari, R. Hardy, H. S. Shim *et al.*, 2009 A Drosophila resource of transgenic RNAi lines for neurogenetics. Genetics 182**:** 1089-1100.

Niki, T., I. Galli, H. Ariga and S. M. Iguchi-Ariga, 2000a MSSP, a protein binding to an origin of replication in the c-myc gene, interacts with a catalytic subunit of DNA polymerase alpha and stimulates its polymerase activity. FEBS Lett 475**:** 209-212.

Niki, T., I. Galli, H. Ariga and S. M. Iguchi-Ariga, 2000b MSSP, a protein binding to an origin of replication in the c-myc gene, interacts with a catalytic subunit of DNA polymerase alpha and stimulates its polymerase activity. FEBS Lett. 475**:** 209-212.

Niki, T., S. Izumi, Y. Saegusa, T. Taira, T. Takai *et al.*, 2000c MSSP promotes ras/myc cooperative cell transforming activity by binding to c-Myc. Genes Cells 5**:** 127-141.

Niki, T., S. Izumi, Y. Saegusa, T. Taira, T. Takai *et al.*, 2000d MSSP promotes ras/myc cooperative cell transforming activity by binding to c-Myc. Genes Cells. 5**:** 127-141.

Nomura, J., K. Matsumoto, S. M. Iguchi-Ariga and H. Ariga, 2005a Positive regulation of Fas gene expression by MSSP and abrogation of Fas-mediated apoptosis induction in MSSP-deficient mice. Exp Cell Res 305**:** 324-332.

Nomura, J., K. Matsumoto, S. M. Iguchi-Ariga and H. Ariga, 2005b Positive regulation of Fas gene expression by MSSP and abrogation of Fas-mediated apoptosis induction in MSSP-deficient mice. Exp. Cell Res. 305**:** 324-332.

Nunez, J. L., J. Sodhi and J. M. Juraska, 2002 Ovarian hormones after postnatal day 20 reduce neuron number in the rat primary visual cortex. J Neurobiol 52**:** 312-321.

Ogiso, Y., K. Tsuneizumi, N. Masuda, M. Sato and T. Tabata, 2011 Robustness of the Dpp morphogen activity gradient depends on negative feedback regulation by the inhibitory Smad, Dad. Dev Growth Differ 53**:** 668-678.

Osterloh, J. M., and M. R. Freeman, 2009 Neuronal death or dismemberment mediated by Sox14. Nature Neuroscience 12**:** 1479-1480.

Oyallon, J., H. Apitz, I. Miguel-Aliaga, K. Timofeev, L. Ferreira *et al.*, 2012 Regulation of locomotion and motoneuron trajectory selection and targeting by the Drosophila homolog of Olig family transcription factors. Dev Biol 369**:** 261-276.

Pai, C. Y., E. P. Lei, D. Ghosh and V. G. Corces, 2004 The centrolsomal protein CP190 is a component of the gypsy chromatin insulator. Molecular Cell 16**:** 737-748.

Park, D., O. T. Shafer, S. P. Shepherd, H. Suh, J. S. Trigg *et al.*, 2008 The Drosophila basic helix-loop-helix protein DIMMED directly activates PHM, a gene encoding a neuropeptide-amidating enzyme. Mol. Cell. Biol. 28**:** 410-421.

Park, J. H., A. J. Schroeder, C. Helfrich-Forster, F. R. Jackson and J. Ewer, 2003 Targeted ablation of CCAP neuropeptide-containing neurons of Drosophila causes specific defects in execution and circadian timing of ecdysis behavior. Development 130**:** 2645-2656.

Park, Y., V. Filippov, S. S. Gill and M. E. Adams, 2002 Deletion of the ecdysis-triggering hormone gene leads to lethal ecdysis deficiency. Development 129**:** 493-503.

Parkhurst, S. M., D. A. Harrison, M. P. Remington, C. Spana, R. L. Kelley *et al.*, 1988 The Drosophila su(Hw) gene, which controls the phenotypic effect of the gypsy transposable element, encodes a putative DNA-binding protein. Genes Dev 2**:** 1205-1215.

Parks, A. L., K. R. Cook, M. Belvin, N. A. Dompe, R. Fawcett *et al.*, 2004 Systematic generation of high-resolution deletion coverage of the Drosophila melanogaster genome. Nat. Genet. 36**:** 288-292.

Peabody, N. C., F. Diao, H. Luan, H. Wang, E. M. Dewey *et al.*, 2008 Bursicon functions within the Drosophila CNS to modulate wing expansion behavior, hormone secretion, and cell death. J. Neurosci. 28**:** 14379-14391.

Peabody, N. C., J. B. Pohl, F. Diao, A. P. Vreede, D. J. Sandstrom *et al.*, 2009 Characterization of the Decision Network for Wing Expansion in Drosophila Using Targeted Expression of the TRPM8 Channel. Journal of Neuroscience 29**:** 3343-3353.

Pierce, S. B., C. Yost, J. S. Britton, L. W. M. Loo, E. M. Flynn *et al.*, 2004 dMyc is required for larval growth and endoreplication in Drosophila. Development 131**:** 2317-2327.

Qu, C., 2010 An enhancer-trap and splice-trap screen for regulators of endocrine functions in the central nervous system and the epitracheal gland of Drosophila melanogaster.

Raftery, L. A., Korochkina, S. and Cao, J., 2006 Smads in Drosophila – interpretation of graded signals in vivo in: Smad Signal Transduction. 55-73.

Raftery, L. A., and D. M. Umulis, 2012 Regulation of BMP activity and range in Drosophila wing development. Current Opinion in Cell Biology 24**:** 158-165.

Reis, T., M. R. Van Gilst and I. K. Hariharan, 2010 A buoyancy-based screen of Drosophila larvae for fat-storage mutants reveals a role for Sir2 in coupling fat storage to nutrient availability. PLoS Genet. 6**:** e1001206.

Ritter, A. R., and R. B. Beckstead, 2010 Sox14 Is Required for Transcriptional and Developmental Responses to 20-Hydroxyecdysone at the Onset of Drosophila Metamorphosis. Developmental Dynamics 239**:** 2685-2694.

Robinow, S., W. S. Talbot, D. S. Hogness and J. W. Truman, 1993 Programmed cell death in the Drosophila CNS is ecdysone-regulated and coupled with a specific ecdysone receptor isoform. Development 119**:** 1251-1259.

Ross, S. E., A. R. Mardinly, A. E. McCord, J. Zurawski, S. Cohen *et al.*, 2010 Loss of inhibitory interneurons in the dorsal spinal cord and elevated itch in Bhlhb5 mutant mice. Neuron 65**:** 886-898.

Ross, S. E., A. E. McCord, C. Jung, D. Atan, S. I. Mok *et al.*, 2012 Bhlhb5 and Prdm8 form a repressor complex involved in neuronal circuit assembly. Neuron 73**:** 292-303.

Roy, A. L., R. Sen and R. G. Roeder, 2011 Enhancer-promoter communication and transcriptional regulation of Igh. Trends Immunol 32**:** 532-539.

Rumpf, S., S. B. Lee, L. Y. Jan and Y. N. Jan, 2011 Neuronal remodeling and apoptosis require VCP-dependent degradation of the apoptosis inhibitor DIAP1. Development 138**:** 1153-1160.

Ryder, E., M. Ashburner, R. Bautista-Llacer, J. Drummond, J. Webster *et al.*, 2007 The DrosDel deletion collection: a *Drosophila* genomewide chromosomal deficiency resource. Genetics 177**:** 615-629.

Ryder, E., F. Blows, M. Ashburner, R. Bautista-Llacer, D. Coulson *et al.*, 2004 The DrosDel collection: a set of P-element insertions for generating custom chromosomal aberrations in Drosophila melanogaster. Genetics 167**:** 797-813.

Sakurai, T., A. Amemiya, M. Ishii, I. Matsuzaki, R. M. Chemelli *et al.*, 1998 Orexins and orexin receptors: A family of hypothalamic neuropeptides and G protein-coupled receptors that regulate feeding behavior (vol 92, pg 573, 1998). Cell 92**:** U29-U29.

Schiml, P. A., and E. F. Rissman, 2000 Effects of gonadotropin-releasing hormones, corticotropin-releasing hormone, and vasopressin on female sexual behavior. Horm Behav 37**:** 212-220.

Schindelin, J., I. Arganda-Carreras, E. Frise, V. Kaynig, M. Longair *et al.*, 2012 Fiji: an open-source platform for biological-image analysis. Nat Methods 9**:** 676-682.

Schneider, L. E., and P. H. Taghert, 1990 Organization and Expression of the Drosophila Phe-Met-Arg-Phe-Nh2 Neuropeptide Gene. Journal of Biological Chemistry 265**:** 6890-6895.

Schubiger, M., A. A. Wade, G. E. Carney, J. W. Truman and M. Bender, 1998 *Drosophila* EcR-B ecdysone receptor isoforms are required for larval molting and for neuron remodeling during metamorphosis. Development 125**:** 2053-2062.

Schuldiner, O., D. Berdnik, J. M. Levy, J. S. Wu, D. Luginbuhl *et al.*, 2008 piggyBac-based mosaic screen identifies a postmitotic function for cohesin in regulating developmental axon pruning. Developmental Cell 14**:** 227-238.

Schwartz, Y. B., D. Linder-Basso, P. V. Kharchenko, M. Y. Tolstorukov, M. Kim *et al.*, 2012 Nature and function of insulator protein binding sites in the Drosophila genome. Genome Res 22**:** 2188-2198.

Seki, Y., J. Rybak, D. Wicher, S. Sachse and B. S. Hansson, 2010 Physiological and morphological characterization of local interneurons in the *Drosophila* antennal lobe. J. Neurophysiol. 104**:** 1007-1019.

Shakiryanova, D., A. Tully, R. S. Hewes, D. L. Deitcher and E. S. Levitan, 2005 Activity-dependent liberation of synaptic neuropeptide vesicles. Nat. Neurosci. 8**:** 173-178.

Shi, L., S. Lin, Y. Grinberg, Y. Beck, C. M. Grozinger *et al.*, 2007 Roles of Drosophila Kruppel-Homolog 1 in neuronal morphogenesis. Developmental Neurobiology 67**:** 1614-1626.

Shiraishi, J., K. Yanagita, M. Fujita and T. Bungo, 2008 Central insulin suppresses feeding behavior via melanocortins in chicks. Domest Anim Endocrinol 34**:** 223-228.

Siekhaus, D. E., and R. S. Fuller, 1999 A role for amontillado, the *Drosophila* homolog of the neuropeptide precursor processing protease PC2, in triggering hatching behavior. J. Neurosci. 19**:** 6942-6954.

Singh, A. P., K. VijayRaghavan and V. Rodrigues, 2010 Dendritic refinement of an identified neuron in the Drosophila CNS is regulated by neuronal activity and Wnt signaling. Development 137**:** 1351-1360.

Sisk, C. L., and D. L. Foster, 2004 The neural basis of puberty and adolescence. Nature Neuroscience 7**:** 1040-1047.

Slaidina, M., R. Delanoue, S. Gronke, L. Partridge and P. Leopold, 2009 A *Drosophila* insulin-like peptide promotes growth during nonfeeding states. Dev. Cell. 17**:** 874-884.

Stanley, B. G., and S. F. Leibowitz, 1985 Neuropeptide-Y Injected in the Paraventricular Hypothalamus - a Powerful Stimulant of Feeding-Behavior. Proceedings of the National Academy of Sciences of the United States of America 82**:** 3940-3943.

Sudo, S., Y. Kuwabara, J. I. Park, S. Y. Hsu and A. J. Hsueh, 2005 Heterodimeric fly glycoprotein hormone-alpha2 (GPA2) and glycoprotein hormone-beta5 (GPB5) activate fly leucine-rich repeat-containing G protein-coupled receptor-1 (DLGR1) and stimulation of human thyrotropin receptors by chimeric fly GPA2 and human GPB5. Endocrinology 146**:** 3596-3604.

Taghert, P. H., R. S. Hewes, J. H. Park, M. A. O'Brien, M. Han *et al.*, 2001 Multiple amidated neuropeptides are required for normal circadian locomotor rhythms in Drosophila. J. Neurosci. 21**:** 6673-6686.

Tan, C. K., H. Lovlie, E. Greenway, S. F. Goodwin, T. Pizzari *et al.*, 2013 Sex-specific responses to sexual familiarity, and the role of olfaction in *Drosophila*. Proc. Biol. Sci. 280**:** 20131691.

Tasan, R. O., N. K. Nguyen, S. Weger, S. B. Sartori, N. Singewald *et al.*, 2010 The central and basolateral amygdala are critical sites of neuropeptide Y/Y2

receptor-mediated regulation of anxiety and depression. J Neurosci 30**:** 6282-6290.

Taylor, T., F. E. Wondisford, T. Blaine and B. D. Weintraub, 1990 The paraventricular nucleus of the hypothalamus has a major role in thyroid hormone feedback regulation of thyrotropin synthesis and secretion. Endocrinology 126**:** 317-324.

Thummel, C. S., 2001a Molecular mechanisms of developmental timing in C-elegans and Drosophila. Developmental Cell 1**:** 453-465.

Thummel, C. S., 2001b Molecular mechanisms of developmental timing in C. elegans and Drosophila. Dev Cell 1**:** 453-465.

Toba, G., T. Ohsako, N. Miyata, T. Ohtsuka, K. H. Seong *et al.*, 1999 The gene search system: A method for efficient detection and rapid molecular identification of genes in Drosophila melanogaster. Genetics 151**:** 725-737.

Truman, J. W., 1996 Steroid receptors and nervous system metamorphosis in insects. Dev Neurosci 18**:** 87-101.

Ubuka, T., S. Haraguchi, Y. Tobari, M. Narihiro, K. Ishikawa *et al.*, 2014 Hypothalamic inhibition of socio-sexual behaviour by increasing neuroestrogen synthesis. Nature Communications 5.

Van der Kloot, W., C. Colasante, R. Cameron and J. Molgo, 2000 Recycling and refilling of transmitter quanta at the frog neuromuscular junction. Journal of Physiology-London 523**:** 247-258.

Vergoni, A. V., H. B. Schioth and A. Bertolini, 2000 Melanocortins and feeding behavior. Biomed Pharmacother 54**:** 129-134.

Veverytsa, L., and D. W. Allan, 2011 Retrograde BMP signaling controls Drosophila behavior through regulation of a peptide hormone battery. Development 138**:** 3147-3157.

Veverytsa, L., and D. W. Allan, 2012 Temporally tuned neuronal differentiation supports the functional remodeling of a neuronal network in Drosophila. Proc Natl Acad Sci U S A 109**:** E748-756.

Vogt, M., 1969 Obituary. Sir Henry Hallett Dale, O.M., F.R.S. Int J Neuropharmacol 8**:** 83-84.

Walkiewicz, M. A., and M. Stern, 2009 Increased insulin/insulin growth factor signaling advances the onset of metamorphosis in Drosophila. PLoS One 4**:** e5072.

Wang, H., X. Chen, T. He, Y. Zhou and H. Luo, 2013 Evidence for tissue-specific Jak/STAT target genes in *Drosophila* optic lobe development. Genetics 195**:** 1291-1306.

Ward, R. E., J. Evans and C. S. Thummel, 2003 Genetic modifier screens in Drosophila demonstrate a role for Rho1 signaling in ecdysone-triggered imaginal disc morphogenesis. Genetics 165**:** 1397-1415.

Watts, R. J., E. D. Hoopfer and L. Q. Luo, 2003 Axon pruning during Drosphila metamorphosis: Evidence for local degeneration and requirement of the ubiquitin-proteasome system. Neuron 38**:** 871-885.

Weeks, J. C., 2003 Thinking globally, acting locally: steroid hormone regulation of the dendritic architecture, synaptic connectivity and death of an individual neuron. Progress in Neurobiology 70**:** 421-442.

Williams, D. W., and J. W. Truman, 2005a Cellular mechanisms of dendrite pruning in Drosophila: insights from in vivo time-lapse of remodeling dendritic arborizing sensory neurons. Development 132**:** 3631-3642.

Williams, D. W., and J. W. Truman, 2005b Remodeling dendrites during insect metamorphosis. Journal of Neurobiology 64**:** 24-33.

Wong, J. J., S. Li, E. K. Lim, Y. Wang, C. Wang *et al.*, 2013 A Cullin1-based SCF E3 ubiquitin ligase targets the InR/PI3K/TOR pathway to regulate neuronal pruning. PLoS Biol 11**:** e1001657.

Woodard, C. T., E. H. Baehrecke and C. S. Thummel, 1994 A molecular mechanism for the stage specificity of the Drosophila prepupal genetic response to ecdysone. Cell 79**:** 607-615.

Wray, S., and G. Hoffman, 1986 Postnatal morphological changes in rat LHRH neurons correlated with sexual maturation. Neuroendocrinology 43**:** 93-97.

Xiao, H. D., S. Fuchs, K. Frenzel, J. M. Cole and K. E. Bernstein, 2003 Newer approaches to genetic modeling in mice: tissue-specific protein expression as studied using angiotensin-converting enzyme (ACE). Am J Pathol 163**:** 807-817.

Yang, H. Y., and M. J. Iadarola, 2006 Modulatory roles of the NPFF system in pain mechanisms at the spinal level. Peptides 27**:** 943-952.

Yaniv, S. P., N. Issman-Zecharya, M. Oren-Suissa, B. Podbilewicz and O. Schuldiner, 2012 Axon Regrowth during Development and Regeneration Following Injury Share Molecular Mechanisms. Current Biology 22**:** 1774-1782.

Yeh, E., K. Gustafson and G. L. Boulianne, 1995 Green fluorescent protein as a vital marker and reporter of gene expression in *Drosophila*. Proc. Natl. Acad. Sci. U S A. 92**:** 7036-7040.

Yu, X. M. M., I. Gutman, T. J. Mosca, T. Iram, E. Ozkan *et al.*, 2013 Plum, an Immunoglobulin Superfamily Protein, Regulates Axon Pruning by Facilitating TGF-beta Signaling. Neuron 78**:** 456-468.

Zhao, T., T. Gu, H. C. Rice, K. L. McAdams, K. M. Roark *et al.*, 2008 A Drosophila gain-of-function screen for candidate genes involved in steroid-dependent neuroendocrine cell remodeling. Genetics 178**:** 883-901.

Zheng, X. Y., J. Wang, T. E. Haerry, A. Y. H. Wu, J. Martin *et al.*, 2003 TGF-beta signaling activates steroid hormone receptor expression during neuronal remodeling in the Drosophila brain. Cell 112**:** 303-315.

Zhu, S. J., A. S. Chiang and T. Lee, 2003 Development of the Drosophila mushroom bodies: elaboration, remodeling and spatial organization of dendrites in the calyx. Development 130**:** 2603-2610.